STRATOSPHERIC PROCESSES
AND THEIR ROLE IN CLIMATE

SPARC

A project of the WMO/ICSU/IOC
World Climate Research Programme



SPARC Intercomparison of Middle Atmosphere Climatologies

December 2002

WCRP - 116
WMO/TD - No. 1142
SPARC Report No.3.


The World Climate Research Programme is jointly sponsored by the World Meteorological Organisation, the International Council for Science and the Intergovernmental Oceanographic Commission of UNESCO.

NOTE

The designations employed and the presentation of material in this publication do not imply the expression of any opinion whatsoever on the part of the Secretariat of the World Meteorological Organisation concerning the legal status of any country, territory, city or areas, or of its authorities, or concerning the delimitation of its frontiers or boundaries.

STRATOSPHERIC PROCESSES
AND THEIR ROLE IN CLIMATE

SPARC

A project of the WMO/ICSU/IOC World Climate Research Programme

---

SPARC Intercomparison of Middle Atmosphere Climatologies

December 2002

Prepared by the SPARC Reference Climatology Group under the auspices of the SPARC Scientific Streering Group

Edited by W. Randel, M.-L. Chanin and C. Michaut

WCRP - 116
WMO/TD - No. 1142
SPARC Report No. 3

SPARC Intercomparison of Middle Atmosphere Climatologies

Table of Contents

Appendices

Preface

SPARC has from its outset been concerned with “Stratospheric Indicators of Climate Change,” “Stratospheric Processes,” and “Troposphere/Stratosphere Modelling.” The SPARC project GRIPS (GCM Reality Intercomparison Project) has focused on comparing troposphere/stratosphere general circulation models with one another, both in terms of their technical formulations and in their results. Of course, another aspect of GRIPS is to examine how well model results compare to observations. Direct model/data comparisons are not so straightforward, however. For instance, the stratosphere displays a great deal of interannual variability, so that model-data comparisons necessarily include statistics of both means and variances over comparable time periods. Additionally, stratospheric data are obtained from complicated inversions of radiances derived from satellite measurements, from direct but sparse balloon or rocket measurements, from time continuous but geographically sparse ground-based remote sensing instruments, and finally from analysis of stratospheric measurements either by statistical techniques or from data assimilation methods. The climatologies derived by these different methods do not agree in all respects. Finally, the entire concept of stratospheric trends means that stratospheric climatology is itself time varying.

The SPARC Reference Climatology Group was established to update and evaluate existing middle atmosphere climatologies for use in GRIPS, and in other SPARC activities. Rather than create a single new “super climatology,” it was decided that a valuable contribution would be to (1) compile existing climatologies and make them easily available to the research community, and (2) carefully compare and evaluate the existing climatologies. The SPARC Data Center was established (in part) as a response to item (1), and this Report is a response to item (2). Here we present detailed intercomparisons of climatological wind and temperature data sets that are currently used in the research community, which are derived from a variety of meteorological analyses and satellite data sets. Special attention is focused on tropical winds and temperatures, where large differences exist among separate analyses. We also include comparisons between the global climatologies and historical rocketsonde temperature and wind measurements, and also with more recent lidar temperature data. These comparisons highlight differences and uncertainties in contemporary middle atmosphere data sets, and allow biases in particular analyses to be isolated. In addition, a brief atlas of zonal mean wind and temperature statistics is provided to highlight data availability and as a quick-look reference. This Report is intended as a companion to the climatological data sets held in archive at the SPARC Data Center (http://www.sparc.sunysb.edu).

Authors

This report was produced by the SPARC Reference Climatology Group

William Randel (Chair)	National Center for Atmospheric Research, Boulder, CO, USA
Eric Fleming	NASA Goddard Space Flight Center, Greenbelt, MD, USA
Marvin Geller	State University of New York at Stony Brook, Stony Brook, NY, USA
Mel Gelman	National Centers for Environmental Prediction, Washington, DC, USA
Kevin Hamilton	International Pacific Research Center, Honolulu, HI, USA
David Karoly	Monash University, Melbourne, Australia
Dave Ortland	Northwest Research Associates, Bellevue, WA, USA
Steven Pawson	NASA Goddard Space Flight Center, Greenbelt, MD, USA
Richard Swinbank	Met Office, Bracknell, United Kingdom
Petra Udelhofen	deceased; previously at SUNY Stony Brook, NY, USA

Contributors

Mark Baldwin	Northwest Research Associates, Bellevue, WA, USA
Marie-Lise Chanin	CNRS - Service d'Aéronomie, Paris, France
Philippe Keckhut	CNRS - Service d'Aéronomie, Paris, France
Karin Labitzke	Freie Universität Berlin, Berlin, Germany
Ellis Remsberg	NASA Langley Research Center
Adrian Simmons	European Centre for Medium Range Weather Forecasts, Reading, UK
Dong Wu	Jet Propulsion Laboratory, Pasadena, CA, USA

Acknowledgments

These climatological comparisons have resulted from work of the SPARC Reference Climatology Group, which has been ongoing since 1994. A majority of the work has centered around obtaining and archiving the numerous data sets in the SPARC Data Center. This activity was primarily organised by Dr. Petra Udelhofen, who unfortunately died during the final stages of preparation of this report. Petra was a valued friend and colleague of everyone involved with this report, and we dedicate it to her memory.

We wish to note special thanks to the NASA ACMAP Research Program, for support of the SPARC Data Center, and for supporting several individuals involved with the Climatology Group. We also acknowledge the careful work of Fei Wu at NCAR, who performed most of the statistical and graphical analyses included here. Marilena Stone (NCAR) expertly prepared the manuscript through many drafts. We also thank Lesley Gray, Kunihiko Kodera, Gloria Manney and Ted Shepherd for careful reviews of the manuscript.

In Memory of Petra Udelhofen

21 May 1960 - 17 May 2002

1 - Introduction

Climatological data sets for the middle atmosphere are useful for empirical studies of climate and variability, and also necessary for constraining the behaviour of numerical models. The earliest comprehensive climatologies for the middle atmosphere were the 1964 and 1972 COSPAR reference atmospheres (CIRA), which were based largely on interpolation of single station balloon and rocket data. An updated version of CIRA in 1986 included early satellite observations of the stratosphere and mesosphere and has served as a community standard since that time. Around 1979, daily meteorological analyses with significant stratospheric coverage that included operational satellite temperature soundings began, and more recently (~1991) sophisticated model-based data assimilation schemes began to produce stratospheric analyses. These analyses (supplemented in the 1990's by extensive retrospective reanalyses) have served as the basis for some more recent middle atmosphere climatologies. Also, satellite observations from the Upper Atmosphere Research Satellite (UARS), launched in 1991 and continuing to operate in 2002, have provided additional climatological data sets for the middle atmosphere. Details of the circulation statistics derived from these various data sets will depend on several factors, including details of data inclusion and analysis techniques, and the respective time periods covered.

The objective of this work is to bring together several middle atmosphere climatological data sets, which are in current use in the research community, and make direct comparisons of some basic measured and derived quantities. These data sets are based on a wide variety of analysis techniques, including manual analyses, objective statistical analyses, and data assimilation systems. Our comparisons are used to identify biases in particular data sets, and also to highlight regions where there is relatively large uncertainty for particular diagnostics (i.e., where large differences are found among several data sets). Where possible, we provide some brief explanations as to why there are uncertainties and/or why the data sets might differ. However, more in-depth and detailed explanations are beyond the scope of this report.

The middle atmosphere climatologies considered here are primarily derived from global meteorological analyses and satellite data. Two independent data sets are also included for comparison, namely historical rocketsonde wind and temperature measurements (covering approximately 1965-1990), and lidar temperature data (covering the 1990's). Because the time and space sampling of the rocketsonde and lidar data are distinct from the global climatologies, direct comparisons require special attention, as discussed in Section 2C below.

An important aspect of numerical modelling for the middle atmosphere is to simulate not just the time mean structure, but also temporal (interannual) variability (e.g., Pawson *et al.*, 2000). To that end we include here comparisons of both long-term means and interannual variance statistics. We also focus particular attention on the tropics, where there are relatively large differences among middle atmosphere

climatological wind and temperature data sets [in particular, for variability related to the quasi-biennial oscillation (QBO) and semi-annual oscillation (SAO)]. We furthermore present some comparisons between the few available sources of mesospheric winds and temperatures. Finally, we provide a brief atlas of middle atmosphere circulation statistics as a quick-look reference, and to highlight data availability.

All of the monthly mean data presented and compared here are available to the research community via the SPARC Data Center (http://www.sparc.sunysb.edu). This atlas is intended to be a companion to those on-line data.

2 - Climatological Data Sets for the Middle Atmosphere

A. Description of fundamental data and types of global analyses

Two fundamental types of observations contribute to global (or hemispheric) stratospheric analyses. Radiosondes are balloon-borne instruments which provide vertical profiles of temperature, pressure and horizontal winds. These measurements cover the lowest 20-30 km of the atmosphere, with a nominal archive vertical resolution of ~ 2 km. The current radiosonde network provides approximately ~ 1100-1200 soundings per day, almost evenly split for measurements at 00UTC and 12UTC; the vast majority of stations are located over land masses of the Northern Hemisphere (NH). Almost all of these soundings (> 1000) reach at least 100 hPa, with ~ 800 reaching 30 hPa, and ~ 350 reaching up to 10 hPa. Satellite-derived temperature profiles provide the other major source of stratospheric data. Operational meteorological polar orbiting satellites provide near-global temperature profile retrievals twice daily up to ~ 50 km altitude, but have the drawback of relatively low vertical resolution (> 10 km) in the stratosphere. A series of operational NOAA satellites has been in orbit since late 1978, containing a suite of instruments that are collectively called the TIROS Operational Vertical Sounder (TOVS) (Smith *et al.*, 1979). An improved set of temperature and humidity sounders (called the Advanced TOVS, or ATOVS) is now replacing the older TOVS series, beginning with the NOAA-15 satellite launched in May 1998, NOAA-16 in September 2000, and NOAA-17 in June 2002. Temperature retrievals or radiances from TOVS and ATOVS data are a primary input to many of the global analyses here (including CPC, UKMO, UKTOVS, NCEP, ERA15 and ERA40 data sets).

Details of the various stratospheric analyses are described below, but the types of global or hemispheric analyses can be summarised as follows. The main objective is to depict the large-scale atmospheric behaviour by some sort of interpolation between sparse observations, or by combining different types of measurements (i.e., radiosondes and satellites). The simplest analyses provide global or hemispheric fields based on hand-drawn analyses (FUB) or objective analysis gridding techniques (CPC and UKTOVS). More sophisticated analyses can be derived by the use of numerical forecast models to predict first-guess fields, and incorporate observations by optimal data assimilation (UKMO, NCEP, ERA15 and ERA40 data). A strength of the simple analyses is that they are most directly dependent on observations, but this can be a drawback in regions with less data availability. The data assimilation techniques have the advantage of incorporating knowledge of prior observations and dynamical balances, but have the disadvantage that details of the numerical model and assimilation method can influence the results. In fact most of the analyses discussed below are based on very similar radiosonde and satellite data, and so the differences revealed in our comparisons highlight the sensitivity of the final statistics to details of the data usage and analysis techniques.

B. Description of data sets

This section presents short descriptions of the climatological data sets included in the comparisons. These are intended to be brief, and more details for each analysis can be found in the listed references. Table 1 provides a summary list of some relevant details for each analysis. For brevity, each data set is referred to throughout this work by the following short acronyms.

Table 1. Summary of middle atmosphere climatological data sets

Data Source	**Type of Analysis**	**Analysis Quantities**	**Time Period Available**	**Vertical Coverage (in pressure)**
UKMO	assimilation	z,T,u,v,w	Nov. 1991-present	1000-0.3 hPa
UKTOVS	objective analysis	z, T (balance winds)	Jan. 1979-Apr 1997	100-1 hPa
CPC	objective analysis (above 100 hPa)	z, T (balance winds)	Oct. 1978-present	1000-0.4 hPa
NCEP reanalysis	assimilation	z,T,u,v,w	1958-present	1000-10 hPa
ERA15 reanalysis	assimilation	z,T,u,v,w	Jan. 1979-Dec. 1993	1000-10 hPa
ERA40 reanalysis	assimilation	z,T,u,v,w	1957-2001	1000-1 hPa
FUB	historical analysis (NH only)	z,T	1957-2001	100-10 hPa
CIRA86 climatology	various	z,T,u	various (1960's-1970's)	1000-0.001 hPa
HALOE temps	harmonic analysis of seasonal cycle	T	Jan. 1992-Dec. 1997	2-0.0046 hPa
MLS temps	harmonic analysis of seasonal cycle	T	Jan. 1992-Dec. 1994	32-0.0021 hPa
URAP winds	UKMO and HRDI data	u	Jan. 1992-Dec. 1998	1000-0.001 hPa

1. UKMO (Met Office Stratospheric Analyses)

Since October 1991 stratospheric analyses have been produced daily using a stratosphere-troposphere version of the Met Office's data assimilation system (Swinbank and O'Neill, 1994). These analyses were formerly referred to as UK Meteorological Office (UKMO) stratospheric analyses, and we retain that name here. The stratosphere-troposphere data assimilation system is a development of the "Analysis Correction" data assimilation system (Lorenc *et al.*, 1991), which was then in use for operational weather forecasting. In this system, observations are assimilated into a 42-level configuration of the Met Office Unified Model to produce a set of stratospheric analyses for 12 UTC every day. The analyses consist of temperatures, wind components and geopotential heights on a global grid of resolution 2.5° latitude by 3.75° longitude. The analyses are output on the UARS standard pressure levels, with six equally spaced levels per decade of pressure (100, 68.1, 46.4, 31.6, 21.5, 14.7, 10,…hPa). The analyses span the range 1000-0.3 hPa (approximately 0-55 km).

The stratospheric analyses were originally produced as correlative data for the NASA UARS (Upper Atmosphere Research Satellite) project, starting from October 1991. The analyses have been used in a number of research studies of stratospheric dynamics, and to help interpret UARS constituent measurements. Since October 1995 the separate UARS assimilation system was discontinued, but stratospheric analyses continue to be produced using a similar data assimilation system, which is run as part of the Met Office operational forecasting suite. Since November 2000 the Met Office stratospheric analyses have been produced using a new 3-D variational (3DVAR) data assimilation system (Lorenc *et al.*, 2000). However, the majority of results presented here were derived from analyses produced before that change. A further note is that the UKMO temperature analyses at the uppermost levels (at and above 1 hPa) were adversely affected by an erroneous ozone climatology in the assimilation model after January 1998, but these do not influence the majority of the comparisons below (which focus on the time period 1992-1997).

The stratosphere-troposphere data assimilation uses essentially the same set of meteorological observations that are used for operational weather forecasting. In the stratosphere the most important observation types are TOVS (and more recently ATOVS) temperature profiles, together with radiosonde soundings of temperatures and winds (although most radiosondes only ascend as far as the lower stratosphere).

2. UKTOVS (Met Office Analyses of TOVS Data)

The Met Office also produced regular stratospheric analyses (not part of a model assimilation) from measurements made by NOAA polar orbiter satellites. The Met Office was formerly referred to as the UK Meteorological Office, and these analyses have been referred to in the research community as UKTOVS (which we retain here). Monthly means from these analyses are available for the period January 1979-April 1997. The analysis method is described by Bailey *et al.* (1993), but a brief

description is given below. Scaife *et al.* (2000) present climatological data and interannual variations diagnosed from the UKTOVS data.

The UKTOVS fields are derived from an independent analysis of TOVS radiance measurements. The daily TOVS data were used to derive geopotential thickness values, covering the layers 100-20, 100-10, 100-5, 100-2 and 100-1 hPa. The thicknesses were then mapped onto a 5 degree resolution global grid, and added to the operational analysis of 100 hPa height (obtained from Met Office operational global analyses) to produce height fields up to 1 hPa. In turn, temperatures and horizontal balanced winds are derived from the height fields. Winds at the equator are interpolated from low latitudes, and resultant tropical variations (e.g., the QBO) are rather weak (as shown below).

3. CPC (Climate Prediction Center)

Operational daily analyses of stratospheric geopotential height and temperature fields have been produced by the Climate Prediction Center (CPC) of the US National Centers for Environmental Prediction (NCEP) since October 1978 (Gelman *et al.*, 1986). NCEP was formerly called the National Meteorological Center (NMC), and these analyses have been referred to in the research community as "stratospheric NMC" analyses. Here they are termed CPC analyses (to differentiate from NCEP reanalyses). The CPC stratospheric analyses are based on a successive-correction objective analysis (Finger *et al.*, 1965) for pressure levels 70, 50, 30, 10, 5, 2, 1 and 0.4 hPa, incorporating TOVS and ATOVS satellite data and radiosonde measurements (in the lower stratosphere of the NH). This analysis system has been nearly constant over time (October 1978-April 2001). The TOVS temperature profiles are provided as layer mean temperatures between standard pressure levels; geopotential thicknesses are calculated from these temperatures, and added to a base level 100 hPa geopotential field taken from operational NCEP tropospheric analyses. Stratospheric temperatures at standard levels are derived by interpolation between the TOVS layer mean temperatures. The fields are produced each day for a nominal time of 1200 UTC, using 12 hours of TOVS data (0600-1800 UTC). The NCEP operationally analysed tropospheric fields over 1000-100 hPa are included, so that CPC analyses cover 1000-0.4 hPa. As a note, the CPC analyses were changed beginning in May 2001, with the data up to 10 hPa based on the NCEP operational analyses, and fields above 10 hPa based solely on ATOVS. However, comparisons here only include data prior to this change.

Satellite temperatures are the sole input to the CPC analyses over the Southern Hemisphere (SH) and tropics, and over the entire globe for levels above 10 hPa. For levels 70-10 hPa in the NH, radiosonde data (for 1200 UTC) are incorporated, using TOVS as a first guess field. TOVS temperatures have been provided by a series of operational NOAA satellites; these instruments do not yield identical radiance measurements for a variety of reasons, and derived temperatures may change substantially when a new instrument is introduced (Nash and Forrester, 1986). Finger *et al.* (1993) have compared the CPC temperatures in the upper stratosphere (pressure levels 5, 2, 1 and 0.4 hPa) with co-located rocketsonde and lidar data, and find systematic biases of order ± 3-6 K. Finger *et al.* (1993) provide a set of recommended

corrections (dependent on time period and pressure level) to the CPC temperature analyses, which have been incorporated in the results here. However, in spite of these adjustments, the CPC analyses still probably retain artefacts of these satellite changes. One additional change of note is that before March 1984 NH fields were only archived over 20°N-pole; prior to this time CPC analyses over 0-20°N are interpolated values.

Horizontal winds are derived from the CPC geopotential data using the 'linear balance' technique (Randel, 1987). The calculations of longitudinally-varying wind fields become ill-behaved in the tropics, and eddy wind statistics are only reliable polewards of ~ 20° latitude. Tropical zonal mean winds are estimated using the second derivative of geopotential height at the equator (Fleming and Chandra, 1989). Extensive climatologies of the stratosphere have been derived from these CPC data by Hamilton (1982), Geller *et al.* (1983) and Randel (1992).

4. NCEP Reanalyses

The NCEP/National Center for Atmospheric Research (NCAR) reanalysis project uses a global numerical weather analysis/forecast system to perform data assimilation using historical observations, spanning the time period from 1957 to the present (Kalnay *et al.*, 1996). For brevity, the NCEP/NCAR reanalyses are referred to as NCEP here. The model used in the NCEP reanalysis has 28 vertical levels extending from the surface to ~40 km, and analyses of winds, temperatures and geopotential height are output on stratospheric pressure levels of 100, 70, 50, 30, 20 and 10 hPa.

5. ERA15 (ECMWF 15-year Reanalysis)

The European Centre for Medium Range Weather Forecasts (ECMWF) produced a global reanalysis for the period 1979-1993, based on data assimilation coupled with a numerical forecast model (Gibson *et al.*, 1997). The forecast model used in that work spanned pressure levels 1000-10 hPa, with analyses output on stratospheric pressure levels of 100, 50, 30 and 10 hPa. An important detail is that the 10 hPa analysis level is at the top level of the model, and this has a detrimental impact on results at this level (as shown in the comparisons below).

6. ERA40 (ECMWF 40-year Reanalysis)

ECMWF is also producing an updated reanalysis, termed ERA40, covering the period 1957-2001. ERA40 will be a comprehensive set of global meteorological analyses, including the stratosphere up to 1 hPa, based on the use of variational data assimilation techniques. One important difference from the ERA15 reanalyses (in addition to the increased vertical domain) is that ERA40 will directly assimilate TOVS and ATOVS radiances, as opposed to retrieved temperature profiles. Production of the full ERA40 reanalyses is an ongoing activity at the time of writing of this atlas. However, we have obtained a subset of early production results for the time period 1992-1997, covering the parameters zonal mean temperature and zonal mean zonal winds (courtesy of Adrian Simmons of ECMWF), and these are included in our comparisons. The ERA40

analyses are available on 23 standard pressure levels spanning 1000-1 hPa, and also on each of the 60 levels of the assimilation model.

7. FUB (Free University of Berlin Analyses)

The meteorological analyses from the Free University of Berlin (FUB) are northern hemispheric, gridded products at four levels: 100, 50, 30, and 10 hPa. Monthly mean data at these levels are available since 1957 (geopotential height) and 1964 (temperature) on a 10-degree grid, with an increase in resolution to five degrees in the early 1970s as technological advances made the automated scanning of the hand-analysed charts a practical reality (the precise date depends on the pressure level). Daily analyses are produced only at the three upper levels (i.e., not at 100 hPa) and are provided only every second day in northern summer, when the flow evolves slowly. The analyses are performed by hand (subjective analysis) by experienced personnel using station observations of geopotential height, wind, and temperature; thermal wind balance is used as a constraint on the analyses, so that even though the wind field is not analysed, it plays an important part in the analysis procedure. Hydrostatic balance and the thermal wind are used as the analyses are built up from the 100-hPa tie-on level (for which data from FUB were used in the early years, but later operational products from the German Weather Service were substituted), to build accurate analyses from the station data at the stratospheric levels.

The FUB data have been used in a large number of studies of the climatology of the middle atmosphere, including trends and low-frequency variability (e.g., Labitzke and Naujokat, 1983; Pawson *et al.*, 1993). Daily data have been extensively exploited to understand the occurrence of very cold regions which are associated with polar stratospheric cloud formation and ozone loss (Pawson and Naujokat, 1999). It should be stressed that these analyses do not include wind as a product; while their utility is restricted by this, they are a valuable record of the stratosphere between about 1957 and 2001, analysed in a consistent and uniform manner throughout this period. Full details of the FUB analysis, together with the entire data set, are available in compact disk (CD) format (Labitzke *et al.*, 2002).

8. CIRA86 Climatology

The COSPAR International Reference Atmosphere, 1986 (CIRA86) of zonal mean temperature, geopotential height, and zonal wind has been described in detail in Barnett and Corney (1985a, 1985b) and Fleming *et al.* (1988, 1990). These reference climatologies extend from 0-120 km and are based on a variety of data sources, briefly summarised here.

Temperatures for 1000-50 hPa are taken from the climatology of Oort (1983), which is based primarily on radiosonde data from the 1960s and early 1970s. Temperatures at 30 hPa over the NH are taken from FUB analyses, and for the SH are taken from the radiosonde climatology of Knittel (1974). For 10-2.5 hPa, values are based on satellite data from the Nimbus 5 Selective Chopper Radiometer (SCR) averaged over 1973-1974. From 2.5-0.34 hPa (~ 40-56 km), the SCR data were merged with temperatures from the

Nimbus 6 Pressure Modulator Radiometer (PMR) averaged over the period July 1975-June 1978. The PMR data were used exclusively for 0.34 hPa-0.01 hPa (~ 56-80 km), with temperatures from the mass spectrometer and incoherent scatter (MSIS-83) empirical model of the thermosphere (Hedin, 1983) used exclusively above 0.002 hPa (~ 90 km). All values were merged to obtain a smooth transition between the original data sets. For the geopotential height climatology temperatures were integrated upwards and downwards from the 30 hPa geopotential heights, which were taken from FUB analyses for the NH and Knittel (1974) for the SH.

The zonal wind climatology in the troposphere is taken from Oort (1983), with winds in the middle atmosphere above 100 hPa based on gradient winds derived from the geopotential height climatology. At high latitudes, the zonal wind is derived by assuming that the relative angular velocity remains constant poleward of 70° latitude. At the equator where the standard gradient wind calculation fails, the zonal wind (above 100 hPa) is based on the second derivative of geopotential height (Fleming and Chandra, 1989). The winds between the equator and 15°S (15°N) are computed by linear interpolation.

9. HALOE Temperatures

The Halogen Occultation Experiment (HALOE) instrument on UARS provides analyses of temperatures in the altitude range ~ 45-85 km (Russell *et al.*, 1993; Hervig *et al.*, 1996; Remsberg *et al.*, 2002). HALOE uses a solar occultation measurement technique, providing 15 sunrise and 15 sunset measurements per day, with each daily sunrise or sunset group near the same latitude on a given day. The latitudinal sampling progresses in time, so that much of the latitude range ~ 60°N-S is sampled in one month; the measurements extend to polar regions during spring through late summer. The vertical resolution of these data are ~ 2 km, with sampling on UARS standard pressure levels (6 levels per decade of pressure). The results shown here are based on HALOE retrieval version 19.

The seasonal temperature analyses here use the combined sunrise plus sunset temperatures binned into monthly samples. The seasonal cycle is derived by a harmonic regression analysis of these monthly data over the period January 1992-December 1999, including annual and semi-annual harmonics at each height and latitude (spanning 60°N-S). This regression provides a useful method of interpolating the irregular temporal sampling of HALOE.

10. MLS Temperatures

Middle atmosphere temperatures have also been obtained from the Microwave Limb Sounder (MLS) instrument on UARS (Fishbein *et al.*, 1996). The data here are from an independent retrieval described in Wu *et al.* (2002), covering the time period January 1992-December 1994. This retrieval is completely independent of other climatologies, using a single temperature profile (an annual mean) as the first guess and linearisation point. The valid altitude range is 20-90 km, with large uncertainties at the two ends; the temperature is reported on the UARS standard pressure grid (six levels

per decade of pressure), but the actual retrieval was carried out at every other pressure surface. Compared to the MLS Version 5 (V5) retrieval, the data here have much better vertical resolution in the mesosphere, while it is about the same in the stratosphere. These data and further descriptions are available to the research community via an ftp site: mls.jpl.nasa.gov/pub/outgoing/dwu/temp.

The orbital characteristics of UARS allow MLS to obtain data from approximately 80°S-32°N or 32°S-80°N for alternating satellite yaw cycles (each approximately one month long). In order to handle these large data gaps in high latitudes, our analyses fit the seasonal cycle at each latitude and pressure level using harmonic regression analyses of monthly sampled data (including annual and semiannual harmonic terms in the analyses).

11. URAP Reference Atmosphere Winds

As part of the UARS Reference Atmosphere Project (URAP), Swinbank and Ortland (2002) compiled a wind data set using measurements from the UARS High Resolution Doppler Imager (HRDI; Hays *et al.*, 1993), supplemented with data from the UKMO stratospheric analyses. The data set comprises zonal-mean wind data from the earth's surface to the lower thermosphere every month for a period of about 8 years starting from the launch of UARS, and the results here use statistics averaged over 1992-1998. The wind data set only includes the zonal (east-west) component of the wind and not the meridional (north-south) component. The wind data are stored on a pressure-latitude grid; the pressures are the UARS standard pressure levels, and the latitudes are equally spaced every 4° from 80°S to 80°N.

There were several periods when HRDI data were not available. The shorter data gaps in the stratospheric data were filled in using a time-smoothing procedure. In the mesosphere tidal variations in the wind field are much more important than in the stratosphere, so a different procedure was used that took into account the local time coverage of the observations (see Swinbank and Ortland, 2002 in preparation). This reduced the impact of tidal variations on the final wind data set as much as possible.

Wind measurements from HRDI span most of the stratosphere and also extend from the middle mesosphere to the lower thermosphere. In order to obtain as full as possible coverage of the atmosphere, the HRDI measurements were combined with UKMO stratospheric analyses. Together, the two data sets cover the troposphere and stratosphere, but there is a gap between the uppermost reliable level of the UKMO data and the lowermost reliable level of HRDI data in the mesosphere. So, the wind data in this region were supplemented with balanced winds calculated from the URAP temperatures (when available). When there were insufficient HRDI data in a particular month, climatological data derived from HRDI data were used instead. In order to provide complete coverage in the data set, interpolated and extrapolated winds were used when no other data were available. The data set includes a quality flag to indicate when the wind values are based on direct measurements and when they are largely derived from climatological or interpolated data.

C. Rocketsonde wind and temperature data

Measurements from small meteorological rockets provide an important source of wind and temperature information for the middle atmosphere, in the 25 to 85 km altitude region. A program of rocketsonde measurements began in the United States in the late 1950s. During the 1960s the program expanded to about a dozen stations making regular measurements once to three times per week (Schmidlin and Rocket, 1986). Other locations made measurements for limited time periods and for special programs. The number of rocketsonde measurements peaked in the late 1970s, at about 1000 to 1500 yearly, including measurements from the former Soviet Union (USSR), Japan and several other countries. Most measurement locations were at middle latitudes of the Northern Hemisphere and tropical locations, but a few stations were located in polar and Southern Hemisphere mid latitude locations. The number of rocketsonde stations and frequency of observations decreased markedly in the 1980s, and by the 1990s fewer than a total of 100 rocketsonde measurements were made each year. Figure A.1 shows a summary of the number of rocketsonde observations for the 1960's, 1970's and 1980's as a function of latitude.

The archived data collected from the 1950s to the 1990s from the rocketsonde network constitutes a valuable independent resource of *in situ,* fine vertical scale, temperature and wind information, for climatology and research. Indeed, when rocketsonde measurements were first made, they constituted the only source of middle atmosphere information above radiosonde levels. Now, it is especially important to be able to compare climatological summaries of the rocketsonde data at their very few measurement locations with climatologies constructed using remotely sensed global satellite information.

There are two types of small meteorological rocketsonde systems, thermistor and sphere. By far, most measurements have been made using an instrumented thermistor package and parachute, ejected from the rocket at apogee and tracked during descent by a ground radar. *In situ* measurements of thermistor temperature are transmitted to a ground station, so that a temperature versus altitude profile is obtained, with 1 km or finer vertical resolution, from apogee (up to 85 km for the USSR system and 70 km for the US system) to data cut-off (approx. 20 to 25 km). A pressure versus altitude profile is obtained with a support radiosonde observation, close in time and from a nearby location, that supplies the needed "tie on" pressure and height values. The horizontal wind versus altitude profile is obtained by ground radar tracking of the horizontal displacement of the descending parachute. Experimental studies for the US system have indicated temperature measurement precision (repeatability) of 1 to 3 K and wind precision of 3 m/s. Corrections have been applied to measured temperatures to account for solar short wave radiative heating, long wave radiative cooling, and frictional heating of the thermistor. Corrections are less than 1 K below 40 km, up to 5 K at 55 km, and rising to several tens of degrees K above 65 km. Wind corrections are large at the upper altitudes because of the high fall velocity of the parachute, but are small below 50 km.

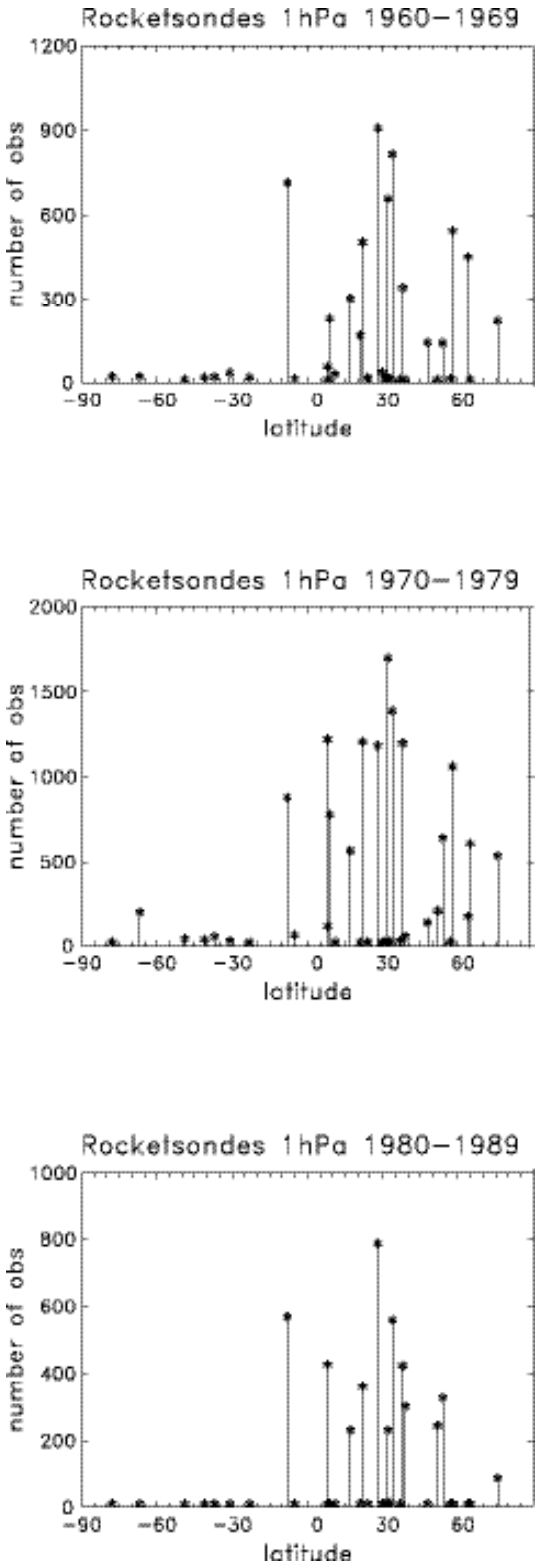

Figure A.1. The availability of rocketsonde wind and temperature measurements as a function of latitude during the 1960's (top), 1970's (middle) and 1980's (bottom). Each line represents data from a single station, which are subsequently sampled in latitude bins centred at 10°S, 10°N, 30°N, 60°N and 80°N.

The number of sphere observations have been relatively small, from a few locations in middle northern latitudes and tropical locations. The sphere system consists of an inflatable mylar balloon, inflated at apogee, and tracked by high-precision ground radar as the inflated sphere descends. Atmospheric density from approximately 90 km down to 35 km is derived from the measured vertical profile of fall velocity of the sphere, assuming zero vertical atmospheric motion. Temperatures are derived from the density profile, using a "guess" temperature value at the top of the profile. The horizontal wind versus altitude profile is obtained by the ground radar tracking of the horizontal displacement of the descending inflated sphere. Studies have found average differences of 3 to 6 degrees K between sphere and thermistor measurements. However, the analyses here make no distinction between these two types of measurements.

The rocketsonde wind and temperature climatologies shown here are based on simple monthly averages, derived by binning all of the available observations during 1970-1989. Due to data availability (Figure A.1), we focus the comparisons on the tropics and extratropical NH. The extratropical bins are centred at 30°, 60°, and 80° latitude, including measurements within ± 10° of the central latitude. The tropical data are separated for measurements near 10°S (mostly from Ascension Is. at 8°S), and near 10°N (mostly from Kwajelein at 8°N). Based on this sampling, there are approximately 100-300 profile observations in each monthly bin, depending on latitude and altitude. Vertical sampling is made on the UARS pressure grid (six levels per decade of pressure). Figure A.2 shows an example of the data availability for rocketsonde zonal winds at 0.1 hPa for the latitude bin centred at 30°N.

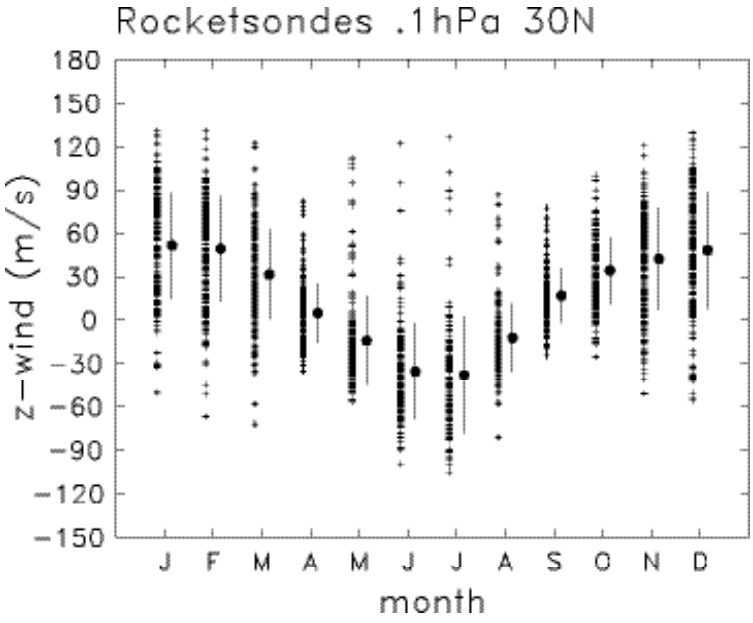

Figure A.2. Distribution of rocketsonde zonal wind measurements at 0.1 hPa (~65 km) for the latitude bin centred at 30°N. The crosses show each individual measurement during 1970-1989 binned into monthly samples, and the circles with error bars show the associated monthly means and ± 1 standard deviations of the individual measurements.

Two important considerations apply to the comparisons of rocketsonde data with global analyses. First, the time periods analysed here for the data are different (1992-1997 for the analyses, and 1970-1989 for the rocketsondes). This is most important for temperatures in the upper stratosphere, and mesosphere, which have experienced strong cooling (of order 2 K/decade near the stratopause, and possibly larger in the mesosphere) during the recent decades (WMO, 1999; Ramaswamy *et al.*, 2001). A large part of the observed rocketsonde-analyses differences in these regions can be attributed to this cooling. Second, the monthly samples from analyses are based on zonal and monthly means of daily data, whereas the rocketsonde statistics are derived from infrequent samples at specific locations, taken over many years. Thus uncertainty levels for the rocketsonde means are significantly larger. Estimates of the standard error of monthly means from the rocketsonde (and lidar) data are calculated as sigma-climatology = sigma $/\sqrt{N}$, where sigma is the standard deviation of the individual soundings within each month and latitude bin (as in Figure A.2), and N is the corresponding number of measurements. These standard error estimates are included in the comparison figures below (although they are typically very small for the large number of rocketsonde measurements).

D. Lidar temperature data

Lidars provide measurements of the vertical temperature profile in the middle atmosphere, and a number of specific sites have made lidar temperature measurements for a decade or longer. The Rayleigh lidar technique uses the backscattering of a pulsed laser beam to derive the vertical profile of atmospheric density, from which the temperature profile is deduced (Hauchecorne and Chanin, 1980; Keckhut *et al.*, 1993). This technique provides an absolute temperature measurement over altitudes ~ 30-75 km, which does not require adjustment or external calibration (derived temperatures above ~ 75 km can be influenced by first guess uncertainties and values below ~30 km by aerosols or details of the lidar measurements). The vertical resolution of the lidar data is approximately 3 km, and the profiles here are sampled on the UARS standard pressure grid.

For the climatological analyses here, we obtained a number of lidar temperature time series (for stations with relatively long records) from the Network for the Detection of Stratospheric Change (NDSC) web site: http://www.ndsc.ws/. The specific locations and available time records are listed in Table 2. The individual profiles are binned into monthly samples, focused on latitude bins centred at 20°N, 40°N and 80°N. We use all the lidar observations over 1990-1999, in order to most directly compare with the meteorological analyses over 1992-1997 (a slightly longer time record for the lidar data provides better monthly sampling). The total number of lidar observations and their latitudinal sampling is shown in Figure A.3. Our monthly and latitudinal sampling produces between ~ 20-80 measurements per bin for latitudes 20°N, and 80°N, and ~ 300 per month for the bin centred at 40°N. The associated monthly means and standard deviations are calculated identically to those for the rocketsonde analyses.

As a note, one important source of variability for lidar and all data sets in the upper stratosphere-mesosphere is the diurnal and semi-diurnal tides, which have large amplitudes above the stratopause. Most lidar observations are taken at night and most rocketsonde observations are taken at a fixed time of day at each station. By contrast the zonal means of gridded global synoptic data sets average over all local times.

Table 2. Lidar temperature data obtained from the NDSC web site: http://www.ndsc.ws/

Location	**available time period**
Eureka (80°N)	1993-1998
Ny Alesund (79°N)	1995-1998
Thule (77°N)	1993-1995
Hohenpeissenberg (48°N)	1987-1999
OHP (45°N)	1991-2000
Toronto (44°N)	1996-1997
Table Mountain (34°N)	1989-2001
Mauna Loa (20°N)	1993-2001
Réunion (22°S)	1994-1998

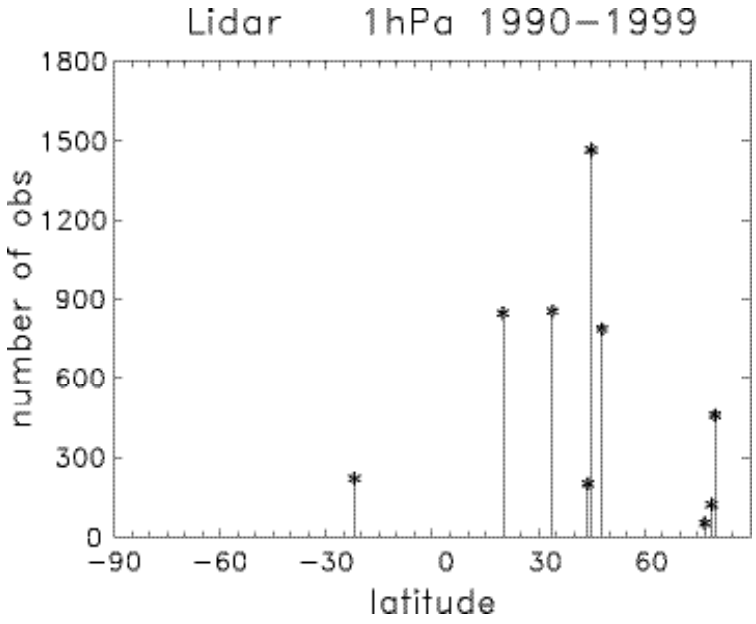

Figure A.3. The number and latitude distribution of lidar temperature measurements during the 1990's, which contribute to the lidar climatology.

3. Data Intercomparisons

In this section we make direct comparisons among the different data sets for global fields of temperature, zonal winds, and zonal averaged eddy fluxes of heat and momentum. The first requirement for such comparisons is to choose a time period which maximises record length for overlap among most data sets. Here we choose the period January 1992-December 1997, which gives direct overlap of the UKMO, CPC, NCEP and ERA40 reanalysis, and FUB fields. The UKTOVS record is slightly shorter (to April 1997). The ERA15 reanalysis has a much shorter record during this 1992-1997 period (January 1992-December 1993). We include comparisons for these data by calculating differences only over this 1992-1993 record, rather than the full 6 years 1992-1997. We also include comparisons with the CIRA86 climatology, although it should be kept in mind that these data are derived from a very different time period (covering the 1960's-1970's). The FUB and NCEP re-analyses have data for the pre-satellite period (prior to 1979), and these are briefly compared separately in Section D below. Rocketsonde data span 1970-1989, while lidar temperatures cover 1990-1999.

A. Temperature

1. Zonal mean climatology

A cross section of January average zonal mean temperature is shown in Figure 1 based on UKMO analyses. The overall latitude-height structure is similar in all data sets, and comparisons are best made by considering differences with a single standard (UKMO in this case; note this is not an endorsement of the UKMO analyses as 'better' or more 'correct', but simply a choice of one data set as a reference). Included in Figure 1 are January temperature differences from the UKMO for each climatology, showing the overall character of the differences. The differences are typically ± 1-5 K, with systematic vertical or latitudinal patterns depending on each data source. Differences that are consistent across several data sets suggest a systematic bias in the UKMO reference, whereas differing biases across many data sets suggest a fundamental uncertainty in estimates of that quantity.

Figure 1

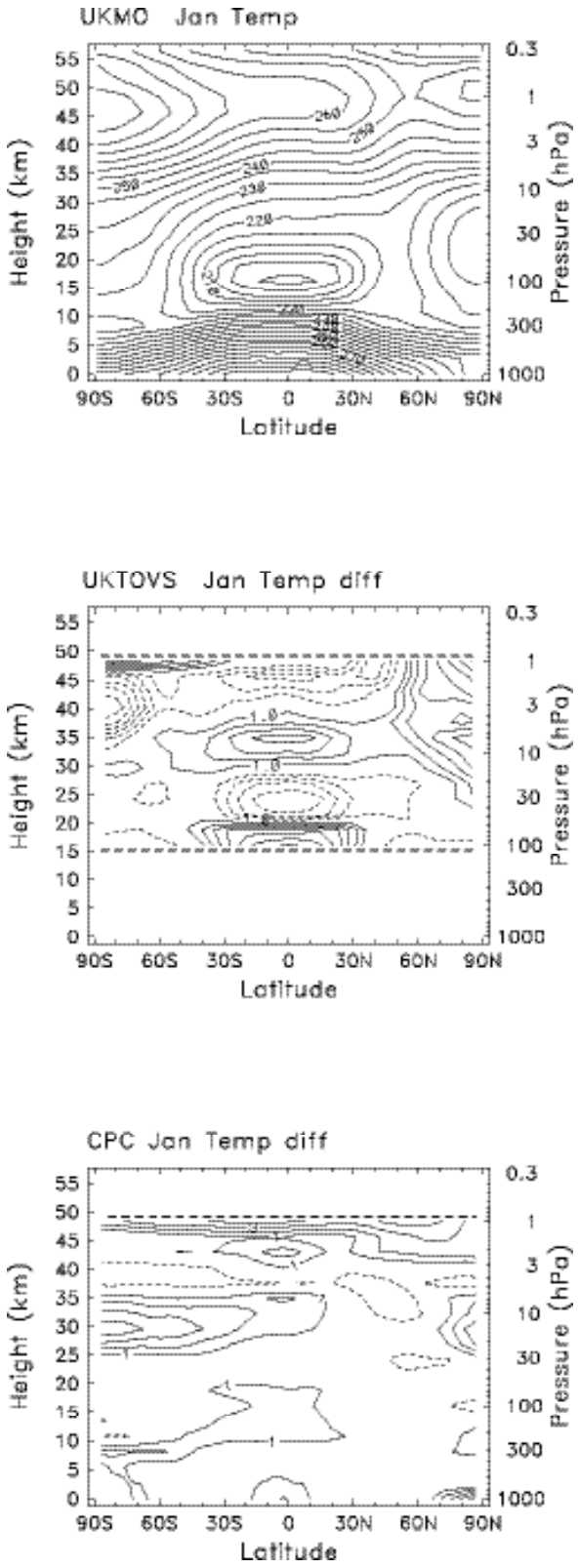

Figure 1. Top panel shows meridional cross section of January average zonal mean temperature (K) derived from UKMO analyses. Each other panel shows a difference field for temperatures from other analyses (i.e., UKTOVS-UKMO, etc.). Contour interval for the difference fields is ± 1, 2, 3 ... (zero contours omitted).

Figure 1 (continued)

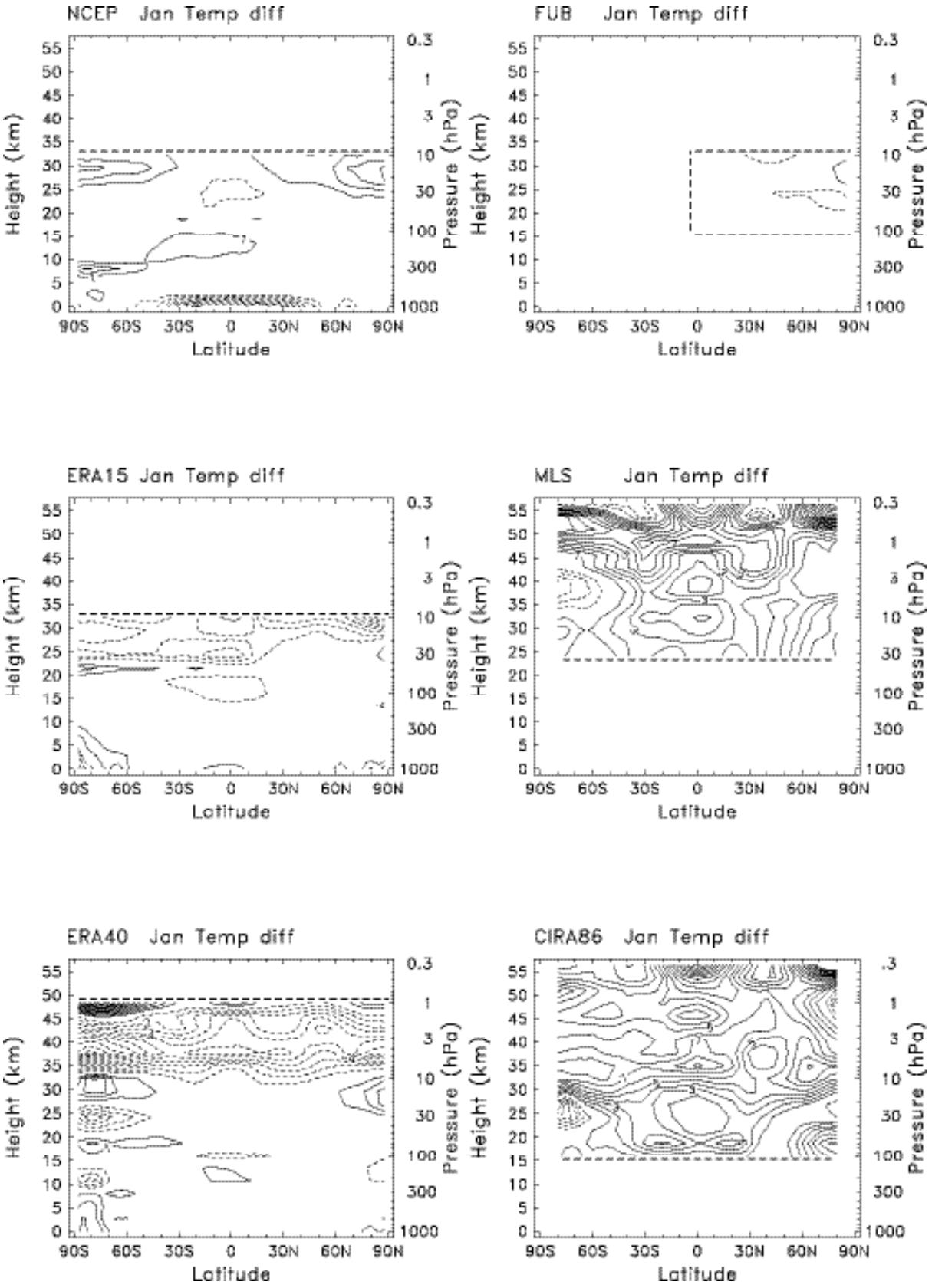

The latitudinal structure of 100 hPa temperature for each data source during January, April, July and October is shown in Figure 2, and differences with the UKMO analyses are shown in Figure 3. The overall latitudinal structure in Figure 2 is similar between the data sets, but there is substantial spread in the tropics and also the polar regions. The UKTOVS data are a notable outlier (> 5 K warmer than all other data sets in the tropics), and are not included in the differences in Figure 3. Aside from UKTOVS, the 100 hPa tropical temperatures fall into two groups, biased warmer (CPC, NCEP and CIRA86) or colder (FUB, ERA15 and ERA40) than UKMO. As discussed in more detail below, the latter (cold) group is probably more realistic, and the former data sets (plus UKMO) have a true warm tropical bias of ~ 2-3 K at 100 hPa. The CIRA86 data exhibit warm biases by up to ~ 5 K in the winter polar regions, and it is likely that at least a part of this may reflect true cooling in the lower stratosphere between the 1960's and 1990's (e.g., Ramaswamy *et al.*, 2001). CPC data show a warm bias over Antarctica in April, July and October, apparently distinct from the other data sources. Manney *et al.* (1996) compared CPC and UKMO lower stratospheric temperature analyses with polar radiosonde data during several winters, finding systematic warm biases (of order 1-3 K) for both CPC and UKMO data in the Arctic. In the Antarctic the CPC data showed similar 1-2 K warm biases, while UKMO biases were smaller (< 1 K).

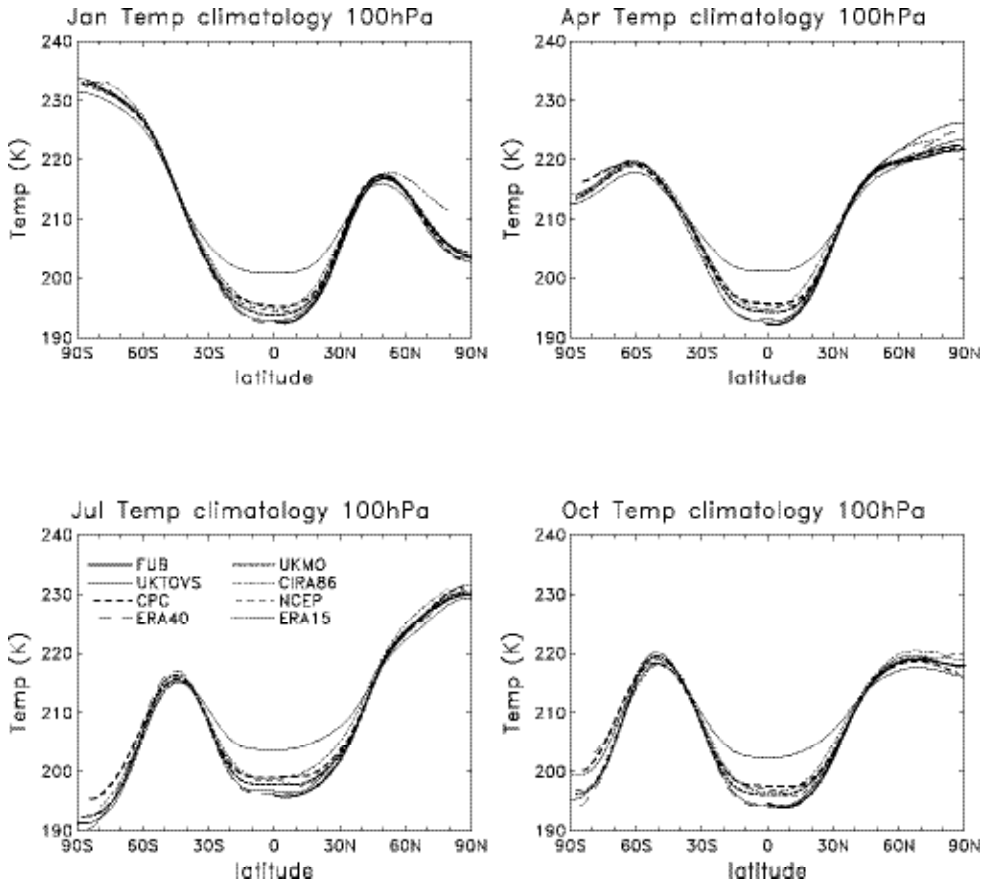

Figure 2. Latitudinal distribution of 100 hPa zonal mean temperature from different analyses, for January, April, July and October.

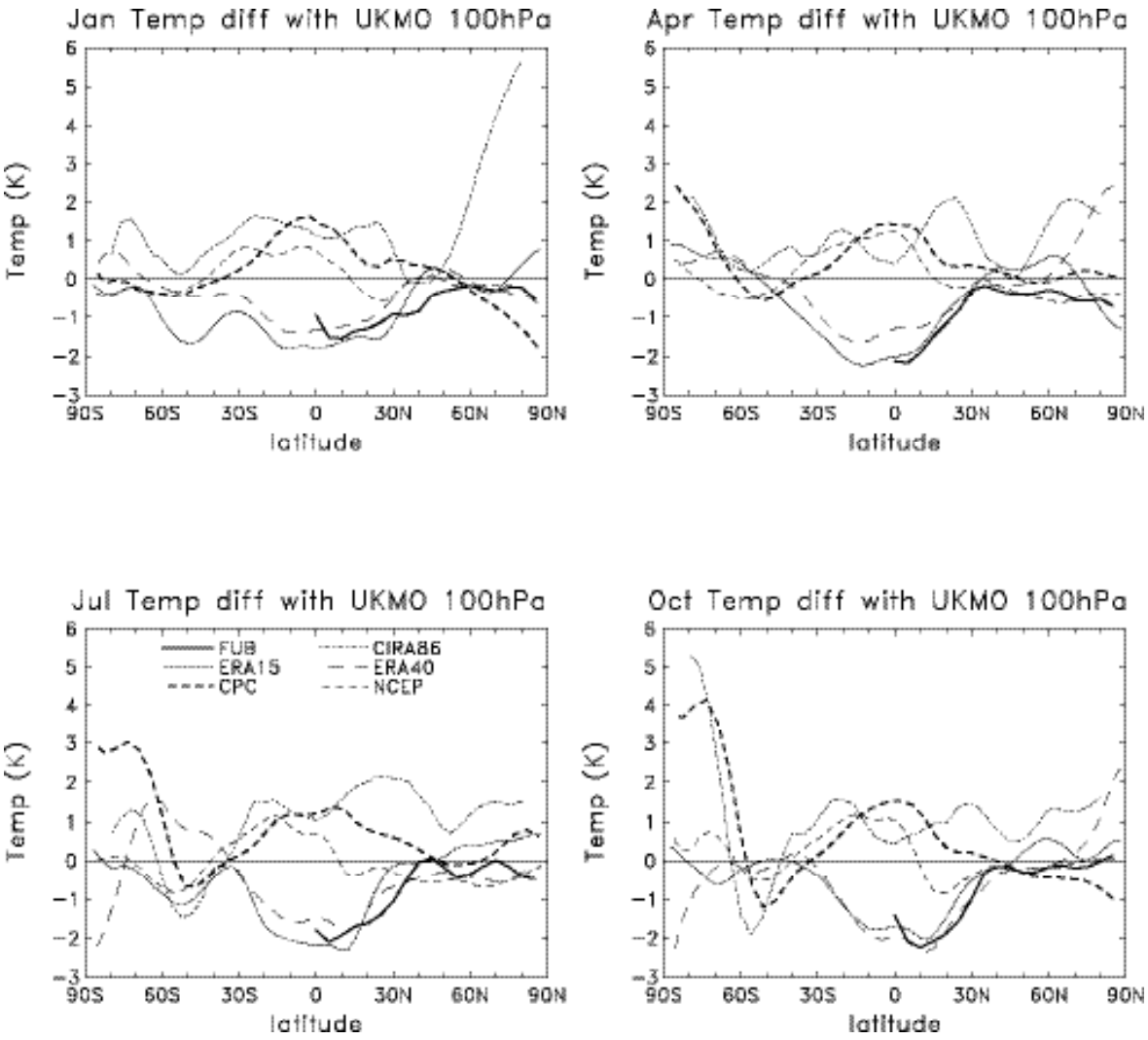

Figure 3. Latitudinal distribution of differences in 100 hPa zonal mean temperature between each analysis and UKMO (i.e., NCEP-UKMO, etc.). The (UKTOVS-UKMO) differences are relatively large in the tropics (~10 K) and not included.

Figure 4 shows difference statistics for the 50 hPa level, for January, March, July and October. Here the differences have been calculated with respect to the UKMO analyses at 46.4 hPa (the closest level), resulting in slight cold differences in the tropics for most data sets. There is reasonable overall agreement between the different data sets over a broad range of latitudes, except for warm biases in CIRA86 (warm by ~ 2-3 K) and cold biases in UKTOVS (cold by up to 5 K). There is also a wide range of biases over Antarctica during spring (October), with differences of ± 2-4 K, and no consensus between data sets.

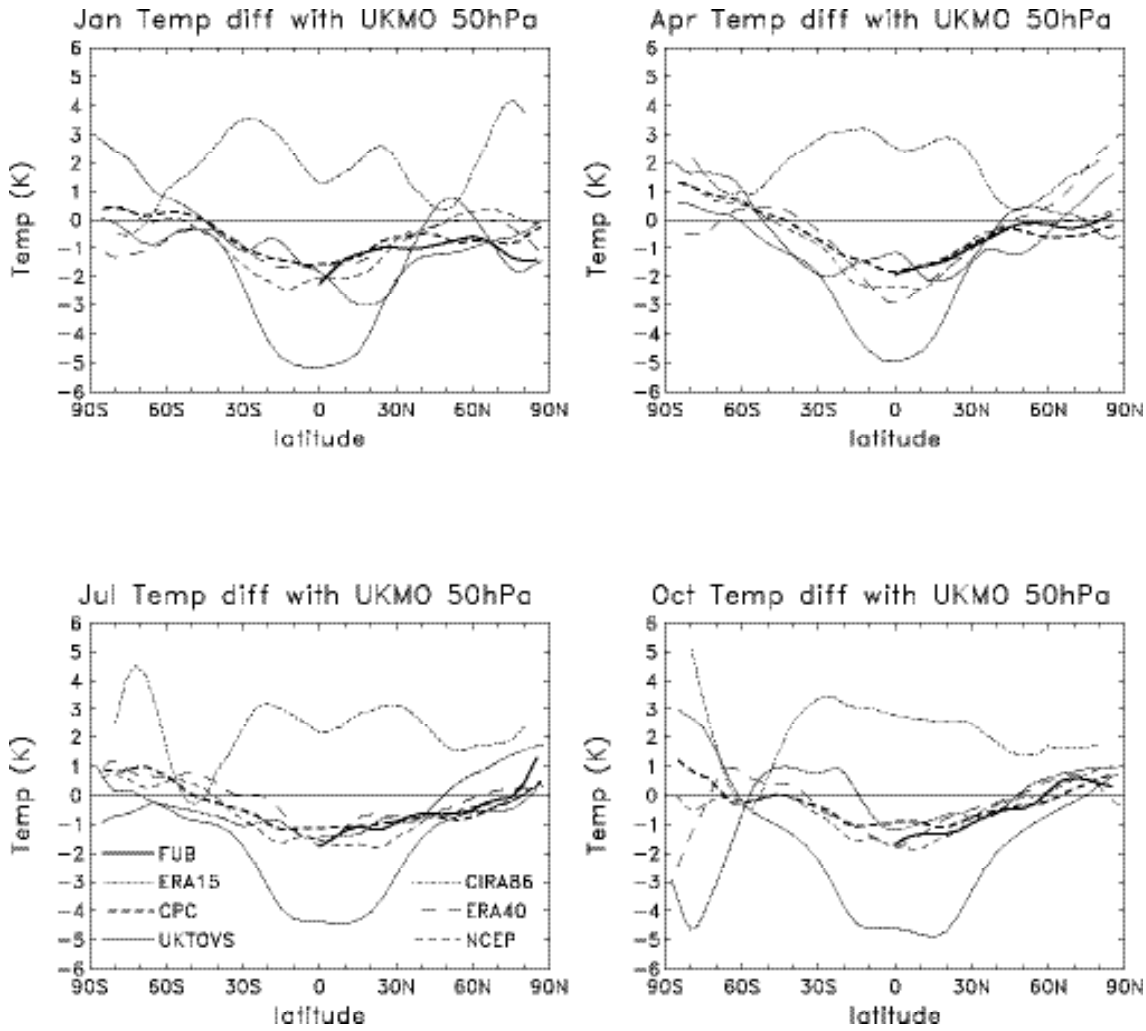

Figure 4. Latitudinal distribution of differences in 50 hPa zonal mean temperature between each analysis and UKMO (i.e., NCEP-UKMO, etc.).

The climatology of 10 hPa zonal mean temperature in January and July, and differences with UKMO, are shown in Figure 5. There is a wider range of differences at this level (typically ± 2-4 K) than at 100 or 50 hPa, showing more uncertainty in the climatology. In the tropics the CIRA86 and MLS data are on the warm side of the ensemble, and the ERA15 10 hPa temperatures are biased cold in the extratropics compared to all other data. The 10 hPa ERA40 data also show large cold biases over SH extratropics in July, and this is part of an oscillatory structure in the ERA40 temperature analyses which are especially large over Antarctica (seen in Figure 1). The cause of this feature is under investigation at ECMWF.

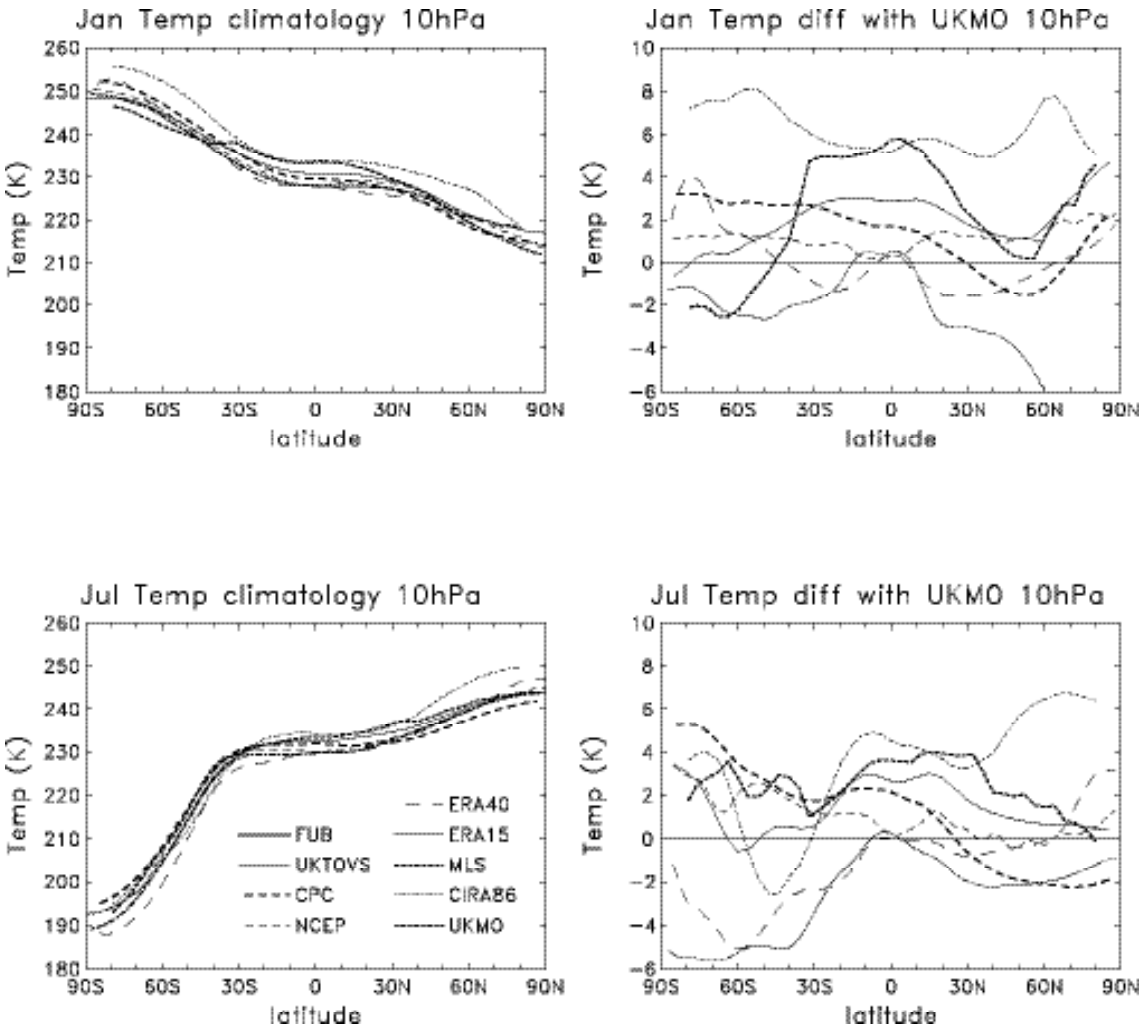

Figure 5. Left panels show latitudinal distribution of 10 hPa zonal mean temperatures in January (top) and July (bottom). Right panels show the corresponding differences with UKMO analyses (i.e., CPC-UKMO, etc.).

Comparisons of temperatures at 1 hPa are shown in Figure 6. Here there are substantial differences of order ~ 5 K between the different data sets, with even larger differences over polar regions. MLS data are relatively warm and UKMO relatively cold compared to the other analyses. The UKTOVS show a slightly different latitudinal structure than the other data sets at high winter latitudes in both hemispheres. This level near the stratopause presents special problems in analyses, because it is not captured accurately in TOVS thick layer radiance measurements, plus it is near the top of the UKMO forecast/assimilation model (at 0.3 hPa).

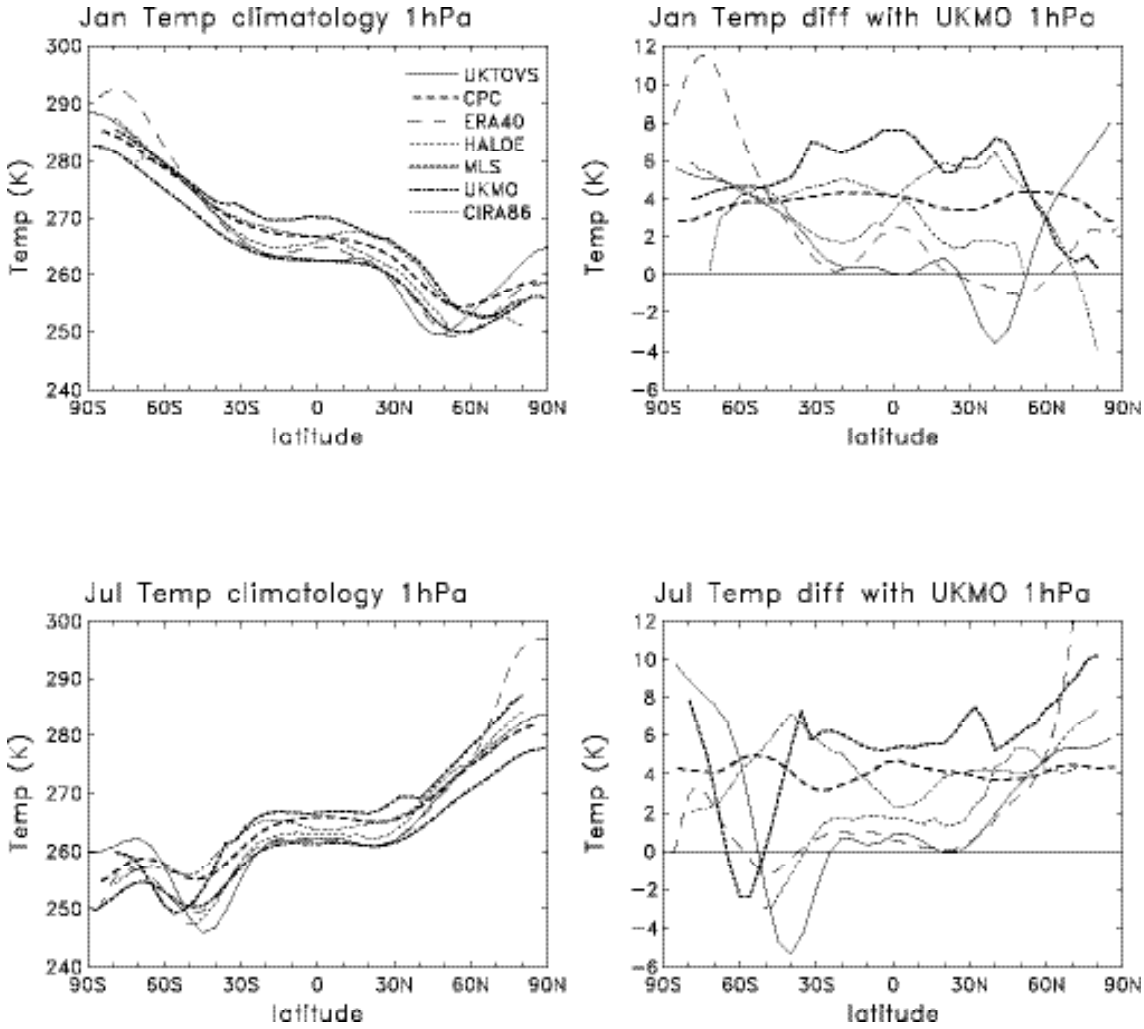

Figure 6. Left panels show latitudinal distribution of 1 hPa zonal mean temperatures in January (top) and July (bottom). Right panels show the corresponding differences with UKMO analyses (i.e., CPC-UKMO, etc.).

Climatologies of mesospheric temperature at 0.1 hPa (~ 65 km) and 0.01 hPa (~ 80 km) are shown in Figure 7, comparing the few available data sets (HALOE, MLS and CIRA86). At 0.1 hPa the latitudinal structure is very similar in all three data sets, with the midlatitude minima most pronounced in MLS and HALOE data. HALOE and MLS data are somewhat colder than the CIRA86 at 0.01 hPa, but absolute comparisons with CIRA86 are difficult in light of the ~ 20 year time difference between these measurements.

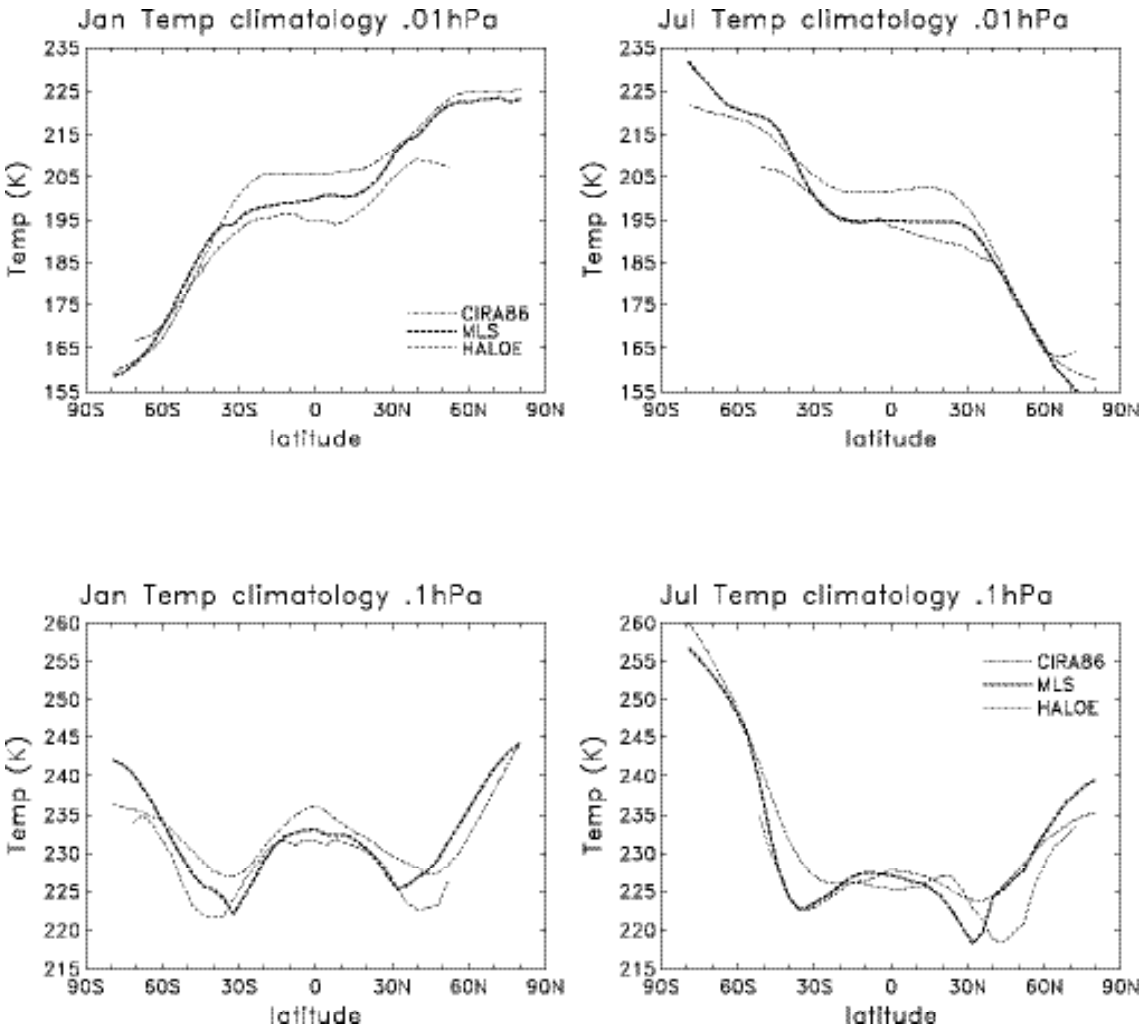

Figure 7. Latitudinal distribution of zonal mean temperatures at 0.01 hPa (~ 80 km) (top) and 0.1 hPa (~ 65 km) (bottom), for January (left) and July (right).

The climatological vertical profiles of temperature in January and July are shown in Figure 8, for data at 80°S, the equator, and 80°N. These plots show the extreme range of global temperature variations, and illustrate regions where there are relatively larger differences between data sets. One obvious region of uncertainty is in the upper stratosphere and near the stratopause, and a further region showing substantial differences (~ 5 K) is in the Antarctic polar stratosphere in July, near the temperature minimum over ~ 25-30 km. A similar level of uncertainty is found in the Antarctic lower stratosphere in October (see Figures 3-4). The seasonal variations of polar temperatures in the lower stratosphere (100 and 50 hPa) are compared among the different climatologies in Figures 9-10. In the NH there is excellent agreement (within 1 K) between UKMO, CPC, FUB and NCEP reanalyses; the UKTOVS have slightly larger differences, while CIRA86 is much warmer in winter (due at least in part to the different time periods involved). In the SH the differences are somewhat larger; the CPC are warmer than UKMO by ~ 2-3 K throughout winter. Large differences are seen in

CIRA86 data over the Antarctic during spring, and a large part of this is due to observed cooling between the respective time periods (associated with ozone depletion, e.g., Randel and Wu, 1999). The climatological minimum 50 hPa temperature over Antartica varies from 184-187 K between the different data sets for the more recent time period (1992-1997), and these comparisons highlight the problem of accurate temperature analyses in the intensely cold Antarctic stratosphere.

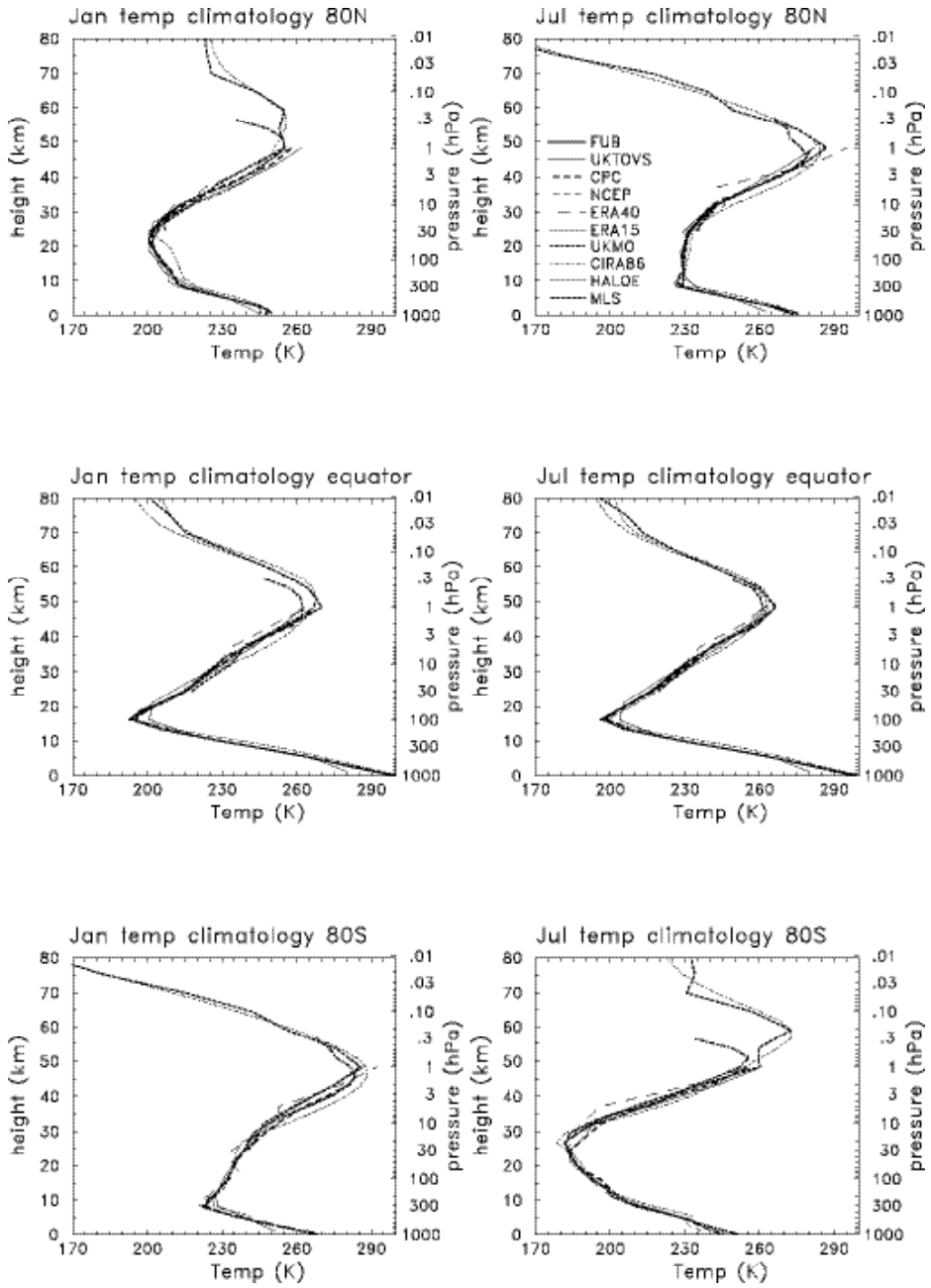

Figure 8. Vertical profiles of zonal mean temperature for January (left) and July (right), for latitudes 80°N (top), the equator (middle) and 80°S (bottom).

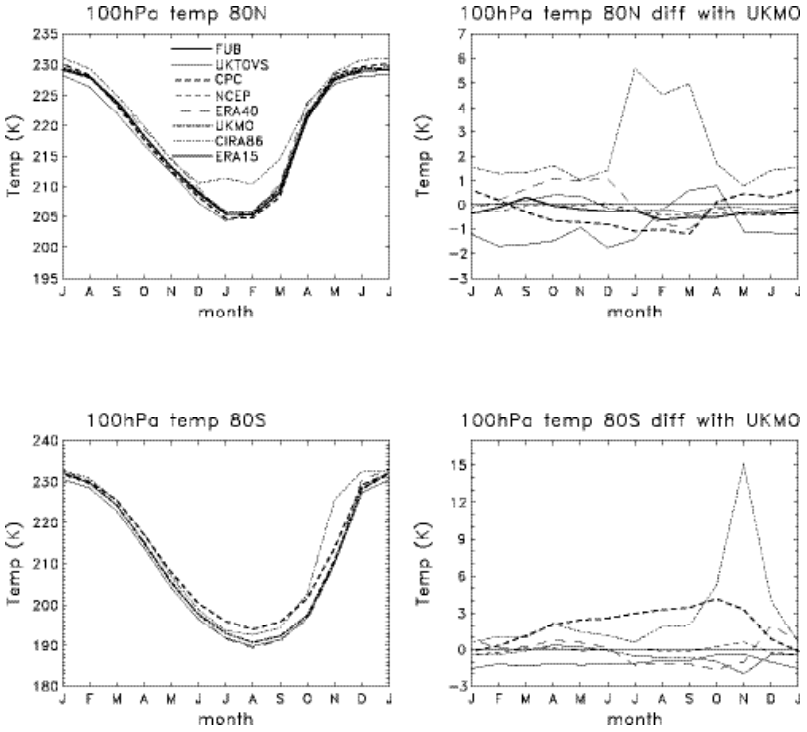

Figure 9. Left panels show seasonal variation of 100 hPa zonal mean temperature at 80°N (top) and 80°S (bottom); note the respective time axes have been shifted by 6 months so that winter is in the middle of each plot. Right panels show the respective differences from UKMO analyses.

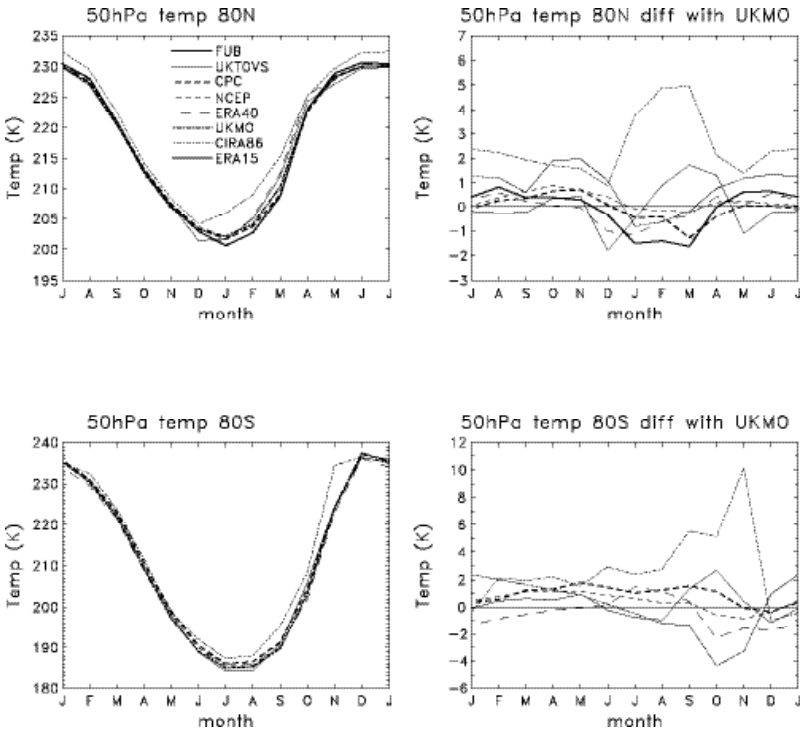

Figure 10. Seasonal variation of polar temperatures as in Figure 9, but for statistics at 50 hPa.

Figure 11 compares the temperature climatologies for January at 40°N, where optimal agreement might be expected in levels below ~ 25-30 km, due to maximum radiosonde coverage. Indeed, Figure 11 shows small differences over these altitudes (~ ± 2 K, aside from CIRA86) and the cluster of differences near –1 K suggest a small systematic bias in UKMO analyses. Above ~ 25 km the differences are larger (~ ± 3-5 K), showing the sensitivity to satellite data types and analyses. As at all other latitudes, relatively large differences are found near the stratopause, with the UKMO being systematically colder than most other analyses.

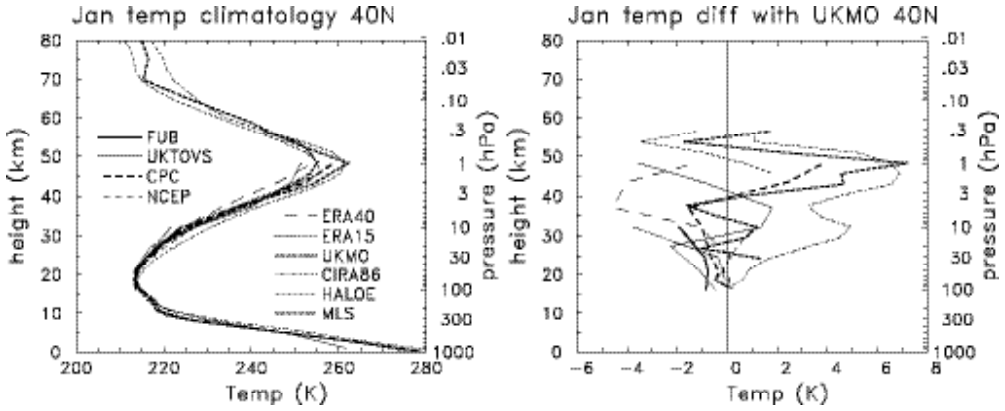

Figure 11. Left panel compares vertical profiles of zonal mean temperature at 40°N; right panel shows the respective differences from UKMO analyses.

Variability at the midlatitude stratopause is explored further in Figure 12, showing the seasonal cycle of 1 hPa temperature at 40°N and 40°S from each analysis. These comparisons demonstrate that some biases vary seasonally. In general, differences between analyses are somewhat larger during local winter. The UKTOVS have an accentuated annual cycle compared to the other analyses, with largest apparent cold biases during local winter. The MLS and CIRA86 data have a relatively warm stratopause throughout the year, while the UKMO, HALOE and ERA40 data are consistently on the cold side.

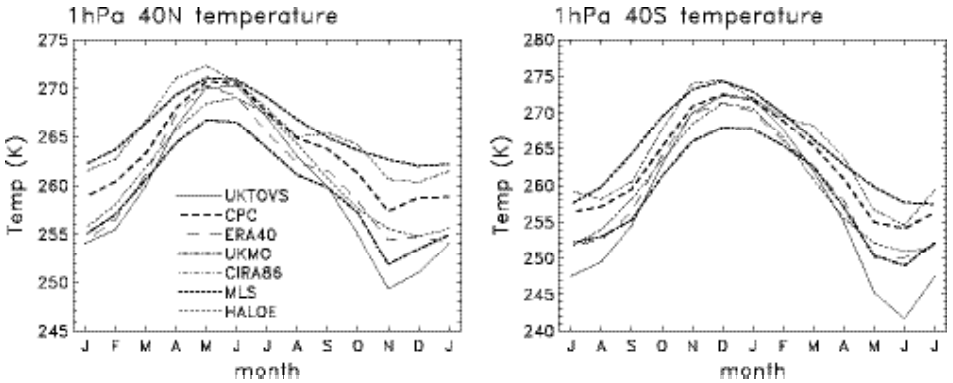

Figure 12. Seasonal variation of 1 hPa zonal mean temperature at 40°N (left) and 40°S (right). Note the respective time axes have been shifted by six months.

a. Comparisons with rocketsondes

As noted above, most of the extratropical rocketsonde data occur in latitude bins near 30°N, 60°N and 80°N, and we focus comparisons on these latitude regions. Figure 13 compares rocketsonde climatology profiles with analyses at 30°N for January and July statistics. The rocketsondes show good overall agreement in the stratosphere, and in locating the altitude of the stratopause. The rocketsonde temperatures in the mesosphere (~ 50-70 km) are warmer than the analyses, especially in January.

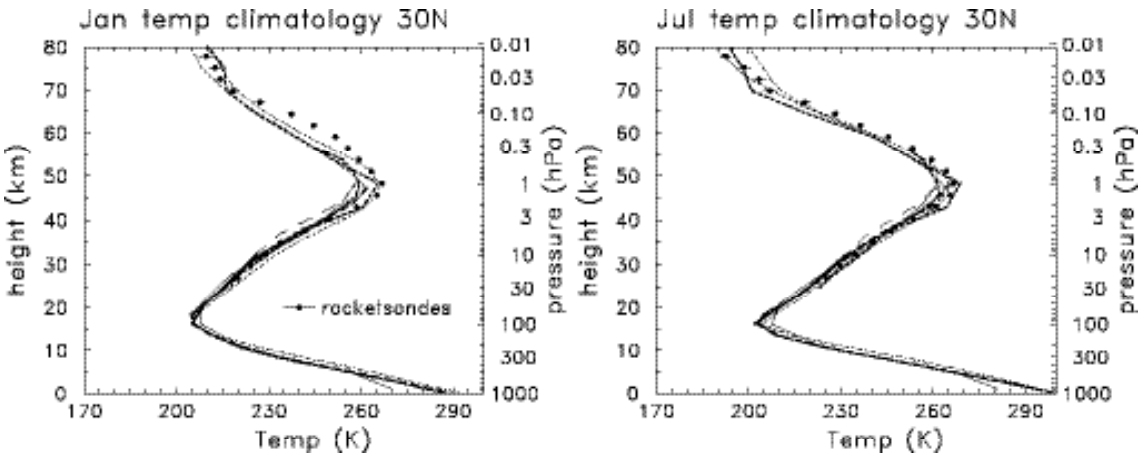

Figure 13. Comparison of rocketsonde temperature statistics at 30°N with zonal mean analyses, showing statistics for January (left) and July (right). Line types denote the same data sources as in Figure 12.

The seasonal variation of temperatures near 30°N from rocketsondes and analyses are compared in Figure 14, for data at 10, 1 and 0.1 hPa. At 10 and 1 hPa the mean rocketsonde temperatures are slightly warmer than most analyses (except CIRA86 at both levels, UKTOVS at 10 hPa and MLS at 1 hPa). At 0.1 hPa the mean rocketsonde values are ~ 5-10 K warmer than MLS or HALOE data, and ~ 3-10 K warmer than CIRA86 (with maximum differences during NH winter).

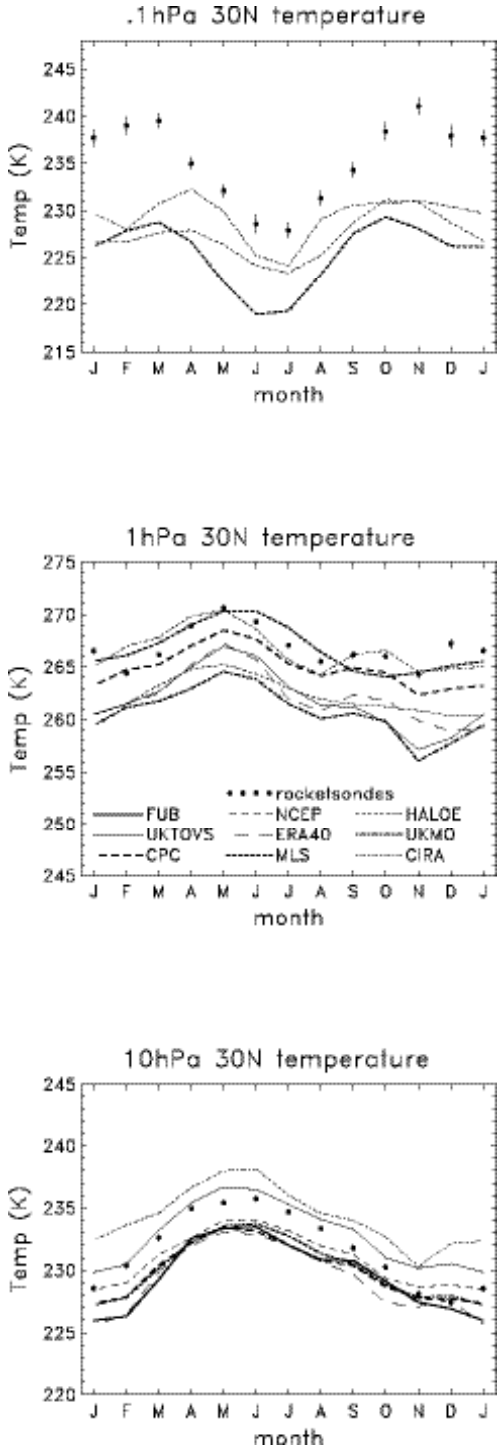

Figure 14. Comparison of the seasonal variation of rocketsonde temperatures near 30°N with zonal mean analyses, for pressure levels 0.1 hPa (top), 1 hPa (middle) and 10 hPa (bottom). Circles denote the rocketsonde means, and error bars the plus/minus two standard errors.

Similar comparisons for temperatures near 60°N are shown in Figure 15. Good agreement is seen at 10 hPa between rocketsondes and all analyses (except CIRA86, with a warm summer bias). At 1 hPa the rocketsondes are also in agreement with most analyses; the comparisons highlight cold biases for UKMO at the warm summer stratopause, and for the HALOE climatology in midwinter (possibly related to the harmonic analysis of sparse HALOE observations near 60°N). At 0.1 hPa, the

rocketsondes are ~ 10-20 K warmer than CIRA86, MLS and HALOE, and only the MLS and rocketsonde data show a similar semi-annual seasonal cycle.

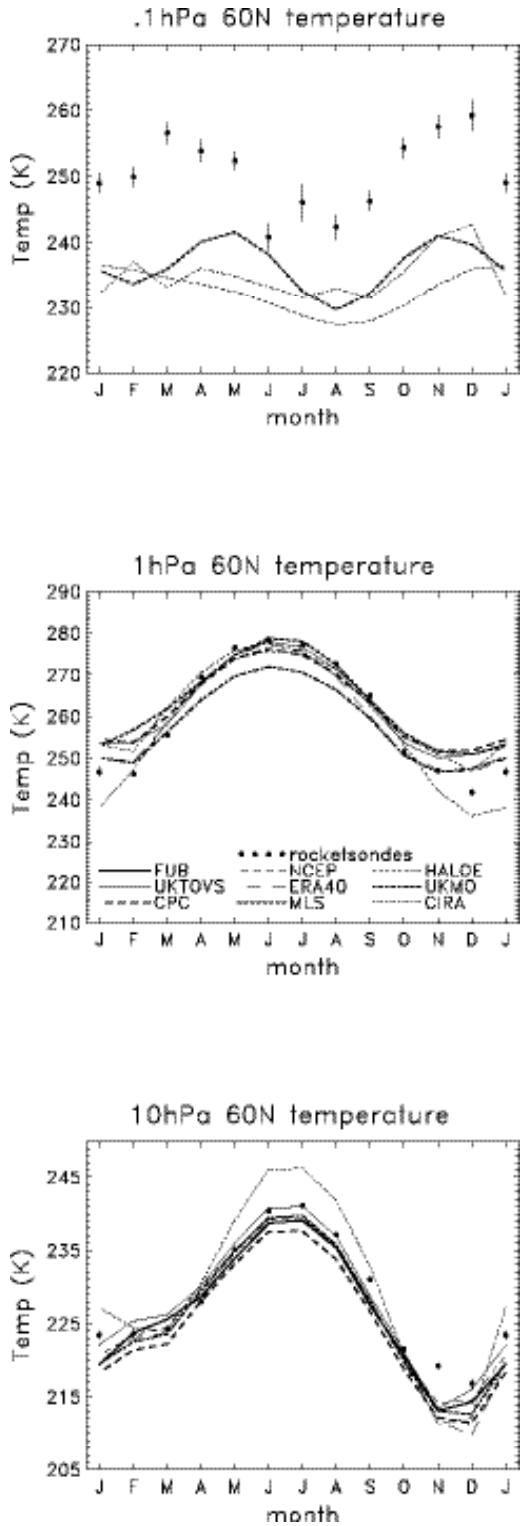

Figure 15. Seasonal cycle comparison of temperatures near 60°N between rocketsondes and zonal mean analyses. Details are the same as in Figure 14.

Comparisons at 80°N (Figure 16) show a similar overall character, with analyses agreeing reasonably well with rocketsondes at 10 and 1 hPa (except for cold rocketsonde

differences at 1 hPa during winter). Systematic warm rocketsonde differences are observed at 0.1 hPa, but these differences are smaller than those observed at 60°N.

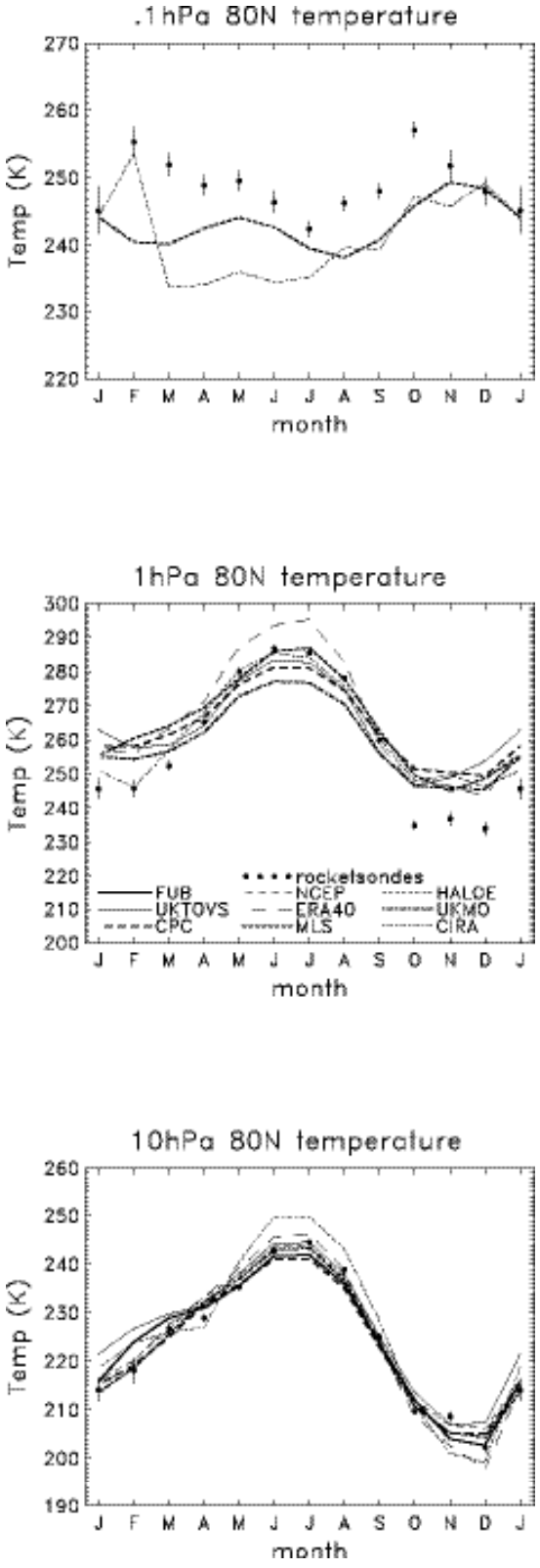

Figure 16. Seasonal cycle comparison of temperatures near 80°N between rocketsondes and zonal mean analyses. Details are the same as in Figure 14.

b. Comparisons with lidars

The lidar temperature measurements have the most data available in the latitude bands near 20°N and 40°N (Figure A.3). Figure 17 shows a comparison of seasonal temperature variations near 20°N between lidar (from Mauna Loa) and zonal mean analyses at 10, 1 and 0.1 hPa. At 10 hPa the analyses form a relatively compact group, except for the warmer CIRA86 and UKTOVS data, and the lidar data are in good agreement with the larger group. At 1 hPa there is a wider spread (~ 5 K) between the analyses, with the lidar measurements generally toward the middle or lower range of analyses. At 0.1 hPa, there is overall reasonable agreement (to within ~ 5 K) between the lidar and temperatures from CIRA86, MLS and HALOE data.

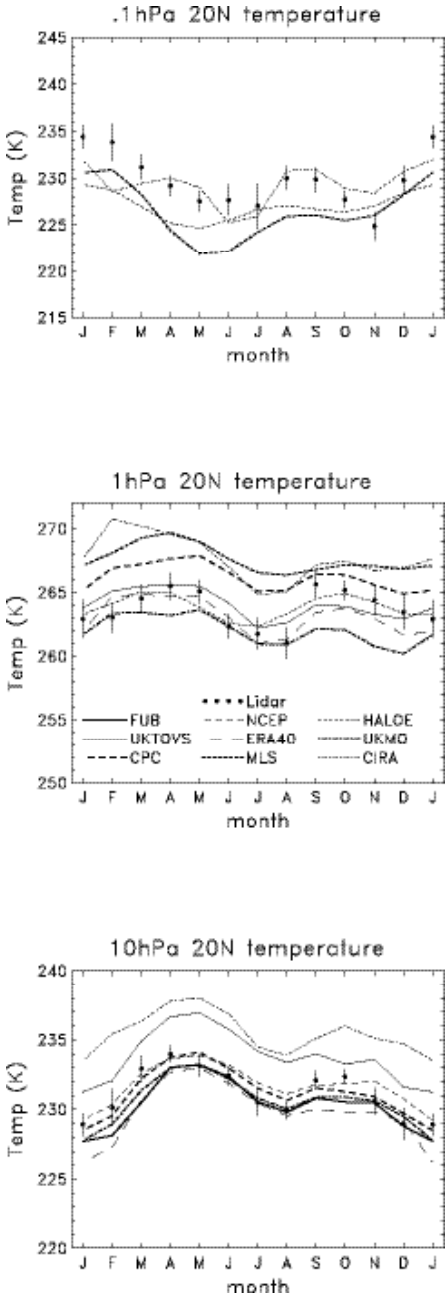

Figure 17. Comparison of the seasonal variation of lidar temperatures near 20°N with zonal mean analyses. Circles denote the lidar means, and error bars the plus/minus two standard errors.

Similar comparisons for measurements near 40°N (lidars from Table Mountain, OHP, Hohenpeissenberg and Toronto) are shown in Figure 18. The overall patterns are very similar to 20°N (Figure 17), with excellent agreement at 10 hPa (again with CIRA86 and UKTOVS as warm outliers). The lidars fall in the mid-range of analyses at 1 hPa, and exhibit reasonably good agreement at 0.1 hPa. We note that the overall good agreement between the lidars and satellite data at 0.1 hPa in Figures 17-18 is further evidence that the larger differences with rocketsondes in the mesosphere (Figures 13-16) are primarily due to the different time periods covered, given the knowledge of strong decadal-scale cooling near and above the stratopause (Ramaswamy *et al.*, 2001).

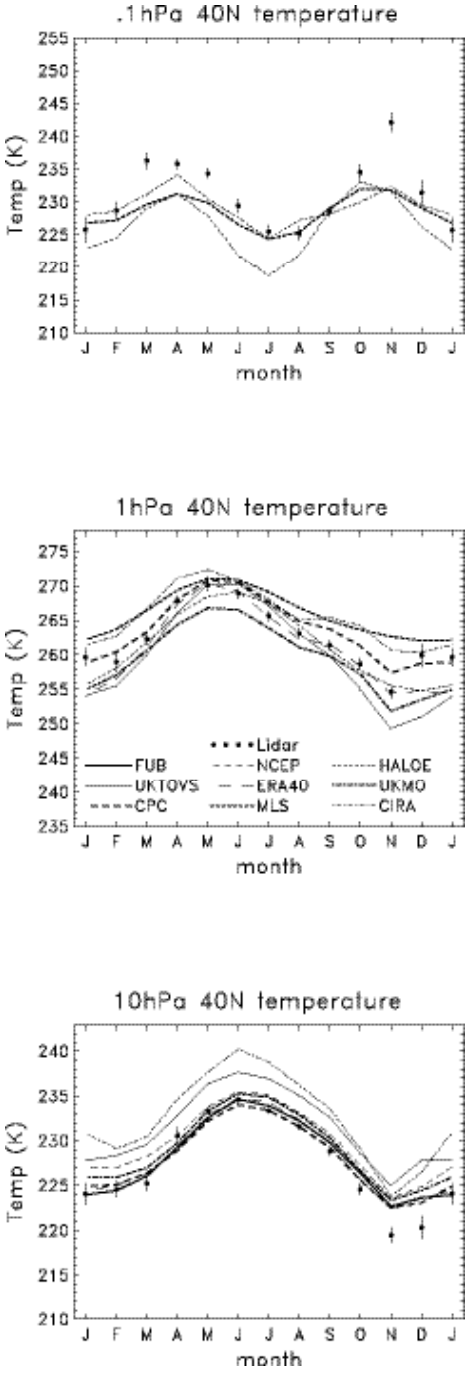

Figure 18. Seasonal cycle comparison of temperatures near 40°N between lidars and zonal mean analyses. Details are the same as in Figure 17.

Figure 19 compares the vertical profiles of temperature measured by lidar near 20°N and 40°N with zonal mean analyses, for NH winter (DJF) and summer (JJA) means, including profiles of the respective differences. Here we have simply averaged the monthly means, and use a sum of squares uncertainty for the lidar data. During DJF at 40°N all of the zonal mean analyses show cold biases with respect to the lidars over ~ 40-45 km; the cause is unknown, but could possibly be due to spatial sampling of the lidars (centred over Europe and North America) and the time-mean longitudinal structure during NH winter. A similar bias is not evident during NH summer at 40°N, or for any season at 20°N. Aside from this bias, there are relatively small differences (of order ± 3 K) between the lidar and analysis data sets; relative outliers are the ERA40 data (persistent cold biases maximizing over ~ 5-2 hPa), and CIRA86 (warm biases over most of the stratosphere).

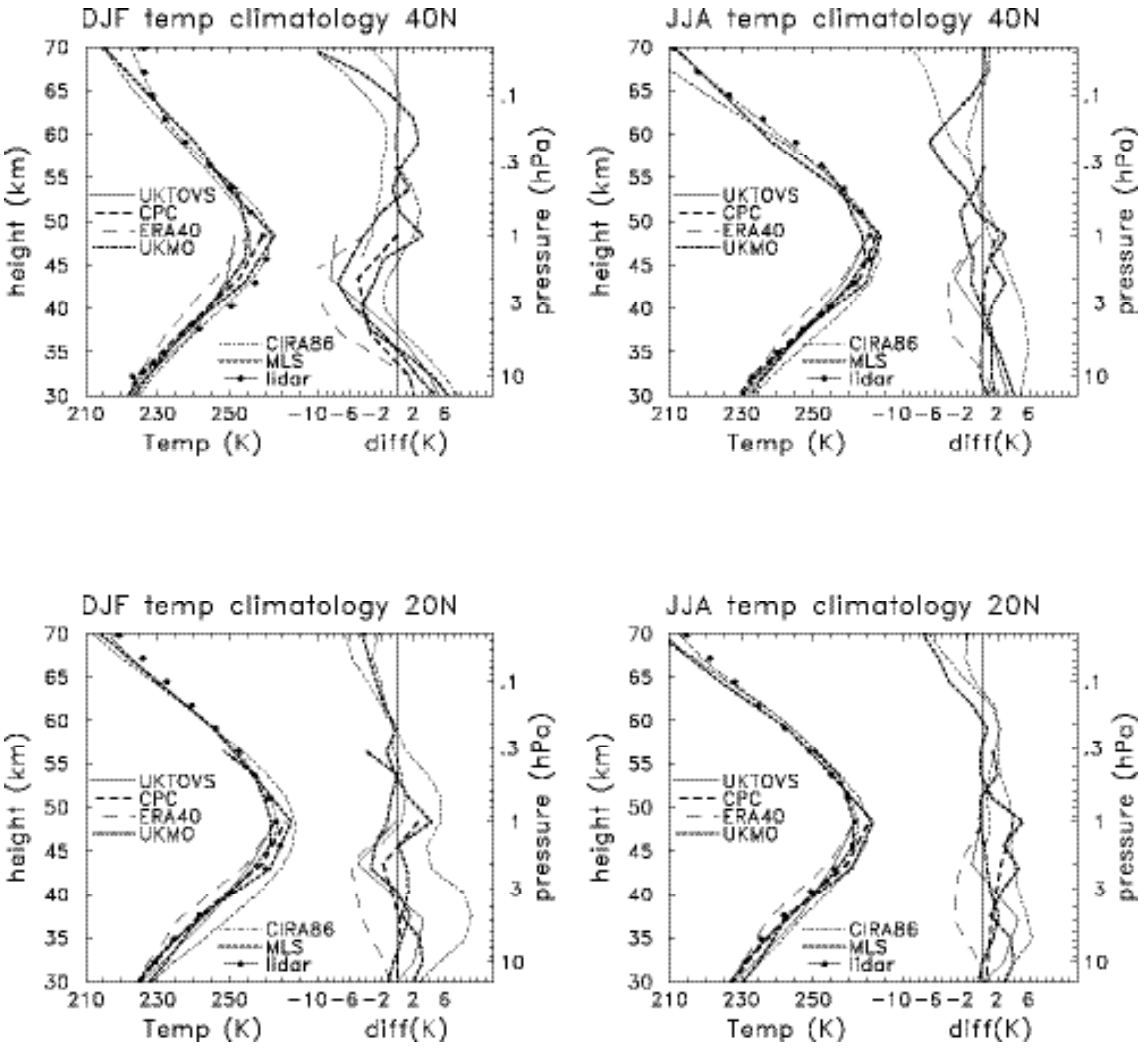

Figure 19. Comparisons of the vertical profile of temperature measured by lidar and zonal mean analyses, for data near 40°N (top) and 20°N (bottom). Statistics are shown for December-February (left panels) and June-August (right panels). Each panel shows the temperature profiles, plus differences from the lidar data.

Lidar data for the Arctic region are primarily available during winter, and a seasonal comparison is not possible. Figure 20 shows profile comparisons for 80°N for DJF, based on lidar data from Eureka, Ny Alesund and Thule. The lidars and analyses show good agreement up to the stratopause (with ERA40 still a cold outlier in the upper stratosphere), and the lidars are ~ 5-10 K colder than the MLS and CIRA86 data in the polar mesosphere.

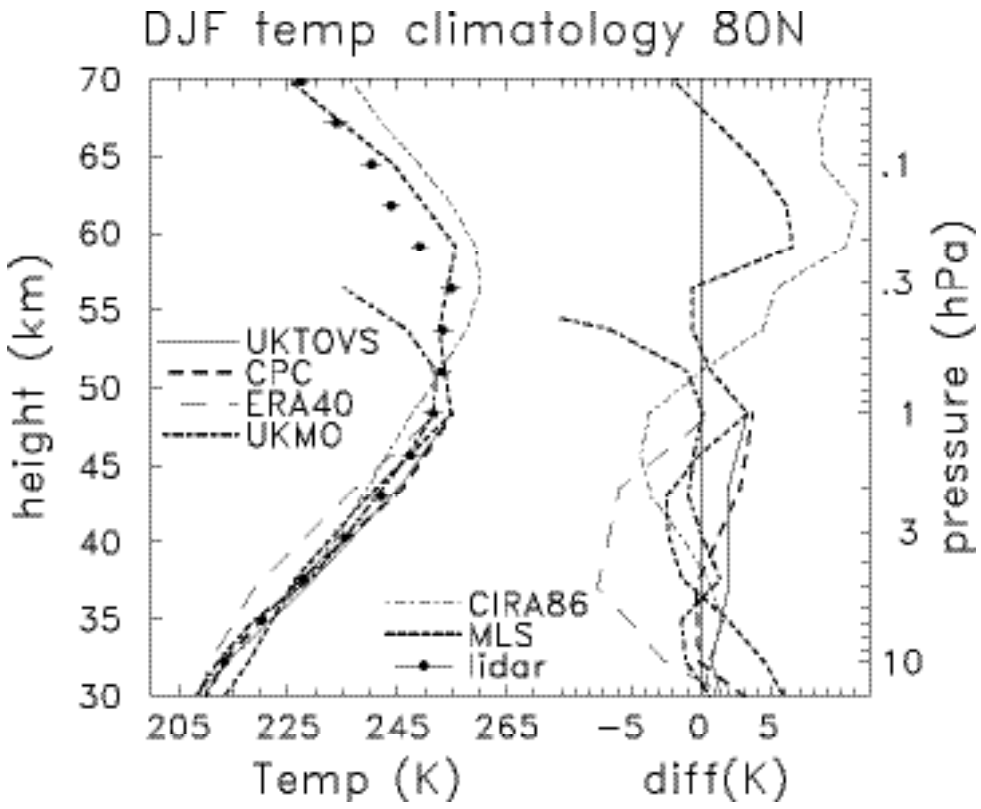

Figure 20. Comparison of the vertical profile of temperature near 80°N in January between lidar measurements and zonal mean analyses, for statistics during December-February.

2. Interannual variability in extratropics

Time series of monthly, zonal mean temperatures are compared here in order to quantify how well year-to-year variability is captured in the various data sets. The focus here is on the extratropical stratosphere during winter and spring (times of maximum variability). Interannual variability in the tropics is discussed separately below.

Figure 21 shows comparisons for February temperatures in the Arctic polar region at 80°N for 1979-1999. Overall there is excellent agreement in detail at 100 hPa, and good correspondence between the different data sets at 10 and 1 hPa (aside from the approximately constant biases discussed above). Similar results are found for other months (not shown). Thus estimates of interannual variability in the Arctic are for

practical purposes not dependent on data type. Figure 22 shows similar comparisons for the Antarctic (80°S) in October. Overall there is somewhat poorer agreement than for the analyses over the Arctic. At 100 hPa the CPC results show much less cooling during the 1990's than the other analyses. Note however that the 100 hPa CPC results are archived from operational NCEP tropospheric analyses, which are subject to continual analysis system improvements and changes; a similar plot at 50 hPa (where the stratospheric analyses are constant in time) does not highlight the CPC results as an outlier. Results at 10 hPa in Figure 22 show reasonable agreement, and the long records of CPC and UKTOVS data at 1 hPa have similar variability.

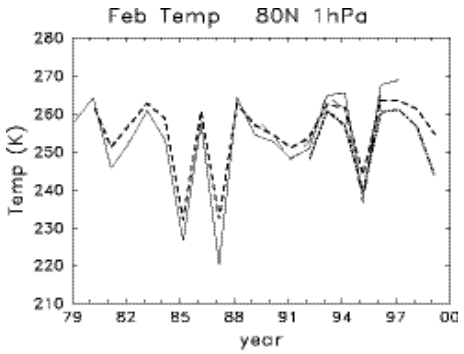

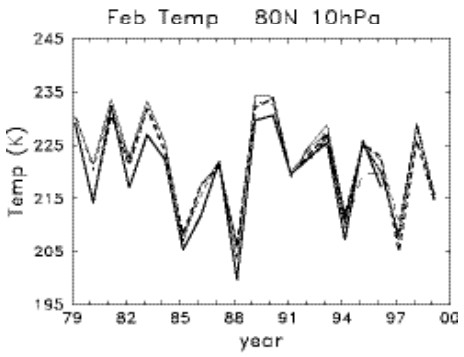

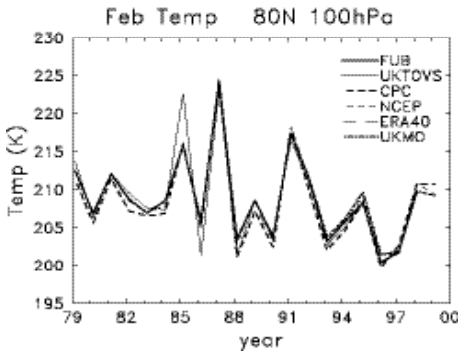

Figure 21. Time series of February average zonal mean temperatures at 80°N from each available data set, comparing interannual variability statistics. Results are shown for 1 hPa (top), 10 hPa (middle) and 100 hPa (bottom).

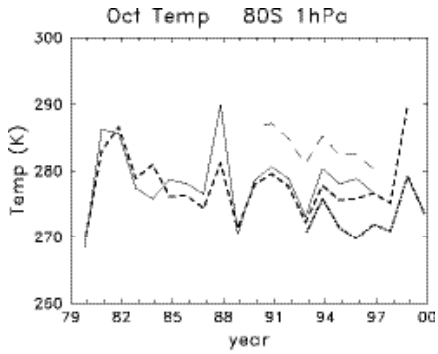

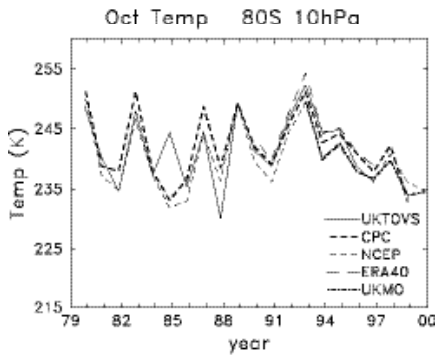

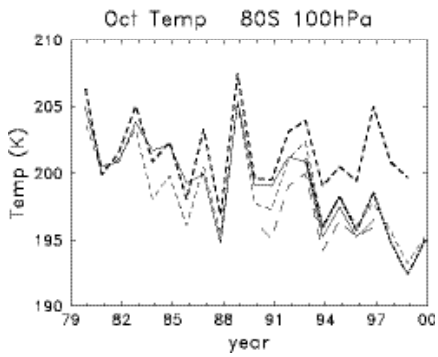

Figure 22. Interannual variability of zonal mean temperatures in the Antarctic (80°S) during October, from each available data set.

3. Longitudinal structure

Comparisons of the full 3-dimensional structures in the temperature climatologies show that differences are primarily a function of latitude, and accurately characterised by zonal means. However, zonal variations are evident in some difference fields, likely related to data availability and analyses, and a few examples are shown here. Figure 23 shows the climatological January NH 10 hPa temperature from UKMO, together with difference fields for CPC and FUB data. The differences with CPC data are positive and linked to the cold polar vortex (i.e., the coldest temperatures are analysed warmer in CPC results). Similar difference patterns tied to vortex structure are found in Southern Hemisphere spring statistics (not shown). In contrast, differences with FUB temperatures in Figure 23 are primarily negative and not as obviously tied to the vortex, but rather they are largest over the North American and European-Asian land masses (where the majority of radiosonde data are available).

4. Tropical seasonal cycle in temperature

The tropics present special problems for analysis of stratospheric temperatures and winds. The tropical tropopause temperature minimum has a sharp vertical structure that is not well resolved by satellite measurements, and it is also problematic for assimilation/forecast models with vertical resolution of ~ 2 km. Temperature anomalies associated with the quasi-biennial oscillation (QBO) have relatively shallow vertical structures, which are also poorly resolved by nadir-viewing operational satellites. Thus it is not surprising to find a wide variance between climatological data sets in the tropics. Here we compare each data set for seasonal variation and interannual variability (the latter focusing on the QBO). The analyses here complement the tropical data comparisons shown in Pawson and Fiorino (1998a, b).

The seasonal variations of equatorial temperature at 100, 50 and 30 hPa derived from each climatological data set are shown in Figure 24. Included in these figures are estimates of monthly temperatures derived for the same 1992-1997 time period from radiosonde measurements at a group of eight near-equatorial stations (within 5° of the equator, including Belem, Bogota, Cayenne, Manaus, Nairobi, Seychelles, Singapore and Tarawa). The radiosonde statistics in Figure 24 include both the means and standard errors calculated from this eight-station group. The amplitude of the seasonal cycle in temperature is reasonably well captured in most data sets at 100 hPa, but there are clear biases among the data sets. In particular, the ERA15, ERA40 and FUB data are the coldest and agree best with radiosondes (except for FUB during January-March), whereas UKMO, CPC, NCEP and CIRA86 data each have a consistent warm bias of ~ 2-3 K (and UKTOVS is almost 10 K too warm, and not shown in Figure 24). At 50 and 30 hPa the seasonal variations are smaller than at 100 hPa, and approximately captured in most analyses (aside from CIRA86 and FUB data at 30 hPa). At 50 hPa the CPC, NCEP and ERA40 data agree best with radiosondes, with FUB ~ 2 K warmer during NH winter. The UKMO analyses appear warm at 50 hPa, but the comparison is not exact since the UKMO pressure level is 46.4 hPa. Likewise, the ERA15 time period is different (1992-1993 versus 1992-1997), and the 1992-1993 period was anomalously

warm in the tropics due to Pinatubo volcanic effects. The CIRA86 and UKTOVS (not shown) are warm outliers at 50 hPa. At 30 hPa most analyses are close to uncertainty estimates of the radiosondes, with FUB and CIRA86 being warm outliers in some months.

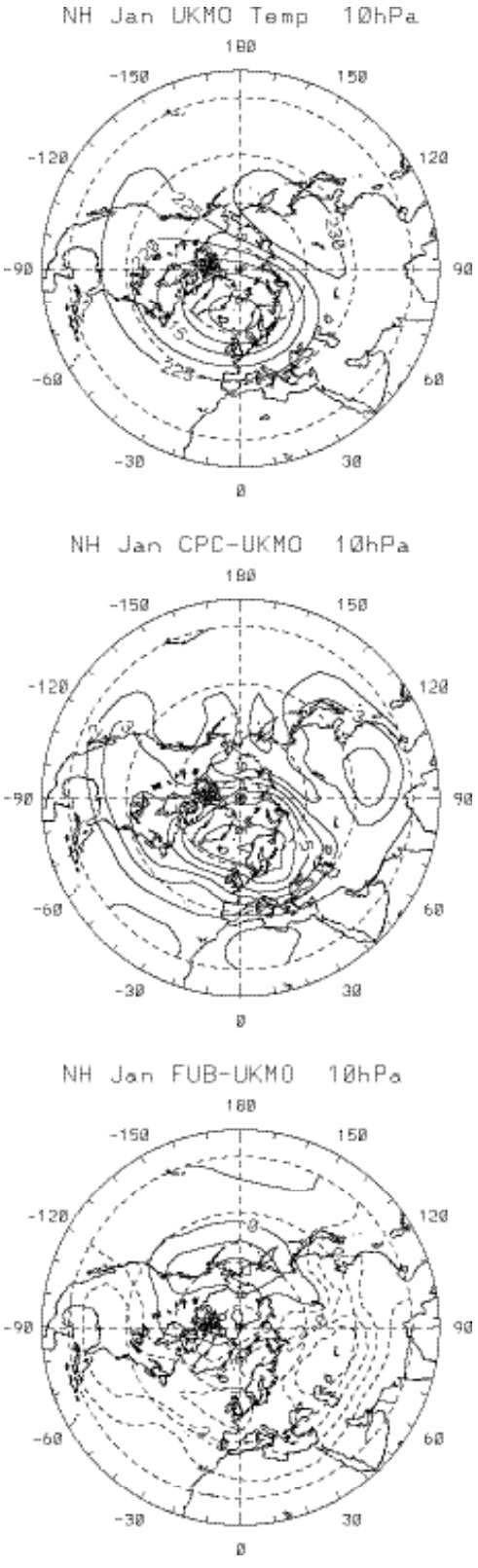

Figure 23. Top panel shows climatological January average 10 hPa temperatures from UKMO analyses. Middle panel shows the differences with CPC analyses (CPC-UKMO), and lower panel differences with FUB (FUB-UKMO). Contour interval in the lower panels is 1 K.

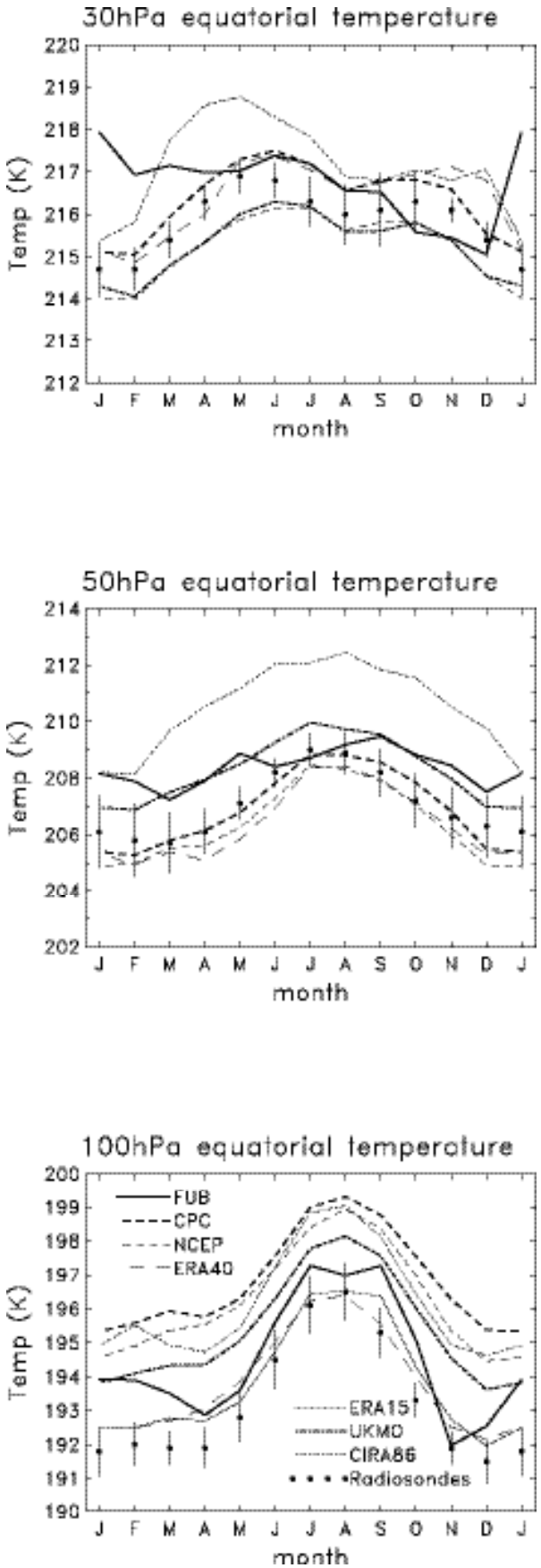

Figure 24. Comparison of the seasonal variation in equatorial temperature from available analyses at 30 hPa (top), 50 hPa (middle) and 100 hPa (bottom). Because of relatively large biases, UKTOVS data are not included here. The circles show a climatology derived from radiosonde measurements at 8 near-equatorial stations (over 5°N-5°S), and the error bars denote the plus/minus two standard errors within the station group.

Figure 25 shows similar statistics for temperature variations at 10, 1, 0.1 and 0.01 hPa, where at each level the dominant variation is a semi-annual oscillation (SAO). There is approximate agreement in the amplitude and phase of the SAO at 10 hPa across many data sets, but biases on the order of 5 K between the different analyses. Similar mean biases are seen at 1 hPa, along with larger differences in SAO amplitude and phase (quantified below). The 0.1 hPa temperatures show quite good agreement between CIRA86, MLS and HALOE, whereas at 0.01 hPa (~ 80 km) there are substantial differences in detail between these three data sets.

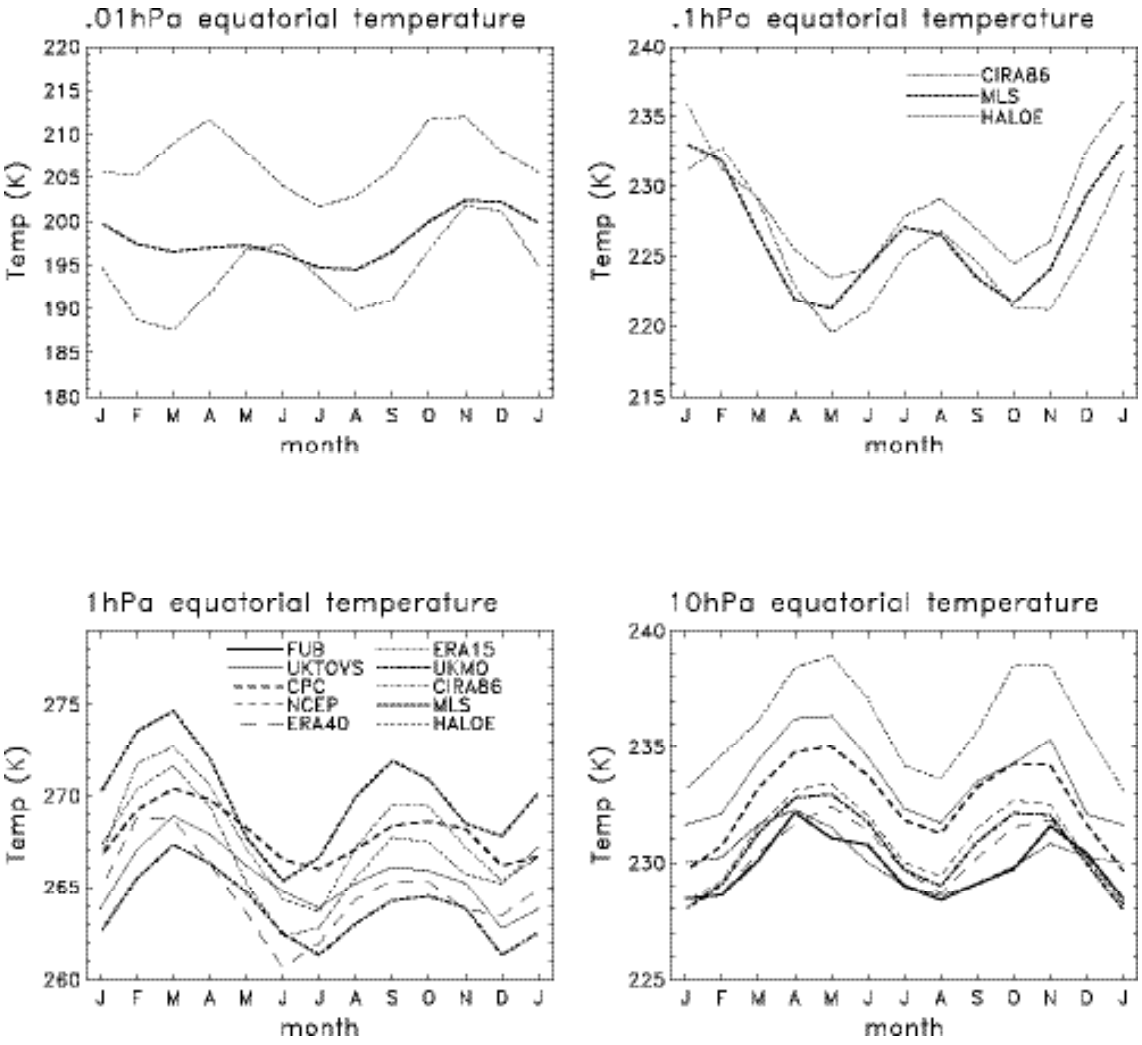

Figure 25. Seasonal variation of equatorial temperature from different analyses, showing results for 0.01 hPa, 0.10 hPa, 1 hPa and 10 hPa.

a. Tropical rocketsondes

Rocketsonde comparisons in the tropics are available near 10°N and 10°S; the temperature comparisons are similar at both latitudes, and we focus here on results near 10°N. Figure 26 shows the 10°N rocketsonde climatology and analysis temperatures at

10, 1 and 0.1 hPa. The SAO amplitude and phase evident in rocketsonde data at 10 and 1 hPa is reasonably consistent with the various analyses, although note that observations near 10°N do not capture the full SAO amplitude at the equator (as shown below in Figure 28). At 0.1 hPa the rocketsondes show a less coherent SAO than that inferred from the CIRA86, MLS and HALOE data, and furthermore the rocketsondes are approximately 10 K warmer.

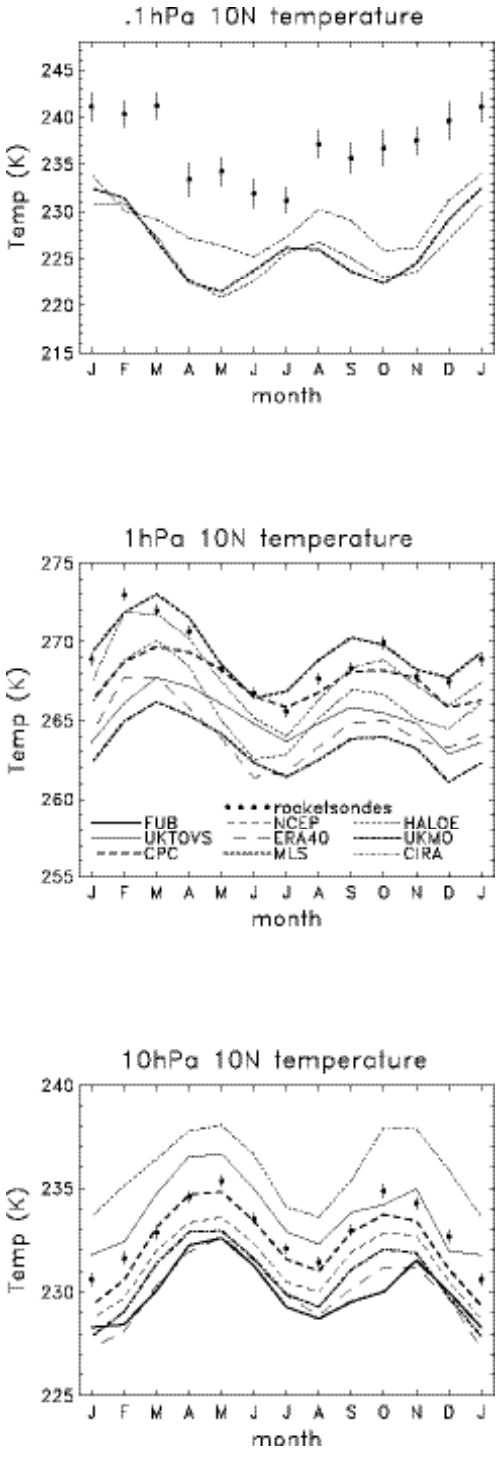

Figure 26. Comparison of the seasonal cycle of temperatures near 10°N between rocketsondes and zonal mean analyses, at 0.1 hPa (top), 1 hPa (middle), and 10 hPa (bottom).

b. Semi-annual oscillation (SAO)

Because the SAO dominates the seasonal variation in equatorial temperatures, it is useful to quantify the SAO amplitude and phase structures derived from the different data sets analysed here. A more comprehensive review and climatology of the SAO (extending to 100 km) is provided in Garcia *et al*. (1997). The results here are based on simple harmonic analyses of the different data sets for the time periods available.

The vertical structure of the temperature SAO amplitude and phase are shown in Figure 27, including results from each data set. As well-known from previous analyses (e.g., Hirota, 1980), the temperature SAO has a double peaked structure in altitude, with maxima below the stratopause (~ 45 km) and mesopause (~ 70 km), and these maxima are approximately 180 degrees out of phase. The maximum near 45 km has an amplitude of ~ 4 K in MLS, HALOE, CIRA86 and ERA40 data sets, and substantially weaker amplitude in CPC, UKMO and UKTOVS data. For the maximum near 70 km the CIRA86, MLS and HALOE show a range of amplitudes of ~ 4-7 K. For further comparison of the upper level peak, the dots in Figure 27 show results derived from Solar Mesosphere Explorer (SME) temperature data for 1982-1986 (taken from Garcia and Clancy, 1990). These SME results show similar amplitude and phases as the other data sets, but don't exhibit an absolute peak near 70 km.

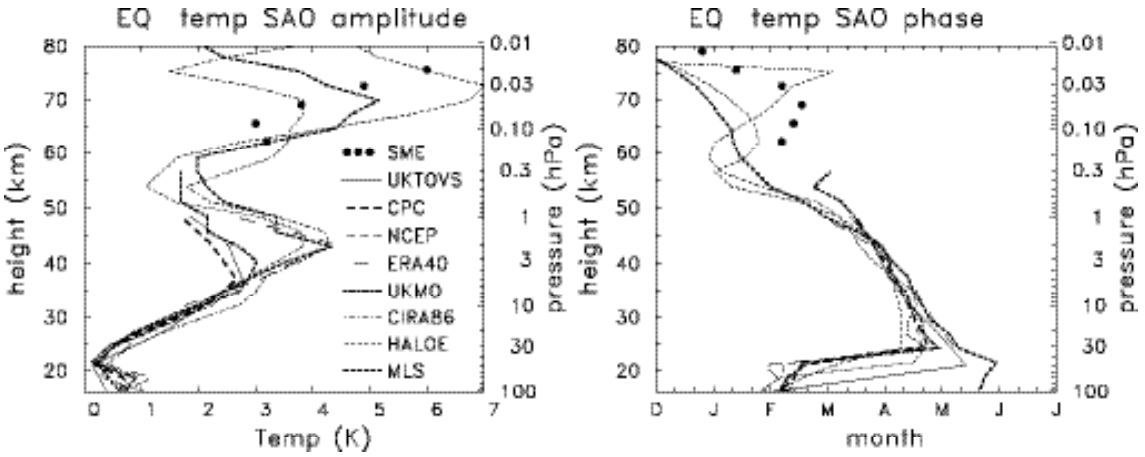

Figure 27. Comparison of the amplitude (left) and phase (right) of the semi-annual oscillation (SAO) in equatorial temperature derived from each temperature data set. Phase refers to month of the first maximum during the calendar year. The dots show the mesospheric results derived from SME satellite data, taken from Garcia and Clancy (1990).

Figure 28 compares the amplitude and phase structure of the temperature SAO as a function of latitude at 2 hPa and 0.046 hPa (near the amplitude maxima seen in Figure 27). The different data sets at 2 hPa show a clear separation in terms of SAO amplitude, with the ERA40, MLS, HALOE and CIRA86 data having amplitudes near 4 K, approximately twice as large as the CPC, UKMO and UKTOVS results. The rocketsonde results (shown as dots near 8°N and 8°S) show amplitudes that agree better with values from the former (larger amplitude) group. Phases at 2 hPa are in good

agreement between all data sets (maximum near April 1). Comparisons at 0.046 hPa show less agreement in amplitude between the few data sets. The HALOE and MLS data both show an equatorial maximum (5-7 K), which is not evident in CIRA86. Rocketsondes have weaker SAO amplitudes than the other data sets at this high altitude.

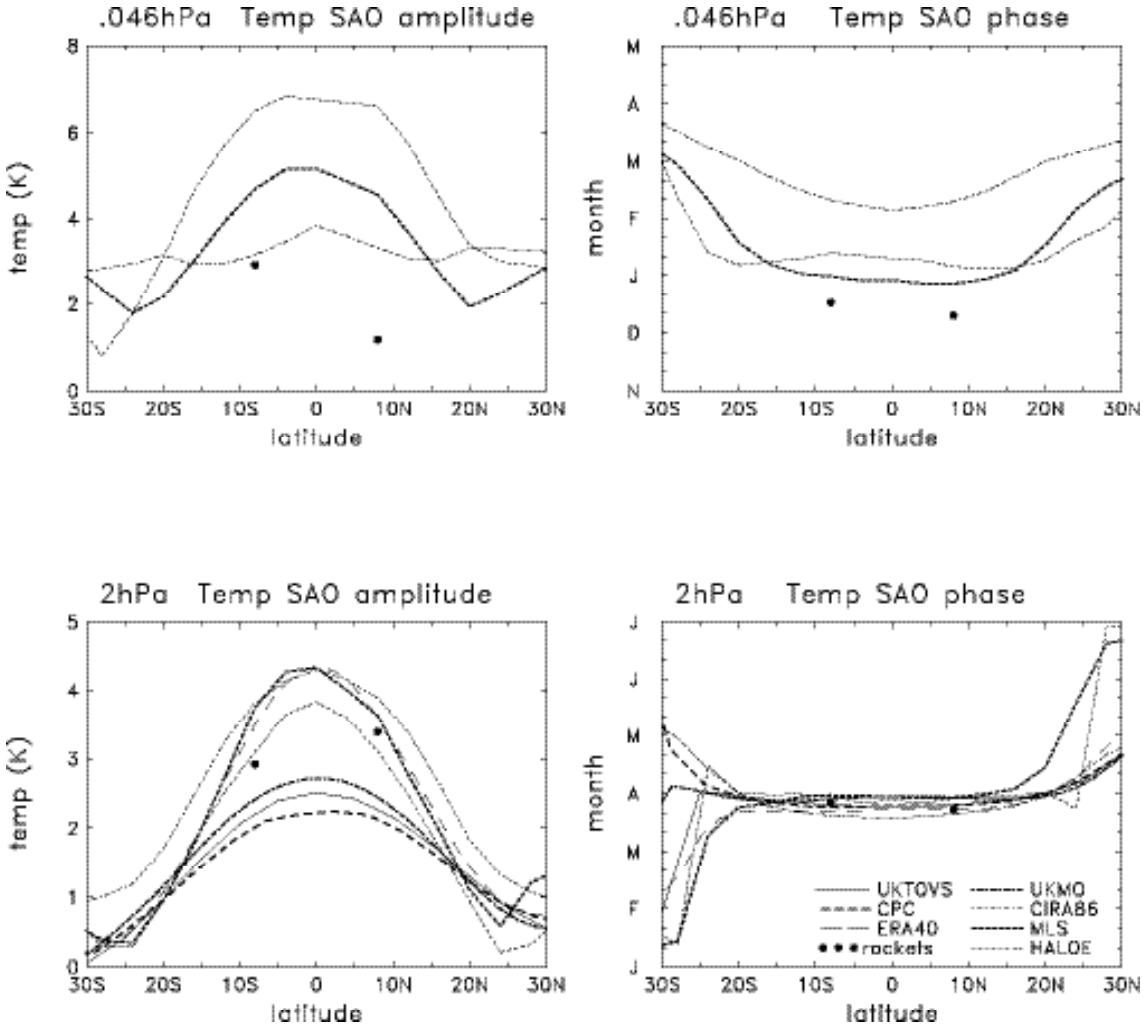

Figure 28. Latitudinal structure of the amplitude (left) and phase (right) of the temperature SAO derived from each data set, for results at 0.046 hPa (~ 70 km) and 2 hPa (~ 44 km). The dots show the corresponding values derived from rocketsonde data near 8°S and 8°N.

5. Tropical temperature interannual variability

Interannual anomalies in 100 and 70 hPa equatorial temperature for the period 1985-1999 are shown in Figure 29, with anomalies calculated as differences from the 1992-1997 mean seasonal cycles shown above. The size of the variations at 100 hPa are small (~ ± 1-2 K), and there are substantial differences among the different data sets regarding the details of these small changes. At 70 hPa (where FUB and UKTOVS are not

available) the interannual temperature changes are ~ ± 2-3 K, larger than those at 100 hPa, and there is overall good agreement among the different data sets (with the latter half of the 1990's being relatively cold).

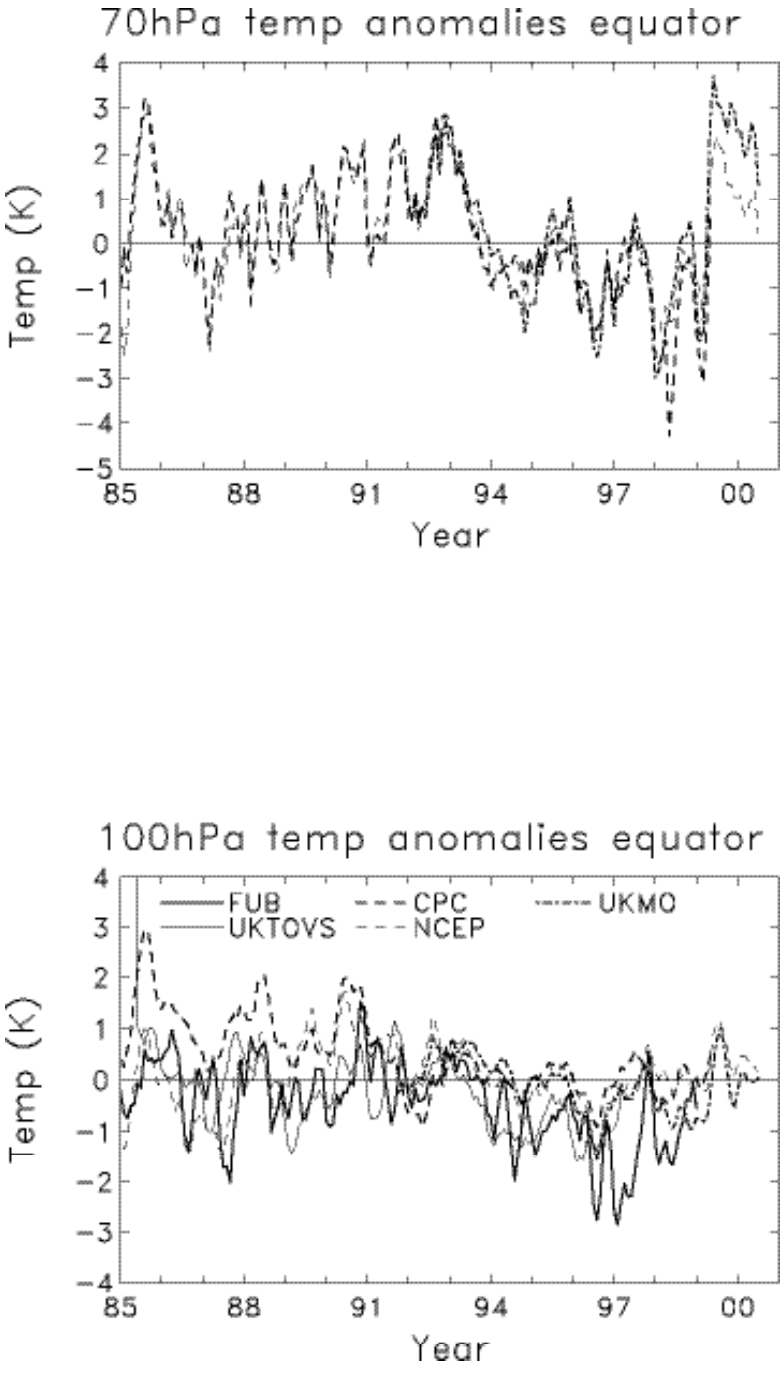

Figure 29. Time series of interannual anomalies in zonal mean temperature at the equator derived from available analyses at 70 hPa (top) and 100 hPa (bottom). Anomalies are defined as differences from the 1992-1997 time average.

Interannual temperature changes at 50, 30 and 10 hPa are shown in Figure 30. Variability at these levels is dominated by the QBO, and while a QBO is evident in each data set, the amplitude varies considerably. For comparison, we include in the 50 and 30 hPa plots in Figure 30 temperature anomalies derived from radiosonde measurements at Singapore (1°N). These comparisons suggest the QBO temperature anomalies are most accurately captured in FUB analyses, and underestimated in each of the other data sets to some degree. Negative temperature anomalies (easterly shear) are particularly poorly sampled. The interannual anomalies at 10 hPa show a clear QBO signal in the FUB analyses after 1991; the QBO is evident but much weaker in the other data sets. Prior to 1990 there are large differences among anomalies derived from the five available data sets (note the FUB 10 hPa temperatures are only available during winter months prior to 1992).

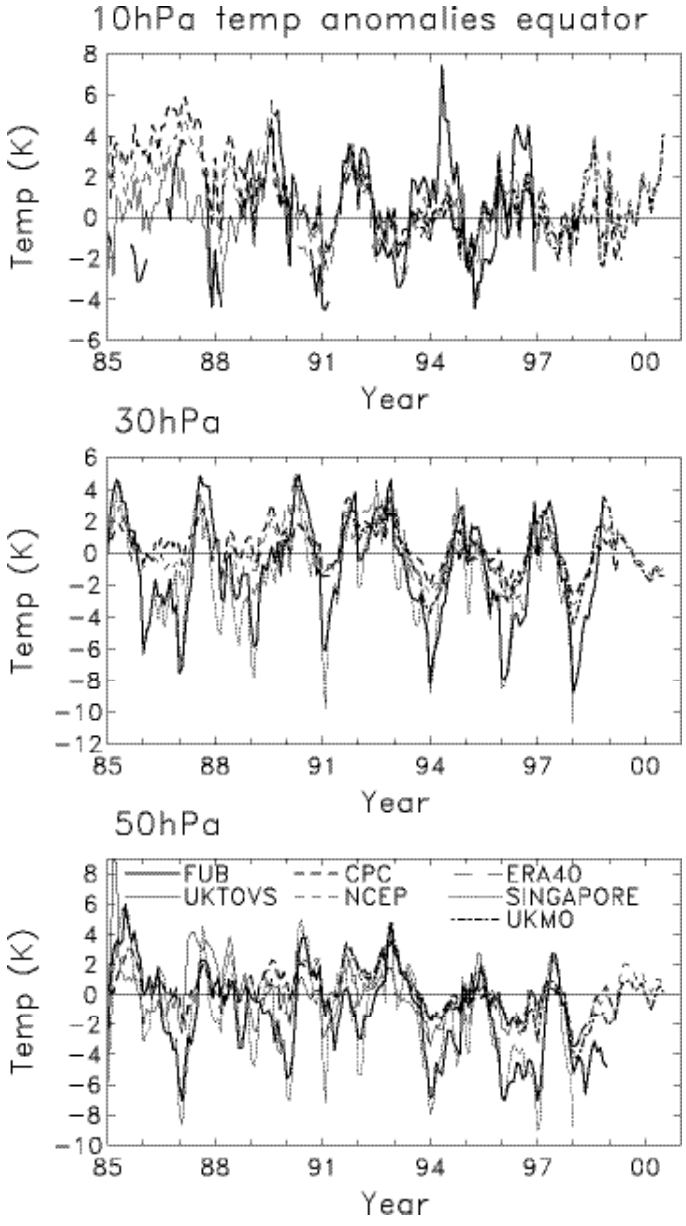

Figure 30. Time series of interannual anomalies in zonal mean temperature at the equator from various analyses, together with results from radiosonde measurements at Singapore (1°N). Statistics are shown for 10 hPa (top), 30 hPa (middle) and 50 hPa (bottom).

The strength of the QBO temperature variation in the different data sets is quantified in Figure 31, where the equivalent "QBO amplitude" is plotted as a function of latitude (at 30 hPa) and height. The QBO amplitude is defined as $\sqrt{2}$ times the rms deviation of deseasonalised anomalies during 1992-1997; this is the equivalent amplitude of a harmonic oscillation, following Dunkerton and Delisi (1985). For comparison, Figure 31 also includes the equivalent result derived from Singapore radiosonde measurements at 50 and 30 hPa. The FUB analyses exhibit the largest QBO signal in temperature, peaking above 4 K at 30 hPa. The next best results are derived from the assimilated data sets (ERA40, ERA15, UKMO and NCEP, in that order), although each underestimates the amplitude to some degree, especially the UKMO and NCEP data. The CPC and UKTOVS data sets provide relatively poor estimates of the temperature QBO.

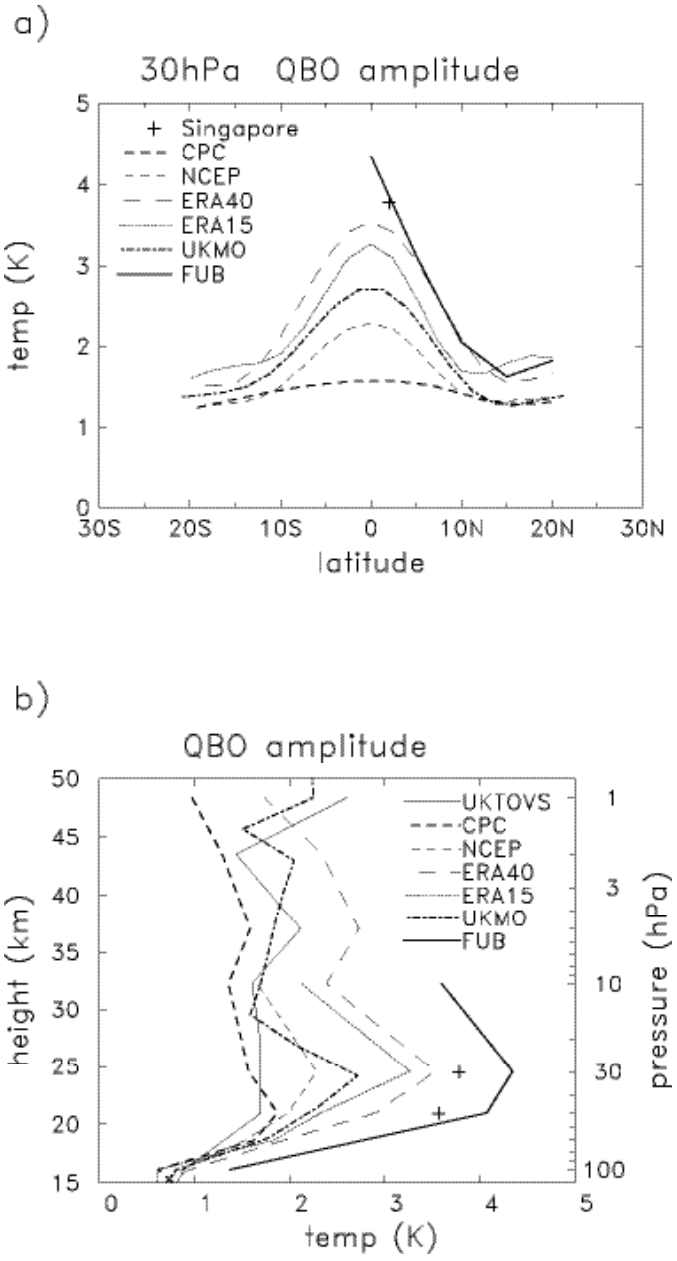

Figure 31.

(a) Latitudinal structure of the equivalent QBO amplitude in temperature at 30 hPa, defined as $\sqrt{2}$ times the rms anomaly values during 1992-1997 (see text).

(b) Shows the vertical structure of the QBO temperature amplitude at the equator. For comparison, plus signs show results derived from Singapore radiosonde data.

Interannual temperature anomalies at 1 hPa are shown in Figure 32, derived from UKMO, CPC and UKTOVS data. The only records extending prior to 1990 are the CPC and UKTOVS analyses, and these show differences of 2-3 K for the pre-1990 period (and hence substantial differences in decadal trends). A separate data set included in Figure 32 shows brightness temperature (radiance) anomalies for 1979-1998 derived from the series of Stratospheric Sounding Unit (SSU) measurements (which are part of the TOVS data that go into the CPC and UKTOVS analyses). The SSU data set in Figure 32 used overlap periods between the different satellite instruments to make adjustments, in an effort to produce a homogeneous long-term data set (see Ramaswamy *et al.*, 2001). The SSU channel 27 data in Figure 32 are representative of a thick layer of the upper stratosphere, spanning approximately 34-52 km, with a peak near 44 km (between 1-2 hPa in pressure), and thus comparisons with the 1 hPa analyses are not exact. Nonetheless, the SSU time series suggests that interannual variations in the CPC temperatures at 1 hPa may have uncorrected biases which influence estimates of long term variability (such as decadal trends or 11-year solar cycle changes); somewhat better overall agreement is seen between SSU and UKTOVS results. The UKMO analyses in Figure 30 show cold anomalies after 1997, which are related to an erroneous ozone climatology in the assimilation model during this time (error introduced on 28 January 1998).

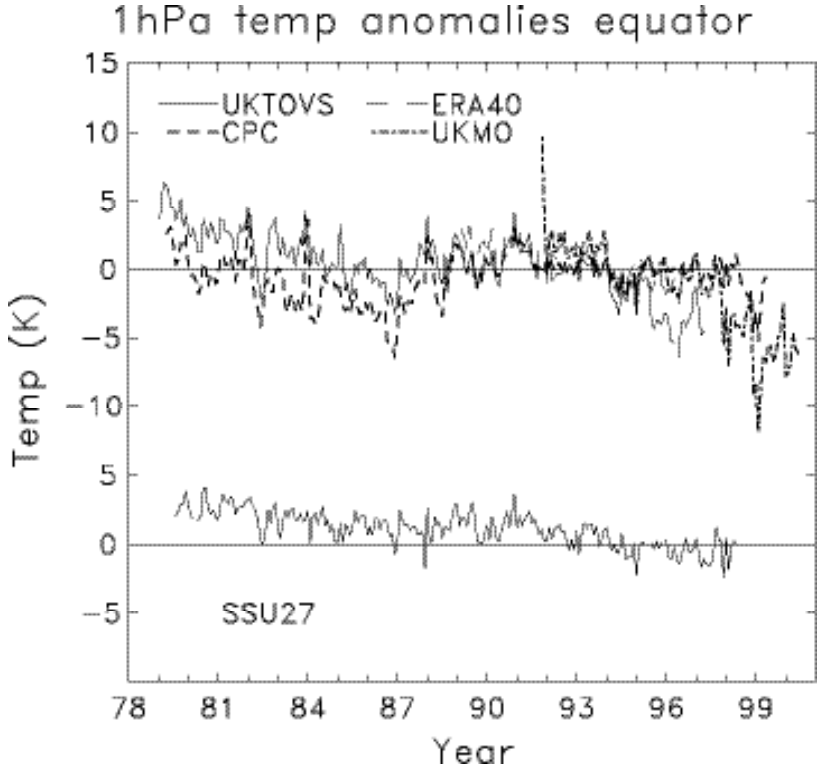

Figure 32. Interannual anomalies in zonal mean temperature at 1 hPa from available data sets (top), together with similar results derived from SSU satellite measurements (bottom). The SSU data represent temperatures over a ~15 km thick layer centered near 1-2 hPa.

6. Temperatures for pre-1979 data

The FUB and NCEP reanalysis data sets have stratospheric temperatures (up to 10 hPa) for the pre-1979 period, i.e., prior to the availability of satellite data. The inclusion of satellite temperatures in the NCEP reanalysis has a significant impact on regions with relatively little radiosonde data (Mo *et al.*, 1995). As an example, Figure 33a shows time series of 100 hPa equatorial temperature from the NCEP reanalysis, showing a clear discontinuity of approximately 3 K prior to and after 1979, coincident with the inclusion of satellite temperatures. The spatial structure of this temperature discontinuity in NCEP reanalyses is shown in Figure 33b, comparing 15-year averages before and after 1979. The largest differences are observed in the tropics and SH middle and high latitudes (regions of few radiosondes); altitudes near the tropopause are warmer with the inclusion of satellite data, while the region of 30-50 hPa is cooler. Corresponding stratospheric zonal wind discontinuities of ± 2-4 m/s are found in the tropics and SH midlatitude and polar regions (not shown here). Extreme caution should be used in analysing long-term variability of NCEP data in these regions.

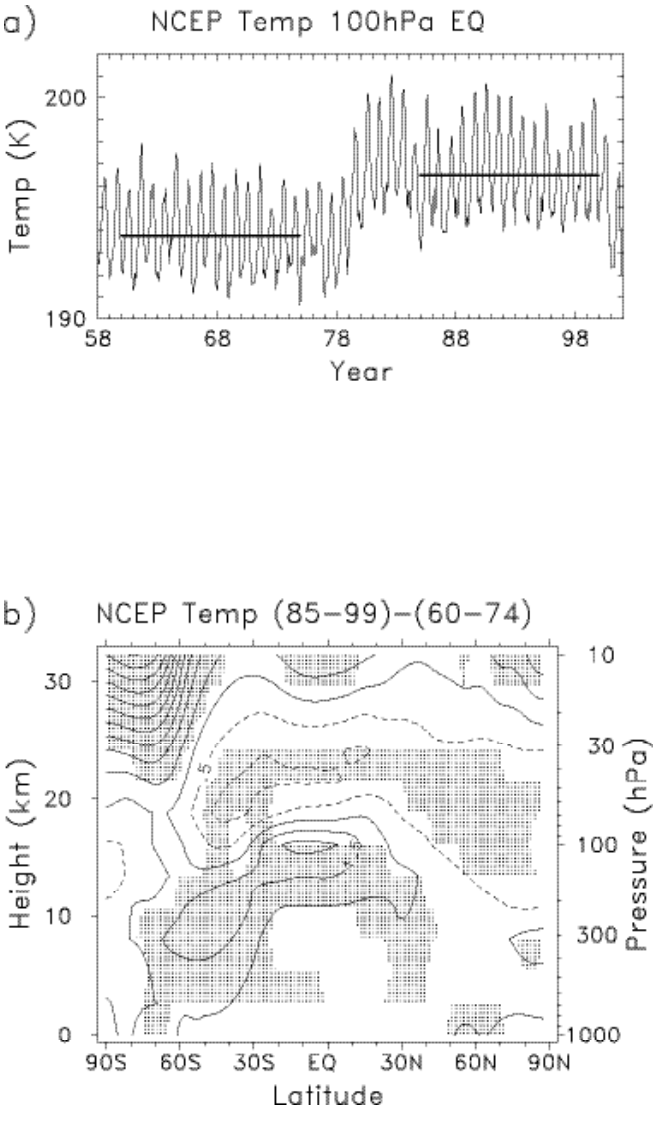

Figure 33.

a) Top panel shows time series of zonal mean equatorial temperature at 100 hPa from the NCEP reanalyses over 1957-2001. Heavy lines denote the time averages for 1960-1974 and 1985-1999. Note the jump in temperatures near 1979, associated with the introduction of satellite data into the reanalyses.

b) Bottom panel shows a cross section of temperature differences between 15-year means before (1960-1974) and after (1985-1999) the satellite discontinuity. Contours are ± 0.5, 1.5, 2.5, ... K, and shading shows statistically significant differences.

Differences between NCEP and FUB temperature analyses over the NH are shown in Figure 34, comparing 5-year periods before (1974-1978) and after (1993-1997) the satellite changes in NCEP data (presumably the FUB data are more homogeneous). Significant differences between the two time periods are found in the tropics at 100 hPa, where the NCEP reanalyses are colder than FUB for 1974-1978, but warmer for 1993-1997. The artificial warming in NCEP data between these periods is consistent with the results in Figure 33. Figure 34 also shows systematic differences in 30 hPa temperature over the entire hemisphere (with NCEP warmer for the satellite period), but the differences are relatively small (~ 1 K). The comparisons in Figure 34 suggest temperatures in other regions are less sensitive to the satellite discontinuity.

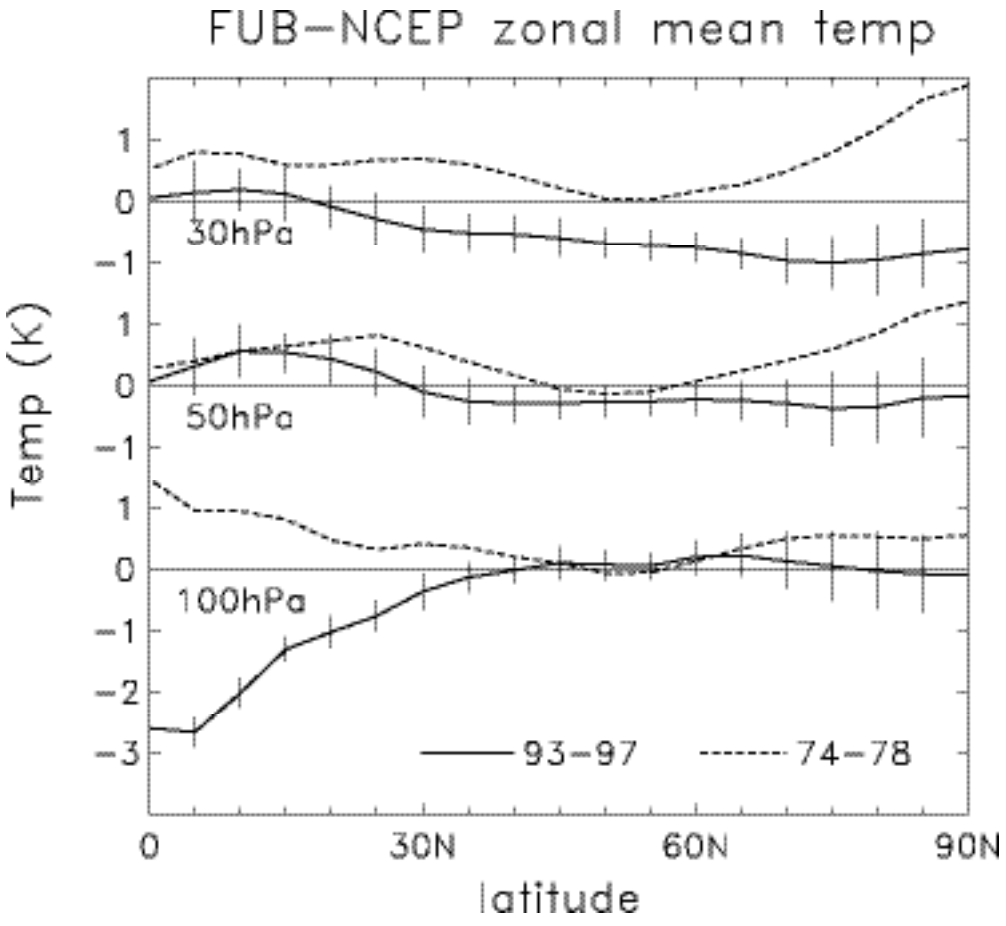

Figure 34. Differences between FUB and NCEP annual average zonal mean temperatures at 30, 50, and 100 hPa, comparing the pre-satellite (1974-1978) and post-satellite (1993-1997) time periods. Error bars show the ± 2-sigma variability values associated 5-year means (just included on the 1993-1997 results for clarity).

B. Zonal mean zonal winds

1. Zonal mean climatology

The January zonal mean zonal wind climatology (for 1992-1997) from UKMO data is shown in Figure 35, together with differences from the other climatological data sets. In general there are relatively large differences in the tropics, related to the uncertainties in deriving balanced winds in low latitudes from temperature (height) data. Detailed comparison of tropical winds are discussed separately below. The difference patterns in NH extratropics show a consistent pattern of positive values near 60°N for each contemporaneous data set (CPC, UKTOVS, NCEP and ERA40), indicating a slightly weaker polar night jet in UKMO data. More complicated global patterns are seen in the CIRA86 differences. Figure 36 shows UKMO climatology and differences with CPC and ERA40 winds for July and October. In July there are relatively small differences (outside of the tropics), and the strength of the intense SH polar jet is similar in each analysis. During October the UKMO SH polar jet is somewhat stronger than the CPC and ERA40 jets. Note these October wind differences are consistent (via thermal wind) with the colder Antarctic polar vortex analyzed in UKMO data (see Figures 3-4).

Figure 37 compares January and July zonal wind climatologies from each data set at 100, 10 and 1 hPa. Outside of the tropics there is reasonable agreement between most analyses, with the CIRA86 climatology showing some biases in detailed structure. The westerly jets are strongest in UKTOVS data.

a. Comparison to rocketsondes

Rocketsondes provide direct measurements of zonal winds, and are unique for comparing to winds derived from analyses (given the caveat of differing time periods). Seasonal climatologies of zonal winds derived from rocketsondes are compared with the various analyses at 30°N and 60°N in Figure 38, for pressure levels 10, 1 and 0.1 hPa. At 30°N there is quite good agreement in the winds at all levels; note especially the strong subtropical mesospheric jet (at 0.1 hPa) in rocketsondes, CIRA86 and URAP data. At 60°N there are some systematic differences with rocketsondes during local winter (November-March) at 10 hPa, with the rocketsonde winds substantially weaker. Given the overall good agreement at other times and locations in Figure 38, these differences may be related to real (decadal-scale) time changes. Note these wind changes are consistent (via thermal wind balance) with observed cooling of the polar lower stratosphere (discussed above).

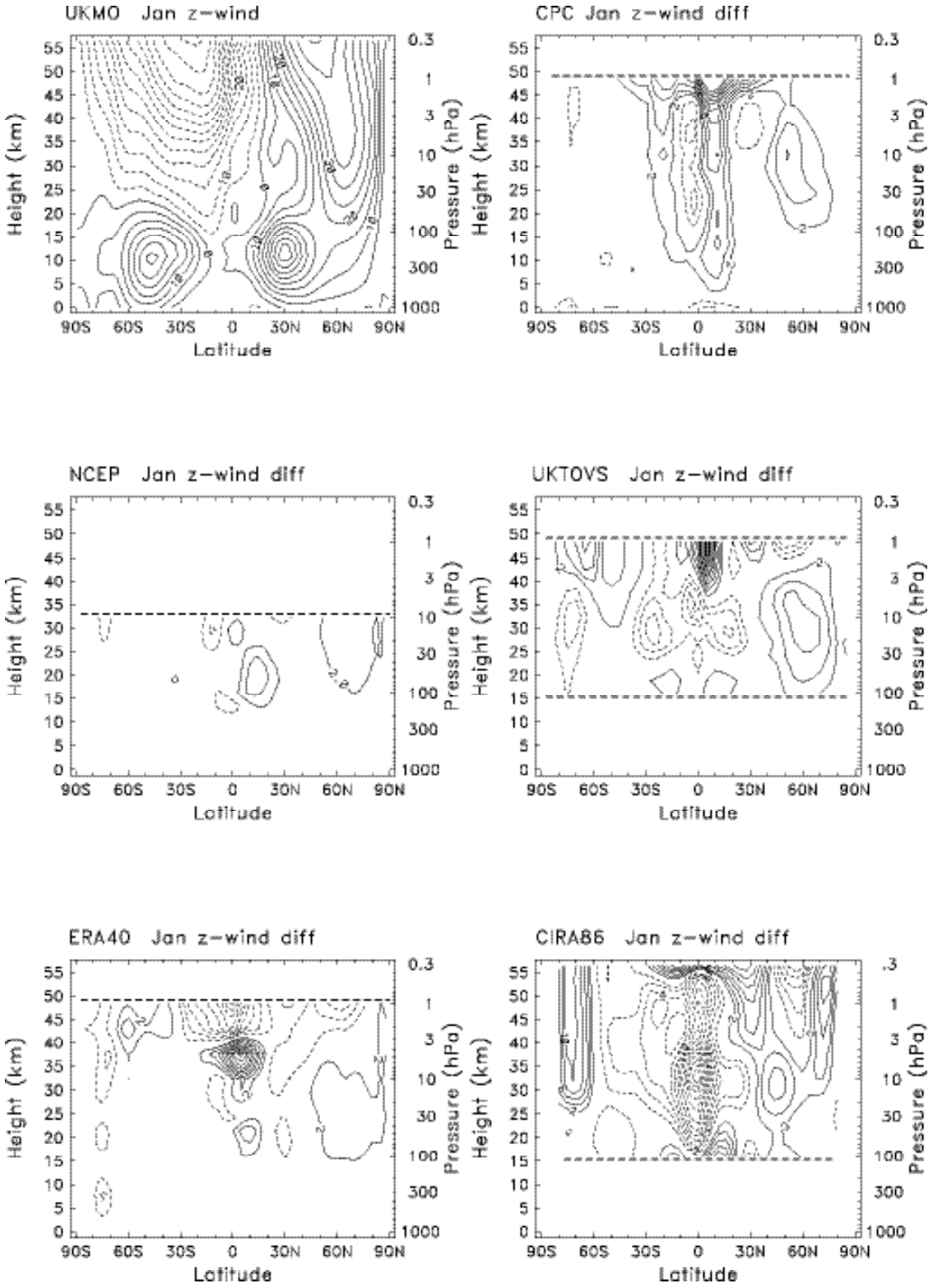

Figure 35. Top left panel shows climatological January average zonal mean wind (m/s) from UKMO analyses. Other panels show the respective differences between each data set and UKMO (i.e., CPC-UKMO), with contours of ± 2, 4, 6, ... m/s (zero contours omitted).

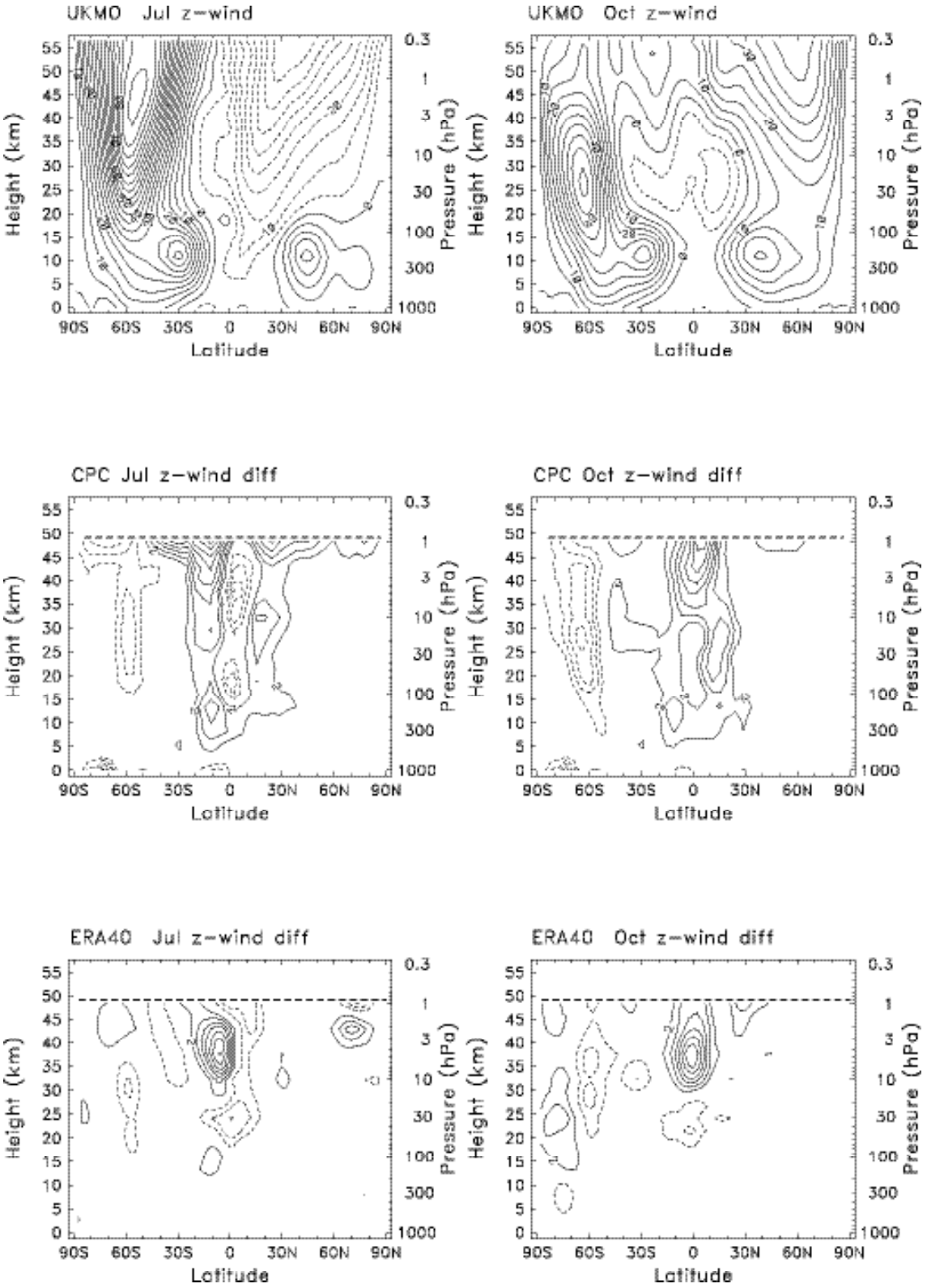

Figure 36. Top panels show climatological zonal mean zonal wind (m/s) from UKMO analyses in July (left) and October (right). Middle and lower panels show the respective differences in CPC and ERA40 reanalyses (i.e., ERA40-UKMO), with contours of ± 2, 4, 6 ... m/s.

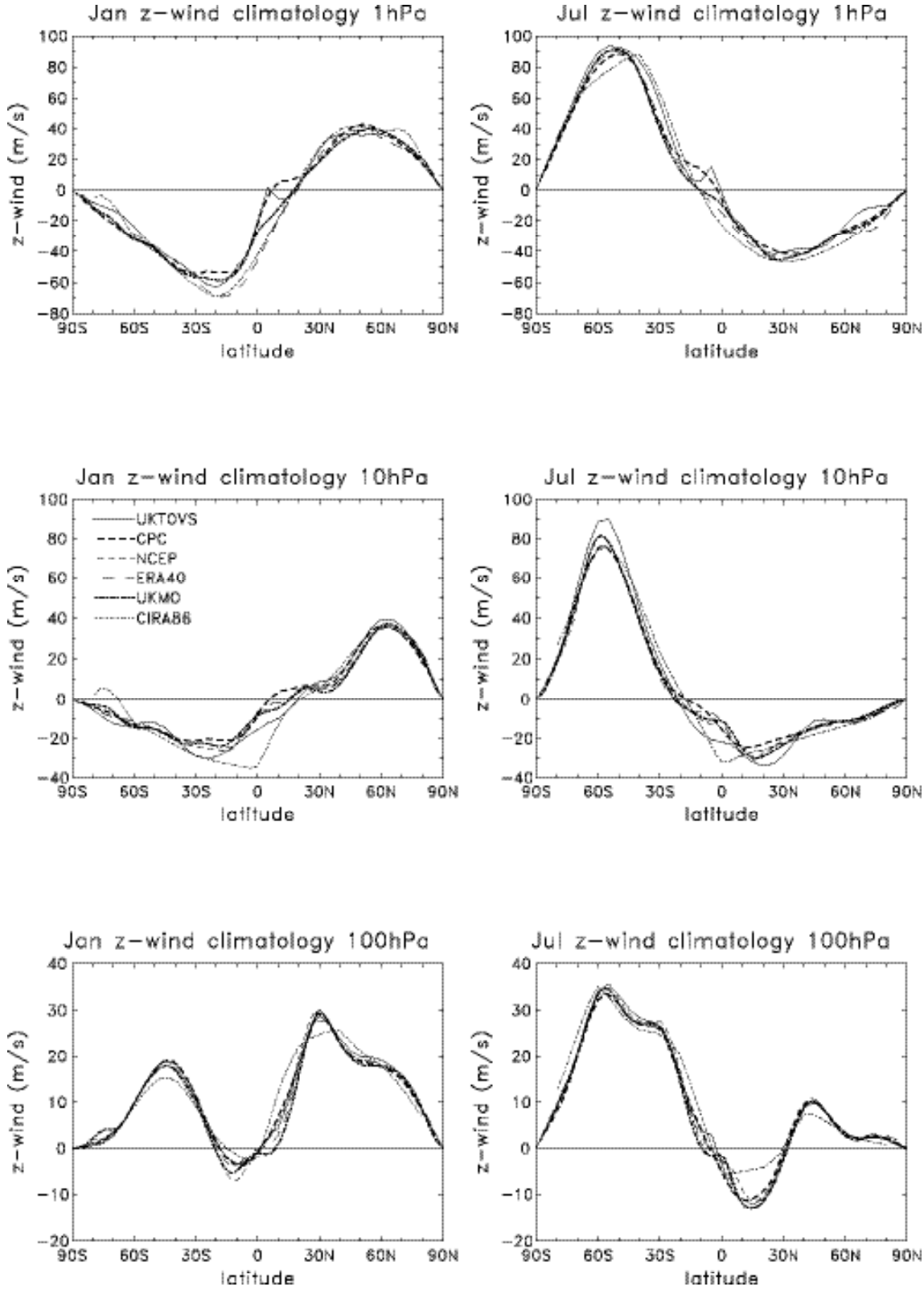

Figure 37. Latitudinal structure of zonal mean zonal wind from various analyses for January (left) and July (right), for statistics at 1 hPa (top), 10 hPa (middle) and 100 hPa (bottom).

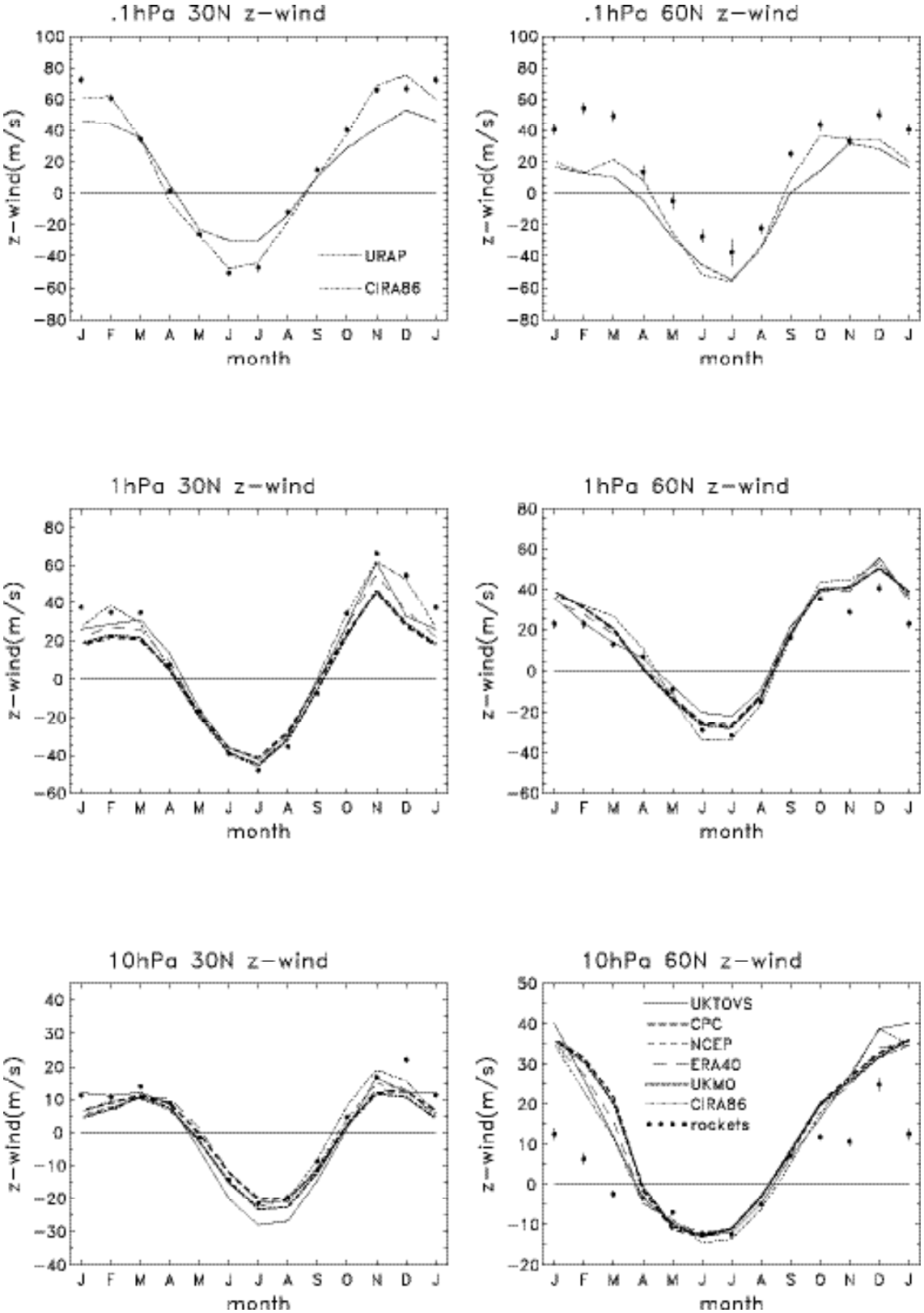

Figure 38. Comparison of the seasonal variation of zonal winds measured by rocketsondes with zonal mean analyses at 30°N (left) and 60°N (right), for statistics at 0.1 hPa (top), 1 hPa (middle) and 10 hPa (bottom).

2. Interannual variability in extratropics

Interannual variability in zonal winds at 100, 10 and 1 hPa is compared in Figure 39 for the Arctic (60°N) in February and Antarctic (60°S) in October (these are periods of maximum variability). Year-to-year changes are nearly identical among the available data sets in the NH. Slightly larger differences are evident in the SH, although the main year-to-year changes are similar across the data sets. Thus overall there is good confidence in estimates of interannual wind variability in high latitudes.

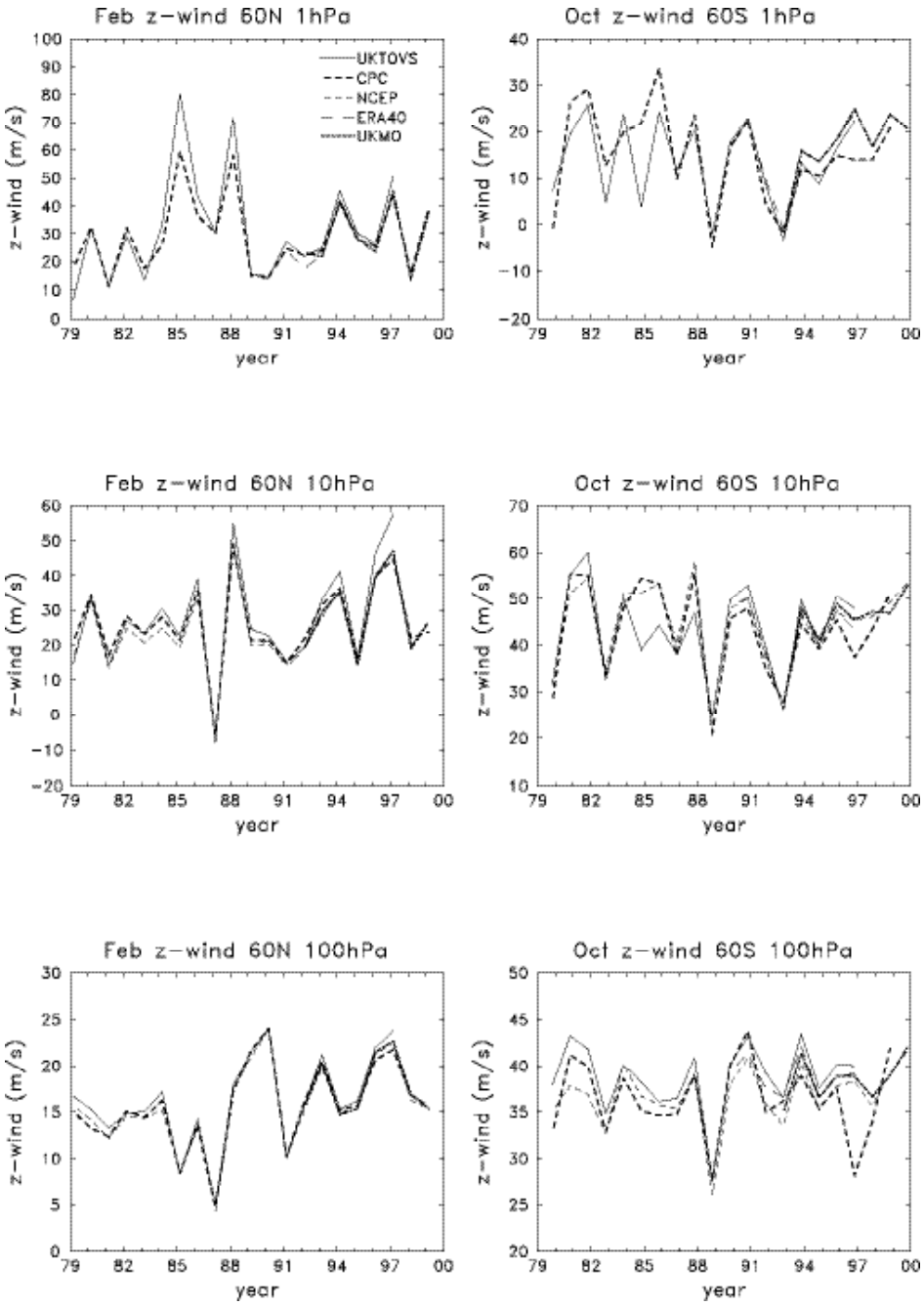

Figure 39. Interannual variation of zonal mean zonal winds during February at 60°N (left) and October at 60°S (right), for pressure levels 1 hPa (top), 10 hPa (middle) and 100 hPa (bottom).

3. Tropical seasonal cycle

Tropical stratospheric winds present particular problems, because there are few direct wind measurements on a daily basis above the lower stratosphere. Also, due to the smallness of the Coriolis parameter, determination of balanced wind in the tropics requires a more accurate estimate of horizontal temperature gradients than at higher latitudes. Thus special attention is required in assessing the quality of tropical winds.

The seasonal variations of equatorial zonal winds at 100 and 50 hPa are shown in Figure 40. An annual cycle is evident at 50 hPa (maximum easterlies during July-September), and a semi-annual variation at 100 hPa, and aside from the CIRA86 results there is overall agreement to within a few m/s among the different data sets. Similar statistics are compared for the 30, 10, 5 and 1 hPa levels in Figure 41. There is approximate agreement among analyses at 30 and 10 hPa, aside from the CIRA86 (strong easterly biases). There is a substantial spread among the data sets at 5 hPa, with ERA40 exhibiting relatively large differences compared to other levels (note the corresponding differences seen in Figures 35-36). There is a pronounced SAO in zonal wind at 1 hPa in Figure 41, which shows similar magnitudes and phases in each data set (discussed more below).

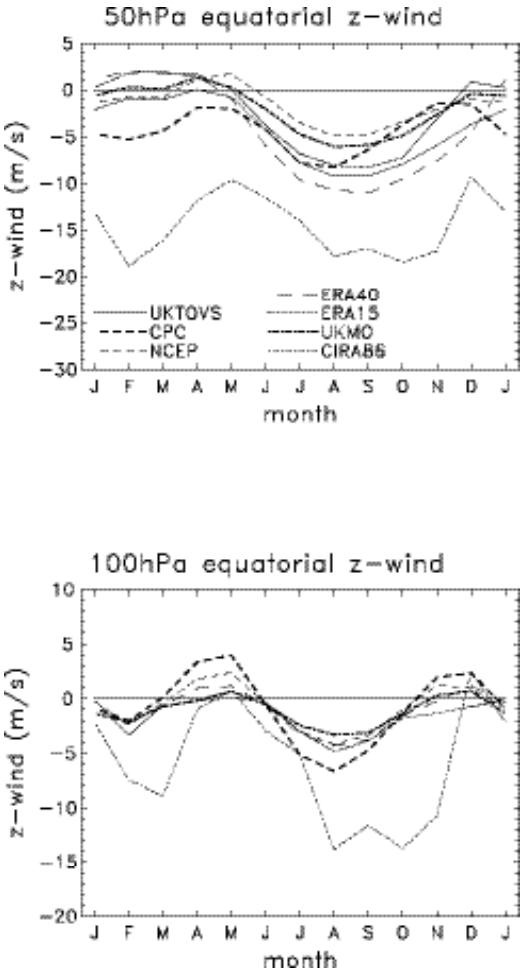

Figure 40. Climatological seasonal cycle of zonal mean zonal winds at the equator from various analyses, for statistics at 50 hPa (top) and 100 hPa (bottom).

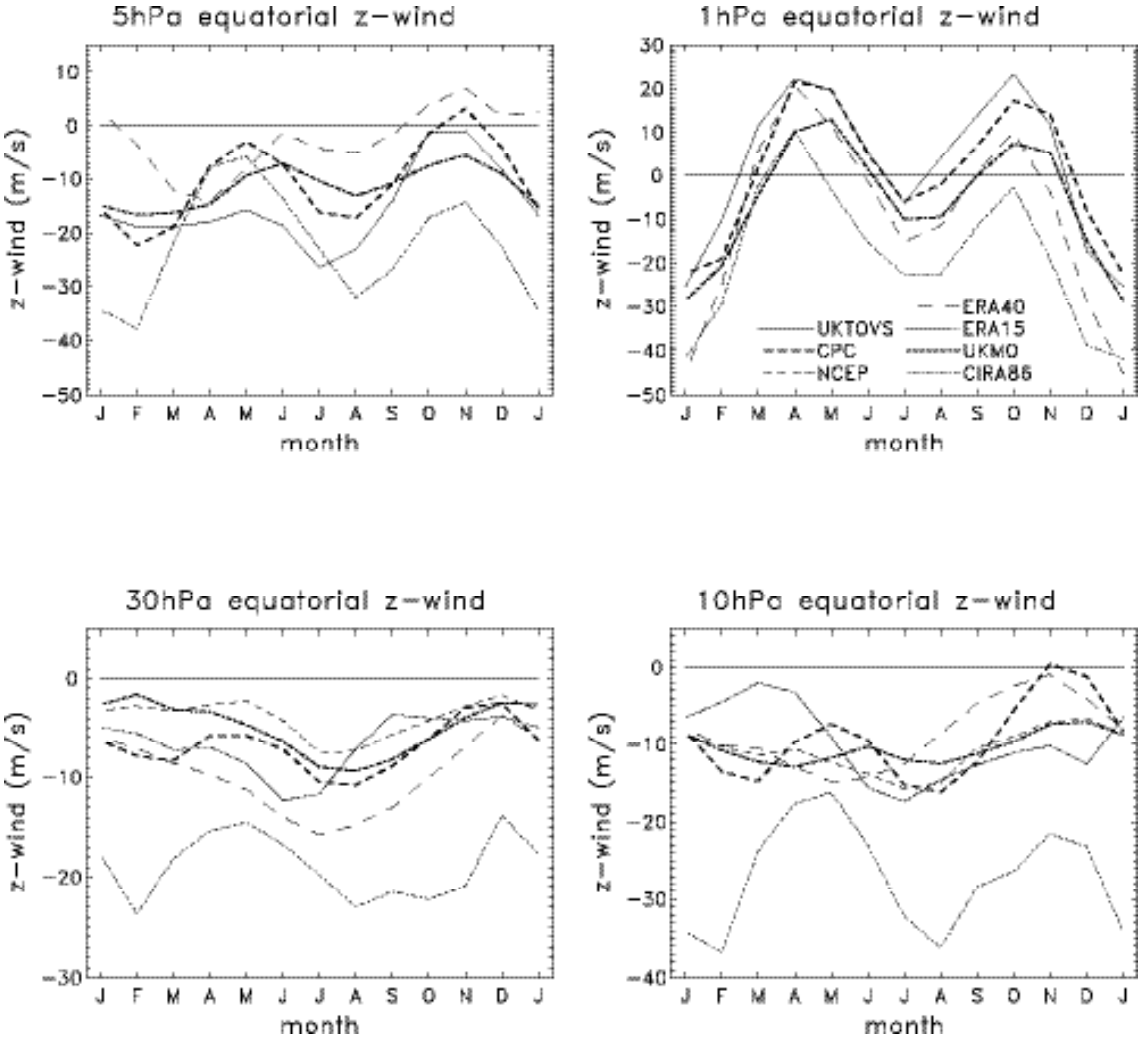

Figure 41. Climatological seasonal cycle of zonal mean zonal wind at the equator from various analyses at 30 hPa (bottom left), 10 hPa (bottom right), 5 hPa (top left), and 1 hPa (top right).

a. Tropical rocketsondes

Rocketsondes are particularly valuable for ground-truth measurements of tropical winds in the middle atmosphere, given the uncertainties in balance wind estimates discussed above. Extensive rocketsonde data are available near 10°N and 10°S, and because there is a substantially different seasonal cycle at these latitudes, we include comparisons for both 10°N and 10°S in Figure 42. The overall impression from Figure 42 is that there is remarkably good agreement between the rocketsonde climatologies and analyses at 10 and 1 hPa, with appropriate seasonal variations and cross-equatorial differences mirrored in all data sets (except for some notable UKTOVS and CIRA86 biases at 10 hPa and 10°S). The rocketsondes at 10°S, 0.1 hPa also show approximate agreement with the CIRA86 and URAP data sets; there are fewer rocketsondes available at 10°N, 0.1 hPa.

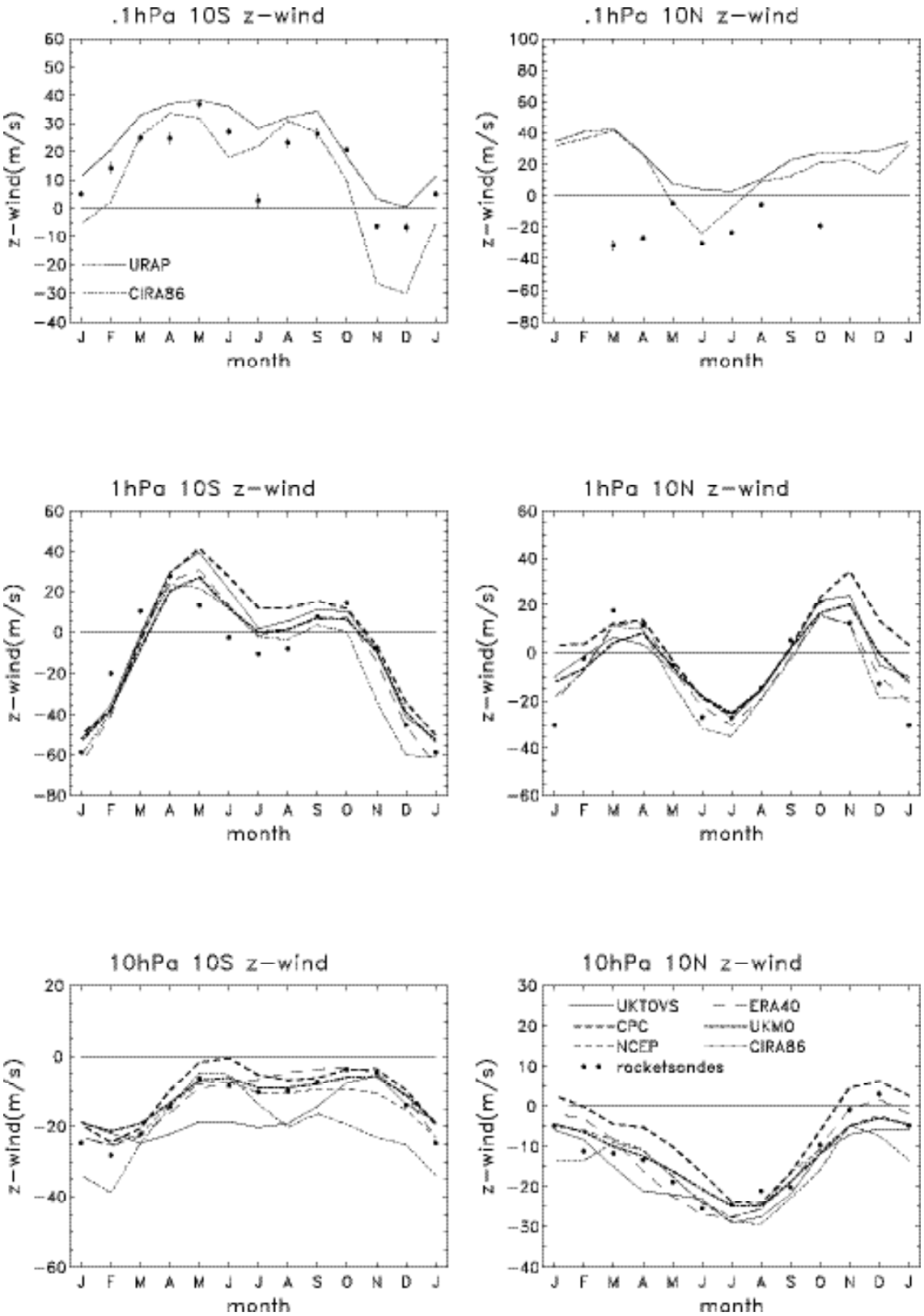

Figure 42. Comparison of the seasonal cycle of zonal winds derived from rocketsondes near 10°S (left) and 10°N (right) with zonal mean analyses. Statistics are shown for 0.1 hPa (top), 1 hPa (middle) and 10 hPa (bottom).

b. Semi-annual oscillation

The vertical and latitudinal amplitude and phase structure of the zonal wind SAO is shown in Figure 43, comparing each data set along with rocketsonde results at 8°N and 8°S. The vertical structure shows an amplitude maximum near the stratopause (~ 50 km), with reasonable agreement between various data sets. A second amplitude maximum near the mesopause (~ 80 km) is suggested in URAP winds. The latitudinal structure at 1 hPa shows maximum SAO amplitude near 10-20°S for most data sets, which is distinct from the equatorially-centred SAO in temperature (Figure 28). The rocketsonde results near 8°N and 8°S suggest a latitudinal asymmetry consistent with analyses (i.e., larger zonal wind SAO in the SH subtropics). The rocketsonde SAO amplitudes are approximately 25% larger than most analyses, while the phases are in good agreement.

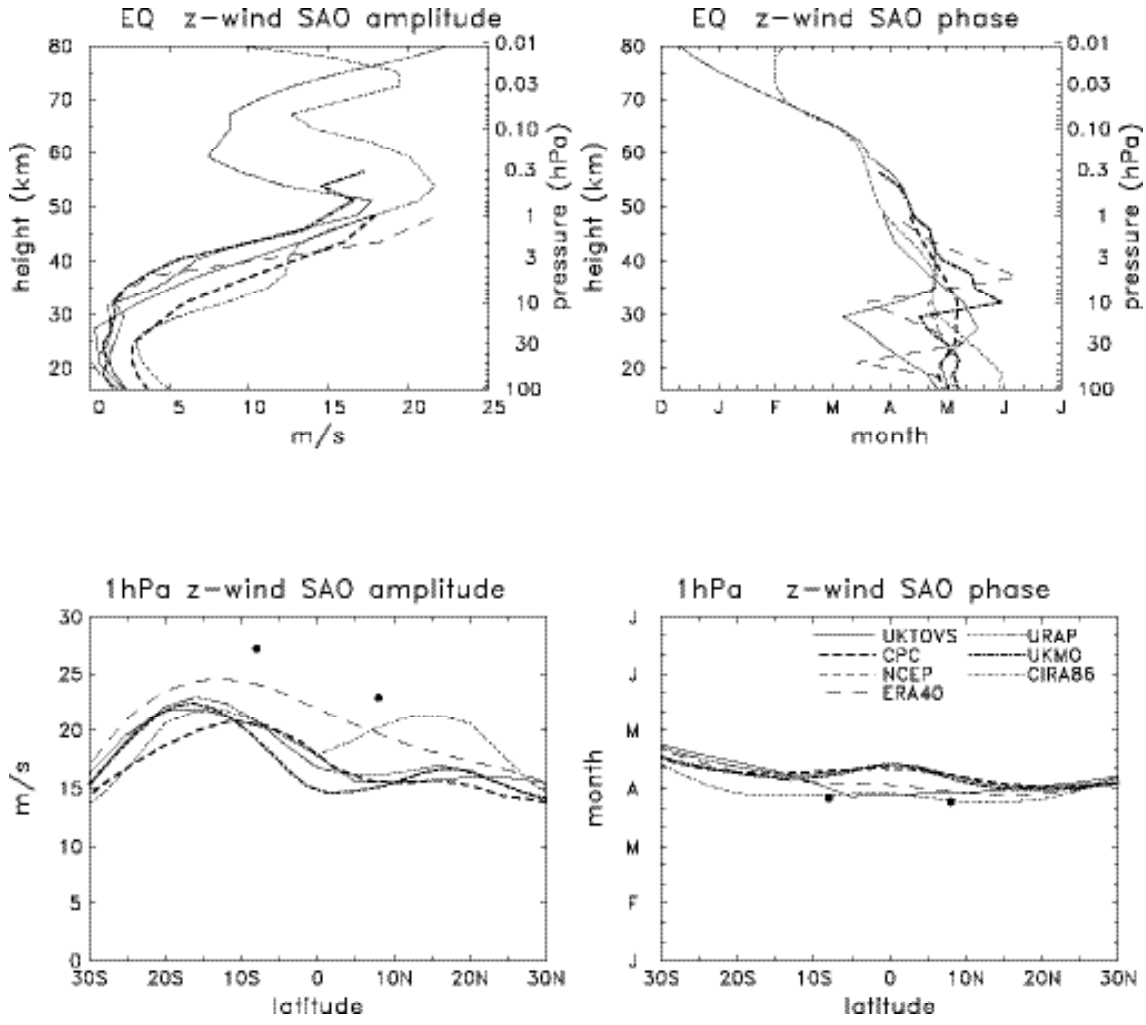

Figure 43. Top panels show the vertical profiles of the amplitude and phase of the zonal wind semi-annual oscillation (SAO) at the equator derived from each available data set. Lower panels show the respective latitudinal structures at 1 hPa, and the dots show results from rocketsonde data at 8°S and 8°N. The phase refers to the time of the first maximum during the calendar year.

4. Tropical interannual variability and the QBO

Figure 44 shows interannual anomalies in equatorial zonal wind at 50, 30 and 10 hPa during 1985-1999 derived from the various analyses. The QBO dominates variability in these time series, and included in Figure 44 are anomalies derived from Singapore radiosonde data, which are a standard reference for the QBO (e.g., Naujokat, 1986). The QBO signal is evident in each analysis, but the amplitude varies strongly between different data (and with altitude). In general the assimilated data sets (UKMO, NCEP, ERA15 and ERA40) have the largest amplitudes, and most closely approach the Singapore data, whereas the balance winds derived from CPC and UKTOVS are much too weak. The strength of the QBO in the different data sets is quantified in Figure 45, where the equivalent QBO amplitude (defined earlier) is plotted as a function of latitude (at 30 hPa) and height. For comparison, Figure 45 also includes the 30 hPa QBO amplitude derived from tropical radiosonde climatologies in Dunkerton and Delisi (1985), plus the equivalent result from Singapore radiosonde measurements over pressure levels 70-10 hPa (using data as in Figure 44). Overall the ERA40 data exhibit the largest QBO amplitude (in good agreement with the radiosonde climatology and Singapore data), with the ERA15, UKMO and NCEP re-analyses somewhat weaker, and CPC and UKTOVS (balance winds) as severe underestimates. The ERA40, ERA15, UKMO and NCEP data show approximately similar amplitudes between 70 and 30 hPh, whereas above 30 hPa there are much larger differences, and only the ERA40 approaches the Singapore amplitudes over 20-10 hPa. Above 10 hPa there is a factor of two difference between the ERA40 and UKMO results, and here the UKMO amplitude is almost certainly too weak.

Figure 46 shows wind anomalies at 1 hPa from UKMO, CPC and UKTOVS data. As with temperatures (Figure 32), there is some approximate agreement after 1990, but larger differences between CPC and UKTOVS for the earlier period. The UKTOVS time series suggests a QBO signal at 1 hPa in the early record, which is seen in all three data sets after 1990 (and which is evident at 1 hPa in rocketsonde data, e.g., Gray *et al.*, 2001).

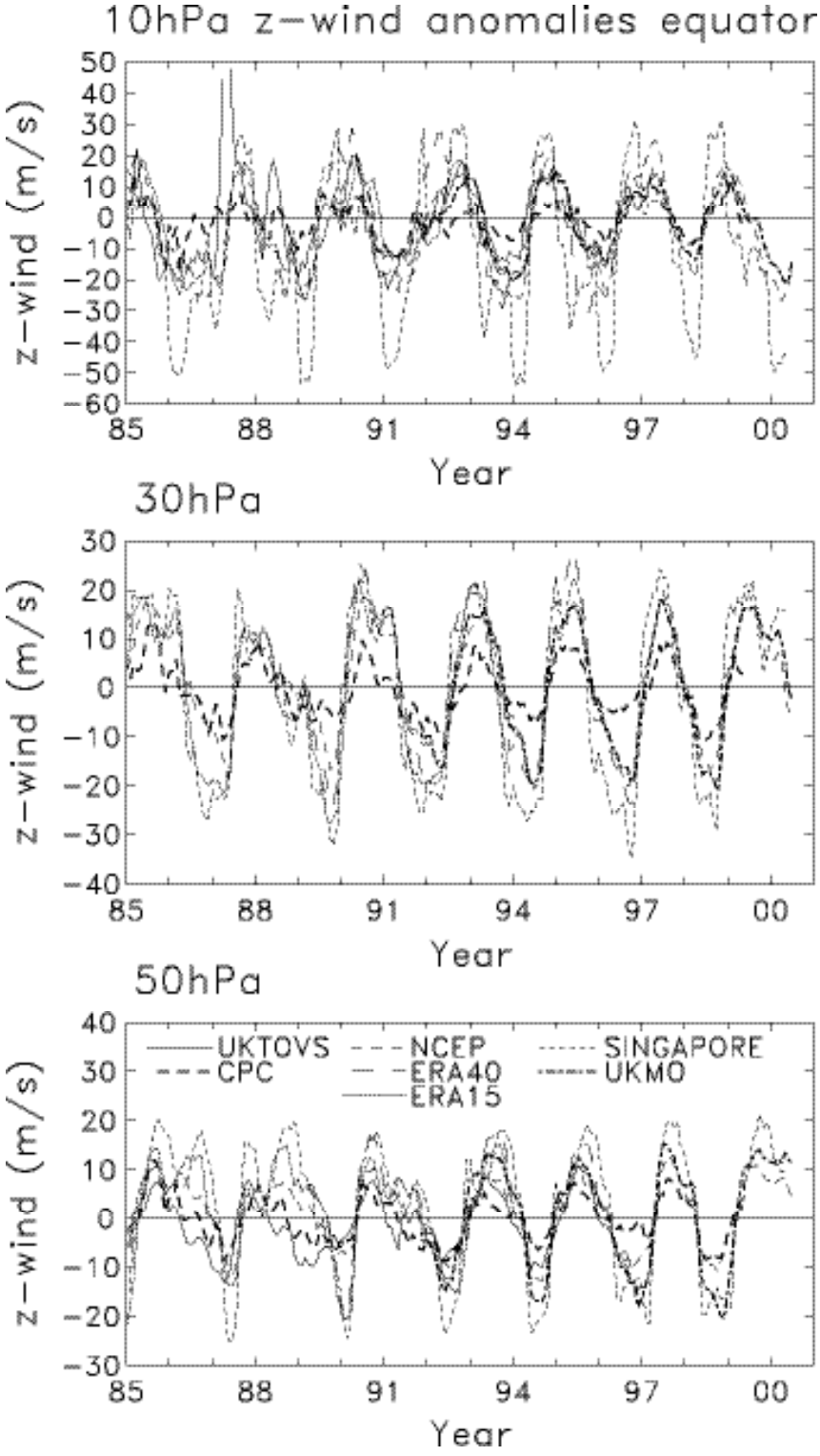

Figure 44. Time series of interannual anomalies in equatorial zonal mean winds from various analyses at 10 hPa (top), 30 hPa (middle) and 50 hPa (bottom). Anomalies are calculated with respect to the 1992-1997 average. For comparison, these plots also show results derived from Singapore (1°N) radiosonde measurements, which are a standard reference for the zonal wind QBO.

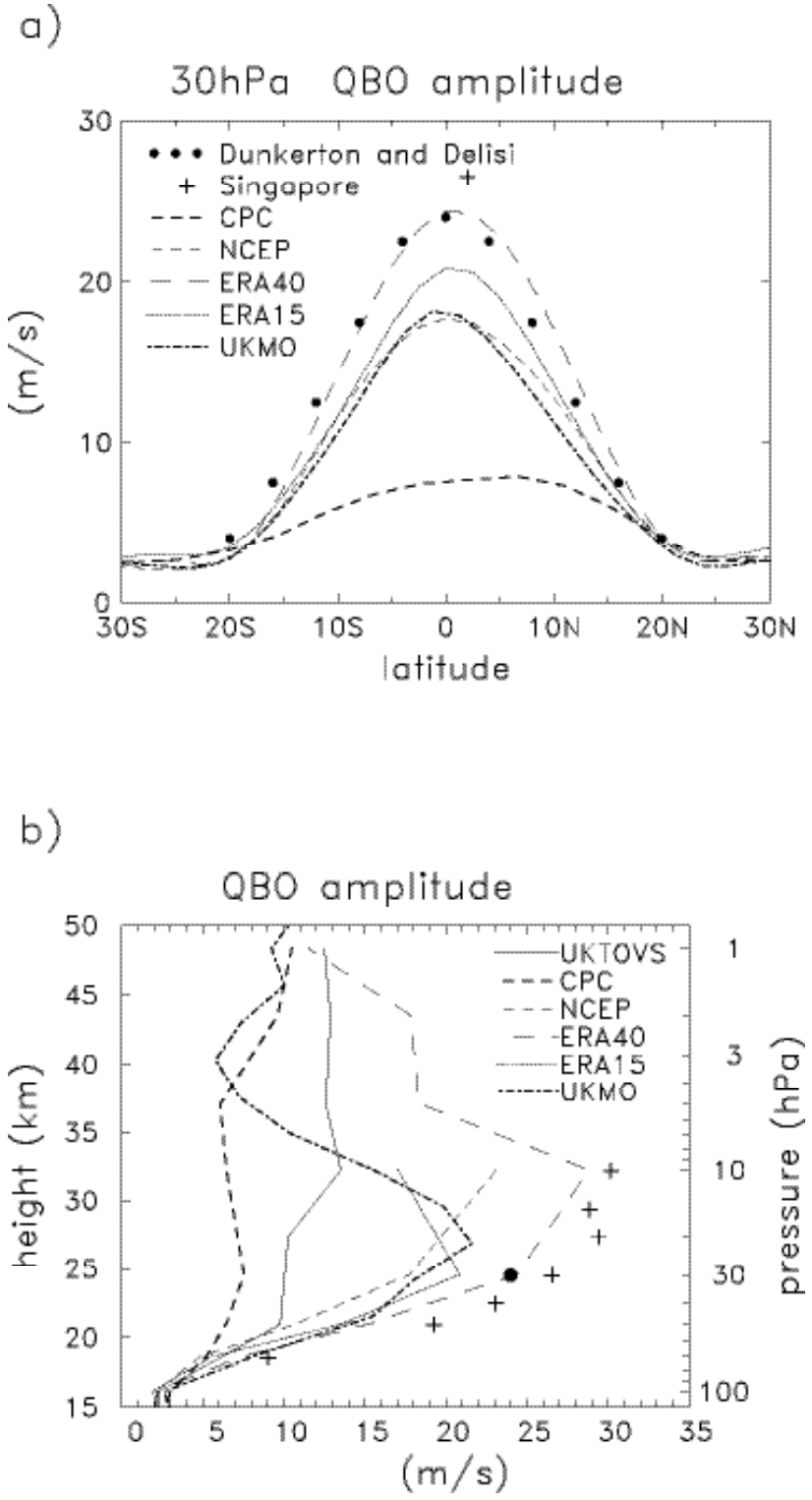

Figure 45. (a) Latitudinal structure of the equivalent QBO amplitude in zonal wind at 30 hPa, defined as $\sqrt{2}$ times the rms anomaly values during 1992-1997 (see text). (b) Shows the vertical structure of QBO amplitude at the equator. For comparison, results of Dunkerton and Delisi (1985) are shown (dots), together with estimates from Singapore radiosondes (plus signs).

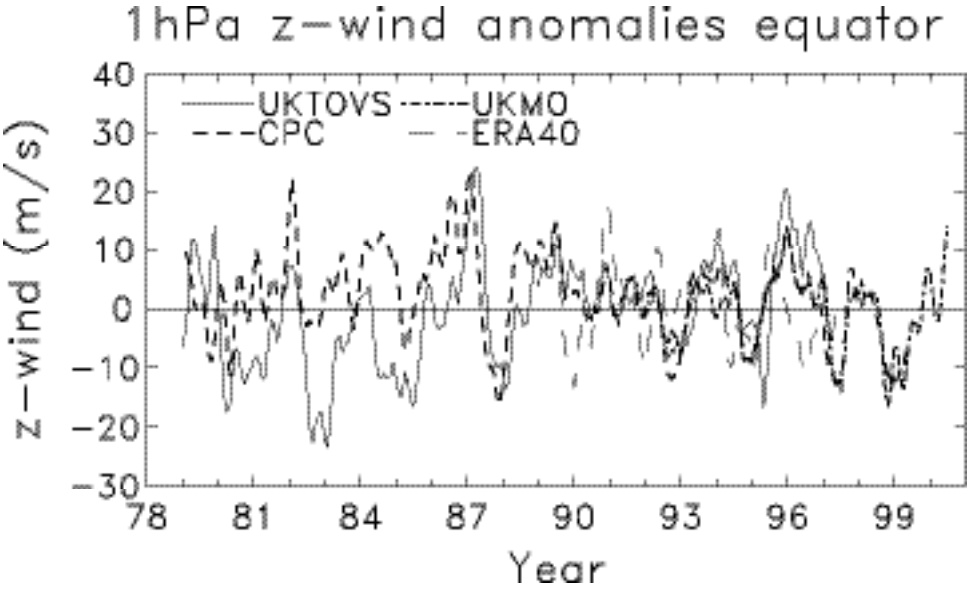

Figure 46. Time series of interannual anomalies in equatorial zonal mean wind at 1 hPa derived from various analyses.

C. Zonally averaged heat and momentum fluxes

The zonally averaged fluxes of heat $\left(\overline{v'T'}\right)$ and momentum $\left(\overline{u'v'}\right)$ are fundamentally important diagnostics of atmospheric wave behaviour and large-scale transport. Their calculation is based on co-variances of eddy winds and temperatures (in longitude), and these fluxes provide sensitive diagnostics of planetary wave behavior and coupling with the mean flow (in both observations and models). The eddy heat and momentum fluxes are primary quantities involved in calculation of the Eliassen-Palm (EP) flux and its divergence (Andrews *et al.*, 1987). Of primary importance is the poleward eddy heat flux $\left(\overline{v'T'}\right)$ in the extratropical lower stratosphere, which is proportional to the vertical wave activity flux (EP flux) from the troposphere into the stratosphere (e.g., Andrews *et al.*, 1987). The fluxes considered here are calculated from daily data and then monthly averaged (i.e., they contain both stationary and transient components). Because daily data are involved in these calculations, we focus on comparisons among UKMO, CPC and NCEP re-analyses. The time period covered is 1992-1997 (a few ERA15 results are also shown for reference, but these are for the period 1988-1993 and are thus not directly comparable). Statistics are compared for NH winter-spring and SH spring seasons, when stratospheric planetary waves and fluxes have maximum amplitude.

January climatological heat fluxes at 100, 50 and 10 hPa are compared in Figure 47. Maximum values are observed approximately over 40-70°N, with similar latitudinal structures for each data set. The seasonal variations of $\left(\overline{v'T'}\right)$ averaged over 40-70°N and 40-70°S at 100 hPa are shown in Figure 48. The magnitude of $\left(\overline{v'T'}\right)$ in the NH varies by ~ 10-20 % between the analyses, with NCEP on the stronger side and CPC slightly

weaker. These uncertainties are consistent with Newman and Nash (2000), who include comparisons with other data sets (for shorter periods). This 10-20 % difference is thus the current level of uncertainty in this derived quantity over NH midlatitudes. Similar statistics for the SH in Figures 47-48 show the CPC data as an outlier with substantially smaller fluxes than the other analyses. Interannual variability of heat fluxes at 50 hPa is shown in Figure 49 for February and March in the NH and October in the SH (including results from ERA15 data). Reasonable agreement between analyses is seen in the NH (differences of ~ 15 %), and the (weak) biased CPC estimates are evident in the SH (although the year-to-year variations are captured to some degree in CPC data).

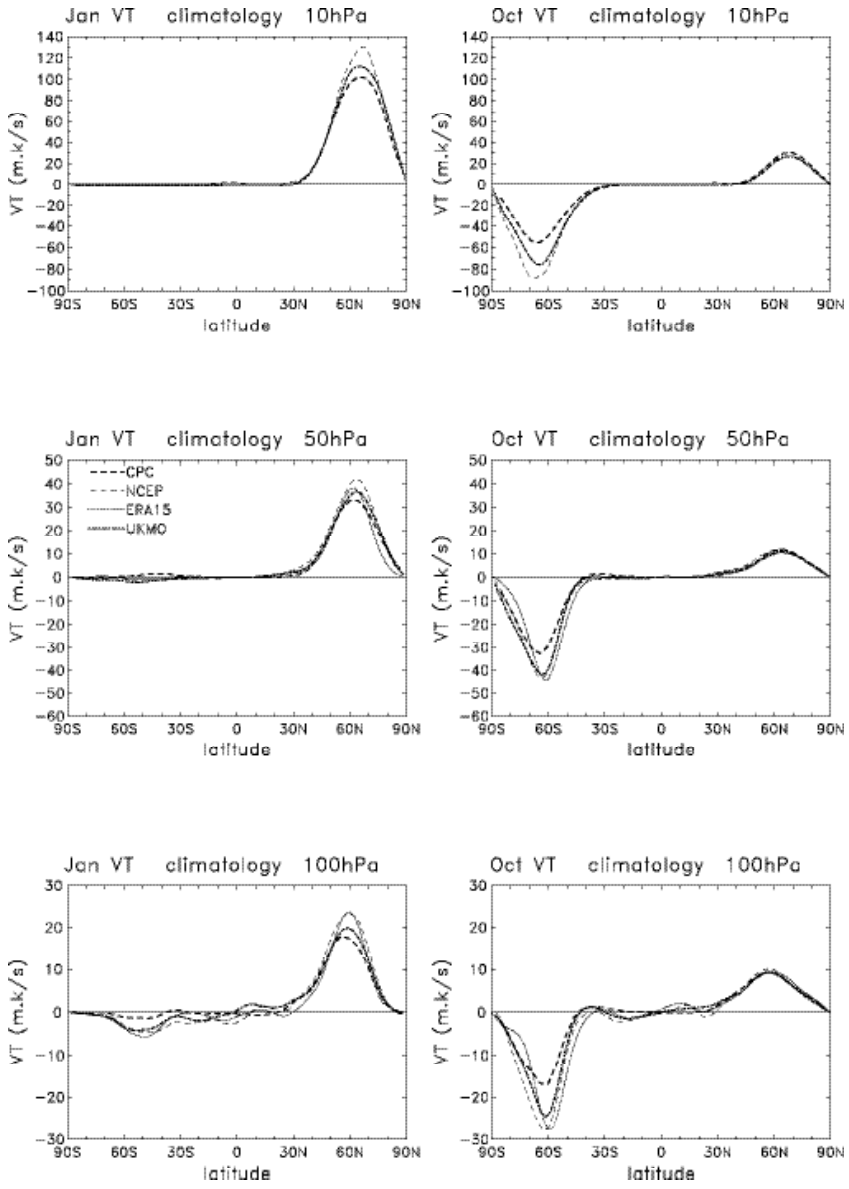

Figure 47. Latitudinal structure of zonal mean eddy heat flux $\left(\overline{v'T'}\right)$ during January (left) and October (right), for statistics at 10 hPa (top), 50 hPa (middle) and 100 hPa (bottom).

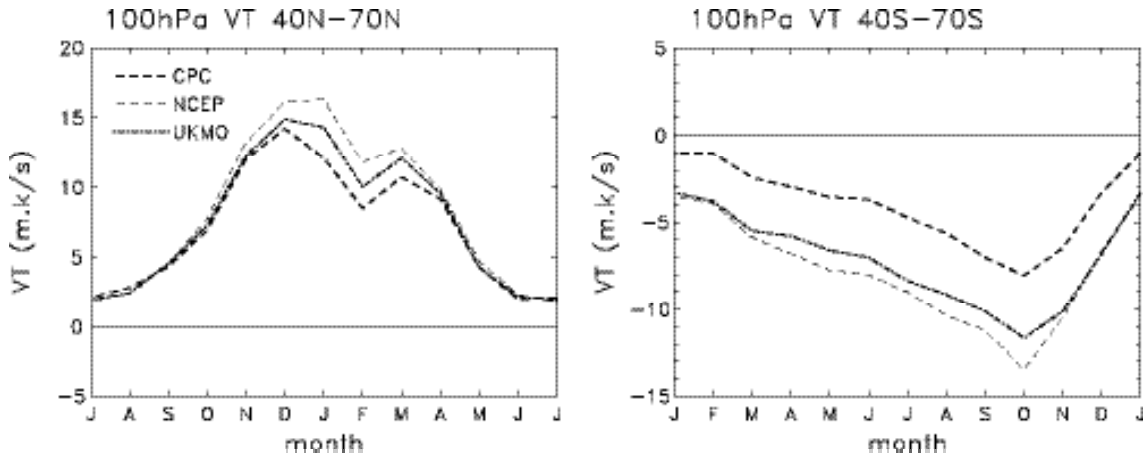

Figure 48. Seasonal variation of zonal mean eddy heat flux $\left(\overline{vT}\right)$ at 100 hPa in the NH (40-70°N, left) and in the SH (40-70°S, right), derived from CPC, NCEP and UKMO analyses over 1992-1997.

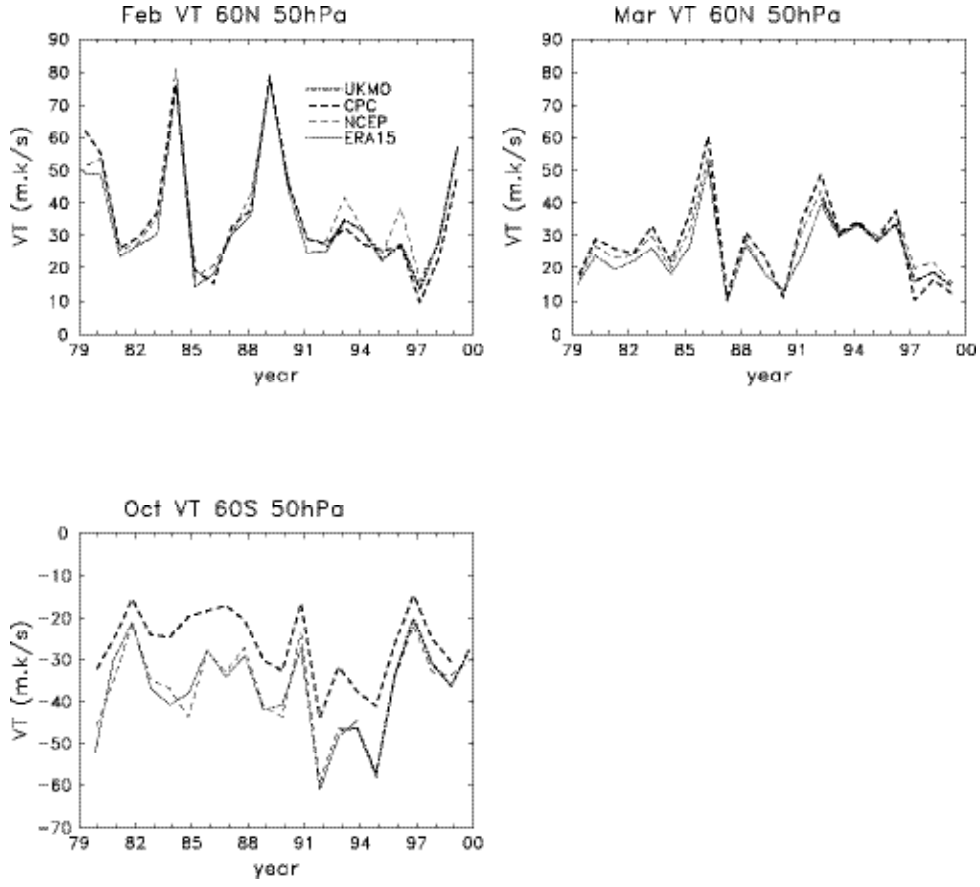

Figure 49. Comparison of interannual variations of zonal mean eddy heat flux at 50 hPa from various analyses. Statistics are shown for the NH during February and March, and for the SH during October.

Climatological comparisons for momentum fluxes $\left(\overline{u'v'}\right)$ are shown in Figure 50. Reasonable agreement is found between the analyses at 100 hPa in both hemispheres (outside of the tropics). At higher levels there are larger differences. The NCEP reanalyses have particularly small $\left(\overline{u'v'}\right)$ in the NH at 50 hPa, and the CPC analyses appear systematically small in the SH, similar to the heat fluxes in Figure 46.

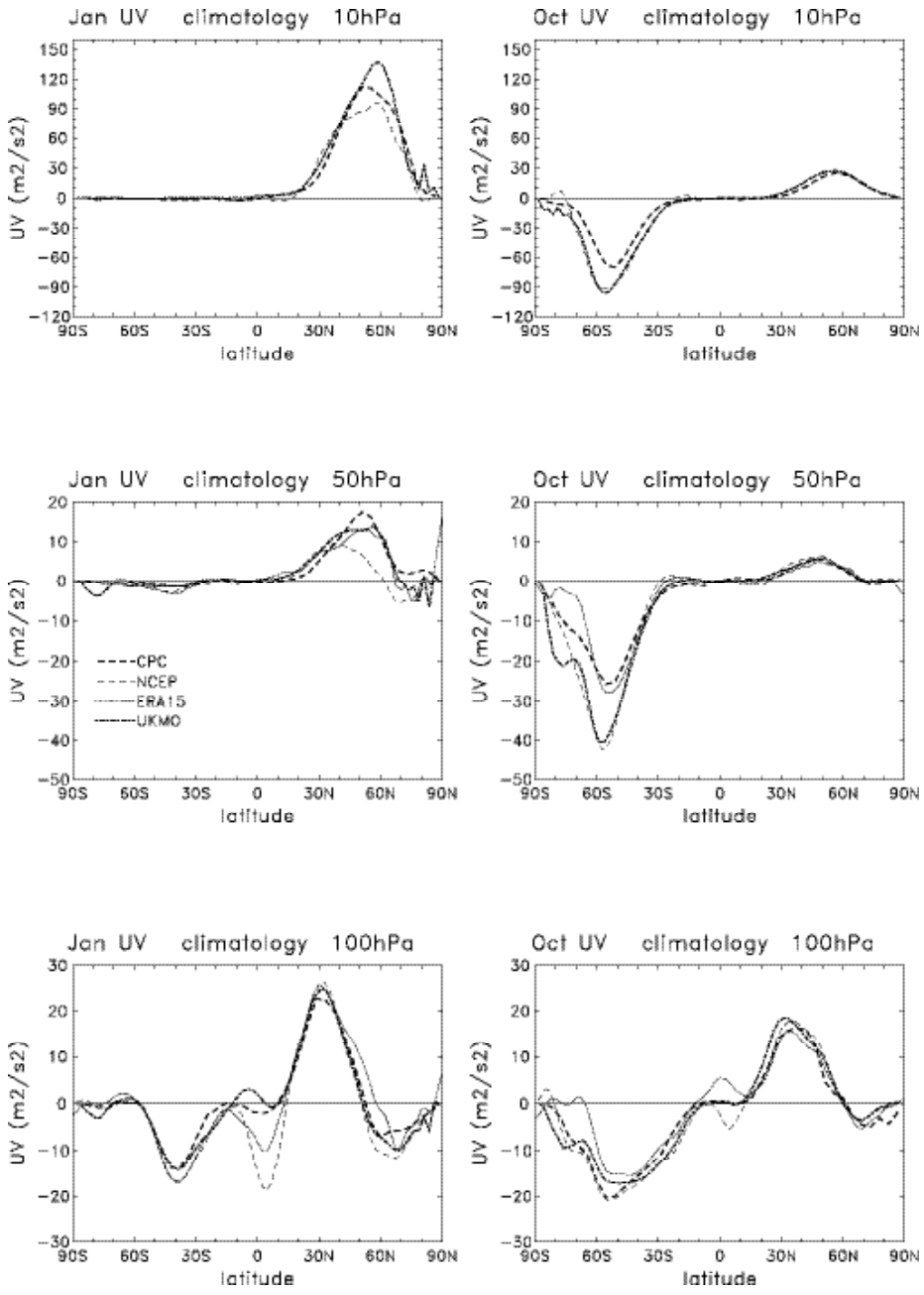

Figure 50. Latitudinal structure of zonal mean eddy momentum flux $\left(\overline{u'v'}\right)$ during January (left) and October (right), for statistics at 10 hPa (top), 50 hPa (middle) and 100 hPa (bottom).

D. Summary: Biases and outstanding uncertainties

1. Summary of largest biases

This study has focused on comparing climatological data sets for the middle atmosphere, which are currently used in the research community. Overall the climatologies developed from analyses (and lidar measurements) for the 1990's agree well in most aspects, although each data set can exhibit 'outlier' behaviour for certain statistics.

The following is a list of the largest apparent biases in each climatological data set, as derived from the foregoing intercomparisons. These are identified when individual data sets are 'outliers' from the group, for these particular features.

UKMO

- cold temperature biases (~ 5 K) near the stratopause (globally)
- warm tropical tropopause temperature (1-2 K)

UKTOVS

- large temperature biases (~ ± 3-5 K) in low latitudes (~ 30°N-S) over much of the stratosphere (20-50 km)
- winter polar night jets somewhat too strong
- weak tropical wind variability (derived from balanced winds)

CPC

- warm temperature biases (~ 3 K) in the Antarctic lower stratosphere during winter-spring
- weak tropical wind variability (derived from balanced winds)
- warm tropical tropopause temperatures (2-3 K)
- weak eddy fluxes in SH

NCEP

- warm tropical tropopause (2-3 K)
- satellite data discontinuity across 1978-1979

ERA15

- global cold biases (~3 K) at 30 and 10 hPa

ERA40

- cold temperature biases (up to 5 K) in the upper stratosphere
- oscillatory vertical structure in temperature, especially large over Antartica

CIRA86

- warm biases of ~ 5-10 K over much of the stratosphere (20-50 km)
- relatively large easterly biases in tropical winds (derived from balanced winds)
- SAO's in mesospheric wind and temperature not well resolved

MLS

- warm biases (~3-7 K) over much of the stratosphere (20-50 km)

Comparisons of the recent climatologies with the historical data sets (CIRA86 and rocketsondes) show reasonable agreement, but the effect of decadal-scale cooling throughout the middle atmosphere is evident, particularly in the polar lower stratosphere (Figures 9-10) and in the upper stratosphere and mesosphere (e.g., Figures 13-16). Decadal changes may also influence zonal mean winds at high latitudes (Figure 38). Despite these differences, the overall quality of the CIRA86 global climatologies is remarkable, given that they were derived from several combined data sets, covering different altitudes and time periods. While the direct wind measurements afforded by UARS and data assimilation techniques provide improved winds (especially in the tropics), the balance winds calculations of CIRA86 captured the overall global climatology reasonably well.

2. Outstanding uncertainties and problem areas

The comparisons here also allow us to highlight aspects of middle atmosphere climatologies that are relatively uncertain. These are identified for statistics that show relatively large variability among each of the different data sets, suggesting a fundamental level of uncertainty or high sensitivity to the details of data analysis. These include:

1) The tropical tropopause region is biased warm (compared to radiosonde data) in many analyses. Relatively smaller biases are found in the ERA15, ERA40 and FUB analyses, which are more strongly tied to radiosonde measurements. The warm biases in this region of sharp temperature gradients probably result from a combination of low vertical resolution in the analyses, plus the less than optimal use by most analyses of thick-layer satellite temperature measurements.

2) The temperature and 'sharpness' of the global stratopause shows large variability among different data sets. This is probably due to the relatively low vertical resolution of TOVS satellite measurements, and also the fact that the stratopause is near the upper boundary for several analyses (UKMO, CPC, UKTOVS).

3) Temperature variability in the tropics (associated with the QBO) is underestimated in all analyses (except FUB), compared to radiosonde measurements. The underestimates are particularly large for analyses that rely primarily on low resolution TOVS satellite data (CPC and UKTOVS). The temperature SAO near the stratopause is also underestimated in these data sets (as well as UKMO).

4) QBO variations in zonal wind are underestimated to some degree in most analyses, as compared to Singapore radiosonde data. The best results are derived from assimilated data sets (ERA40, ERA15, UKMO and NCEP, in that order), and only ERA40 has realistic wind amplitudes above 30 hPa. The use of balance winds in the tropics (derived from geopotential data alone) is problematic for the QBO, and produces large underestimates of variability in CPC and UKTOVS data sets.

References

Andrews, D.G., J.R. Holton and C.B. Leovy, Middle Atmosphere Dynamics. *Academic Press*, 1987.

Bailey, M.J., A. O'Neill and V.D. Pope, Stratospheric analyses produced by the United Kingdom Meteorological Office, *J. Appl. Meteorol.*, **32**, 1472-1483, 1993.

Barnett, J.J. and M. Corney, Temperature data from satellites, "Middle Atmosphere Program, Handbook for MAP," Vol. 16, ed. K. Labitzke, J. J. Barnett and B. Edwards, 2-11, 1985a.

Barnett, J.J. and M. Corney, Middle atmosphere reference model from satellite data, "Middle Atmosphere Program, Handbook for MAP," Vol. 16, ed. K. Labitzke, J. J. Barnett and B. Edwards, 47-85, 1985b.

Dunkerton, T.J. and D.P. Delisi, Climatology of the equatorial lower stratosphere, *J. Atmos. Sci.*, **42**, 376-396, 1985.

Finger, F.G., H.M. Wolf and C.E. Anderson, A method for objective analysis of stratospheric constant pressure charts, *Mon. Wea. Rev.*, **93**, 619-638, 1965.

Finger, F.G., *et al*., Evaluation of NMC upper stratospheric analyses using rocketsone and lidar data, *Bull. Amer. Meteor. Soc*., **74**, 789-799, 1993.

Fishbein, E., *et al*., Validation of the UARS Microwave Limb Sounder temperature and pressure measurements, *J. Geophys. Res.*, **101**, 9983-10,016, 1996.

Fleming, E.L., *et al*, Monthly mean global climatology of temperature, wind, geopotential height, and pressure for 0-120 km, NASA Tech. Memo, NASA TM-100697, 85 pp., 1988.

Fleming, E.L. and S. Chandra, Equatorial zonal wind in the middle atmosphere derived from geopotential height and temperature data, *J. Atmos. Sci.*, **46**, 860-866, 1989.

Fleming, E.L., *et al*., Zonal mean temperature, pressure, zonal wind, and geopotential height as functions of latitude, COSPAR International Reference Atmosphere: 1986, Part II: Middle Atmosphere Models, *Adv. Space Res.*, (10), **12**, 11-59, 1990.

Garcia, R.R. and R.T. Clancy, Seasonal variation of equatorial mesospheric temperatures observed by SME, *J. Atmos. Sci.*, **47**, 1666-1673, 1990.

Garcia, R.R., *et al*., Climatology of the semiannual oscillation of the tropical middle atmosphere, *J. Geophys. Res.*, **102**, 26,019-26,032, 1997.

Geller, M.A., M.-F. Wu and M.E. Gelman, Troposphere-stratosphere (surface-55 km) monthly winter general circulation statistics for the Northern Hemisphere-Four year averages, *J. Atmos. Sci.*, **40**, 1334-1352, 1983.

Gelman, M.E., *et al.*, Detection of long term trends in global stratospheric temperature from NMC analyses derived from NOAA satellite data, *Adv. Space Res.*, **6**, 17-26, 1986.

Gibson, J.K., *et al.*, ERA description, Reanalysis Project Rept. 1, Eur. Center for Medium-Range Weather Forecasts, Reading, England, 1997.

Gray, L.J., *et al.*, A data study of the influence of the equatorial upper stratosphere on Northern Hemisphere stratospheric sudden warmings, *Q.J.R. Meteorol. Soc*., **127**, 1985-2004, 2001.

Hamilton, K., Stratospheric Circulation Statistics. NCAR Technical Note NCAR/TN-191 STR, 174 pp., 1982.

Hauchecorne, A. and M.-L. Chanin, Density and temperature profiles obtained by lidar between 35 and 70 km, *Geophys. Res. Lett.*, **7**, 565-568, 1980.

Hays, P.B., *et al.*, The high-resolution Doppler imager on the Upper Atmosphere Research Satellite, *J. Geophys. Res.*, **98**, 10,713-10,723, 1993.

Hedin, A.E., A revised thermospheric model based on mass spectrometer and incoherent scatter data: MSIS-83, *J. Geophys. Res.*, **88**, 10,170-88, 1983.

Hervig, M.E., *et al.*, Validation of temperature measurements from the Halogen Occultation Experiment, *J. Geophys. Res.*, **101**, 10,277-10,286, 1996.

Hirota, I., Observational evidence of the semiannual oscillation in the middle atmosphere: A review, *Pine Appl. Geophys*., **118**, 217-238, 1980.

Kalnay, E., *et al*., The NCAR/NCEP 40-year reanalysis project, *Bull. Am. Meteorol. Soc*., **77**, 437-471, 1996.

Keckhut, P., A. Hauchecorne and M.-L. Chanin, A critical review of the data base acquired for the long term surveillance of the middle atmosphere by the French Rayleigh lidar, *J. Atmos. Ocean. Technol*., **10**, 850-867, 1993.

Knittel, J., Ein Beitrag zur Klimatologie der Stratosphaere der Suedhalbkugel, *Meteorol. Abh. Met. Inst.*, Berlin, A2, No. 1, 1974.

Labitzke, K., and B. Naujokat, On the variability and trends of the temperature in the middle atmosphere, *Beitr. Phys. Atmos*. **56**, 495-507, 1983.

Labitzke, K., and collaborators, 2002: The Berlin Stratospheric Data series. CD-rom from Meteorological Institute, Free University of Berlin.

Lorenc, A.C., R.S. Bell and B. Macpherson, The meteorological office analysis correction data assimilation scheme, *Quart. J. R. Meteorol. Soc*., **117**, 59-89, 1991.

Lorenc, *et al.,* The Met Office global 3-dimensional variational data assimilation scheme, *Q.J.Roy. Meteorol. Soc*., **126**, 2992-3012, 2000.

Manney, G.L. *et al.*, Comparison of UK meteorological office and US NMC stratospheric analyses during northern and southern winter, *J. Geophys. Res*., **101**, 10,311-10,334, 1996.

Mo, K., *et al.,* Impact of satellite data on the CDAS-reanalysis system, *Mon. Wea. Rev*., **123**, 124-139, 1995.

Nash, J. and G.F. Forrester, Long-term monitoring of stratospheric temperature trends using radiance measurements obtained by the TIROS-N series of NOAA spacecraft, *Adv. Space Res.*, **6**, 37-44, 1986.

Naujokat, B., An update of the observed quasi-biennial oscillation of the stratospheric winds over the tropics, *J. Atmos. Sci.*, **43**, 1873-1877, 1986.

Newman, P.A. and E.R. Nash, Quantifying the wave driving of the stratosphere, *J. Geophys. Res.*, **105**, 12,485-12,497, 2000.

Oort, A.H., Global atmospheric circulation statistics, 1958-1983, NOAA Professional Paper 14, 1983.

Pawson, S., *et al*., Climatology of the Northern Hemisphere stratosphere derived from Berlin analyses. Part I. Monthly means, Met. Abh. FU-Berlin, Neue Folge Serie A, Band 7, Heft 3, 1993.

Pawson, S., *et al.*, The GCM-reality intercomparison project for SPARC (GRIPS): Scientific issues and initial results. *Bull. Am. Meteorol. Soc*., **81**, 781-796, 2000.

Pawson, S. and M. Fiorino, A comparison of reanalyses in the tropical stratosphere. Part 1: Thermal structure and the annual cycle, *Climate Dyn.*, **14**, 631-644, 1998a.

Pawson, S. and M. Fiorino, A comparison of reanalyses in the tropical stratosphere. Part 2. The quasi-biennial oscillation, *Climate Dyn.*, **14**, 645-658, 1998b.

Pawson, S., and B. Naujokat, The cold winters of the middle 1990's in the northern lower stratosphere, *J. Geophys. Res.*, **104**, 14,209-14,222, 1999.

Ramaswamy, V., *et al.*, Stratospheric temperature trends: observations and model simulations, *Rev. Geophys*., **39**, 71-122, 2001.

Randel, W.J., The evaluation of winds from geopotential height data in the stratosphere, *J. Atmos. Sci.*, **44**, 3097-3120, 1987.

Randel, W.J., Global Atmospheric Circulation Statistics, 1000-1 mb, NCAR Technical Note, NCAR/TN-366 STR, 256 pp., 1992.

Randel, W.J. and F. Wu, Cooling of the Arctic and Antarctic polar stratospheres due to ozone depletion, *J. Climate*, **12**, 1467-1479, 1999.

Remsberg, E.E., *et al.*, The validation of HALOE temperature profiles in the mesosphere using Rayleigh backscatter lidar and inflatable falling sphere measurements, *J. Geophys. Res.*, submitted, 2002.

Russell, J.M., *et al.*, The Halogen Occulation Experiment, *J. Geophys. Res*., **98**, 10,777-10,979, 1993.

Scaife, A.A., *et al*., Seasonal and interannual variability of the stratosphere diagnosed from UKMO TOVS analyses, *Quart. J. R. Meteorol. Soc*., **126**, 2585-2604, 2000.

Schmidlin, F.J, Rocket techniques used to measure the neutral atmosphere, Middle Atmosphere Program Handbook for MAP Volume 19, ed. Richard A. Goldberg, pp. 1-28 and references therein, March 1986.

Smith, W. L., *et al*., The TIROS-N operational vertical sounder, *Bull. Am. Meteorol. Soc*., 60, 1177-1187, 1979.

Swinbank, R. and A. O'Neill, A stratosphere-troposphere data assimilation system, *Mon. Wea. Rev.*, **122**, 686-702, 1994.

Swinbank, R. and D. A. Ortland, Compilation of wind data for the UARS reference atmosphere project, submitted to *J. Geophys. Res.*, 2002.

World Meteorological Organization (WMO), Scientific assessment of ozone depletion: 1998. WMO Report No. 44, Geneva, 1999.

Wu, D. L., *et al.*, Mesospheric temperatures from UARS MLS: Retrieval and validation, *J. Atmos. Solar-Terr. Phys*., submitted 2002.

4. An Atlas of Middle Atmosphere Temperatures and Zonal Winds

This section presents a brief atlas of monthly mean temperatures and zonal winds (over 0-85 km), together with estimates of interannual variability in these quantities over 0-50 km. The zonal mean temperature climatology is derived using UKMO analyses over 1000-1.5 hPa, combined with the HALOE temperature climatology over pressures 1.5-0.0046 hPa (~ 85 km). The monthly HALOE climatology is best sampled for the latitude range 50°N-S, and mesospheric temperatures poleward of 50°N and 50°S are derived from the MLS climatology, with offsets at each pressure level used to match the HALOE data at 50°N and 50°S (i.e., the polar latitudinal gradients from MLS are used). The monthly zonal wind climatology (over ~ 0-85 km) is derived from the URAP wind analyses, based primarily on UKMO and UARS HRDI data (see Section 2.9). In order to provide smooth monthly estimates, we use a harmonic analysis of the available time series over 1992-1997, including annual and semi-annual harmonic components.

Estimates of the interannual variability of the zonal mean temperatures and zonal winds are derived using UKMO analyses for the time period 1992-2000. The UKMO analyses have a shorter time record than the CPC or UKTOVS data sets, but provide improved estimates of tropical zonal winds. Interannual standard deviations are calculated from the standard formula

$$\sigma = \left[\frac{1}{N-1} \sum_{i=I}^{N} \left(x_i - \bar{x} \right)^2 \right]^{1/2}$$

where $\bar{x}$ represents the ensemble (climatological) mean, x_i is the monthly mean for each year, and N is the number of available years (N = 9 for 1992-2000).

As a note, the UKMO temperature analyses had some significant errors introduced after January 1998 at the uppermost levels (at and above 1 hPa), due to an ozone climatology problem in the assimilation model (as seen in Figure 31). In order to avoid large effects on the interannual variability estimates, temperature variability at and above 1 hPa use statistics derived from the shorter record 1992-1997.

Climatological means and standard deviations are shown below, in the forms of:

(1) latitude-height cross sections for each month (Figure 51),

(2) latitude-time sections at a few selected pressure levels (Figure 52), and

(3) height-time sections at a few latitudes (Figure 53). In the latitude-height and height-time sections we include heavy dashed lines indicating the location of the tropopause (defined by the lapse rate criterion and taken from the NCEP reanalyses), and the stratopause (defined by the local maximum in temperature near 50 km).

Figure 51. pp74 to pp 79

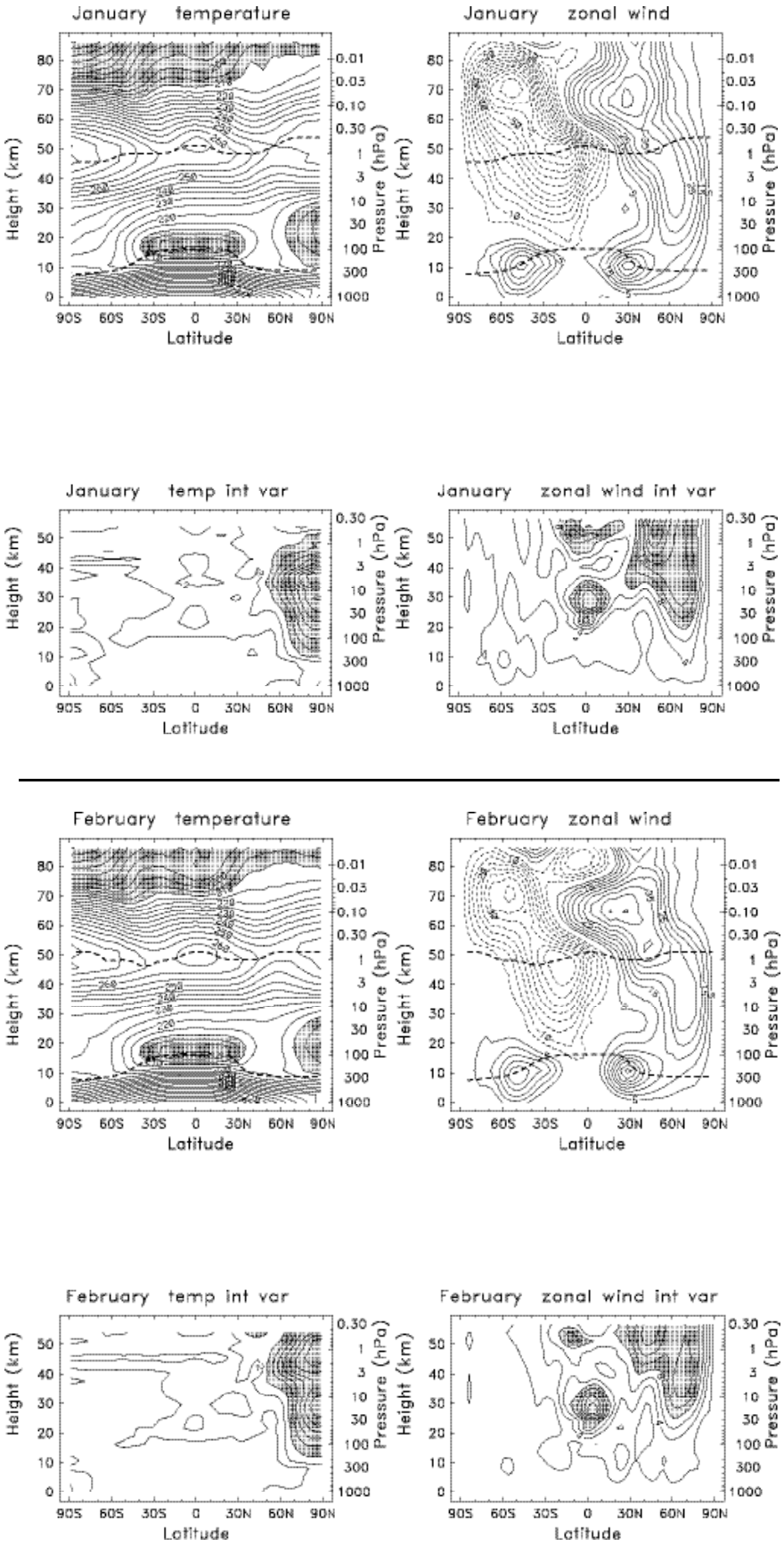

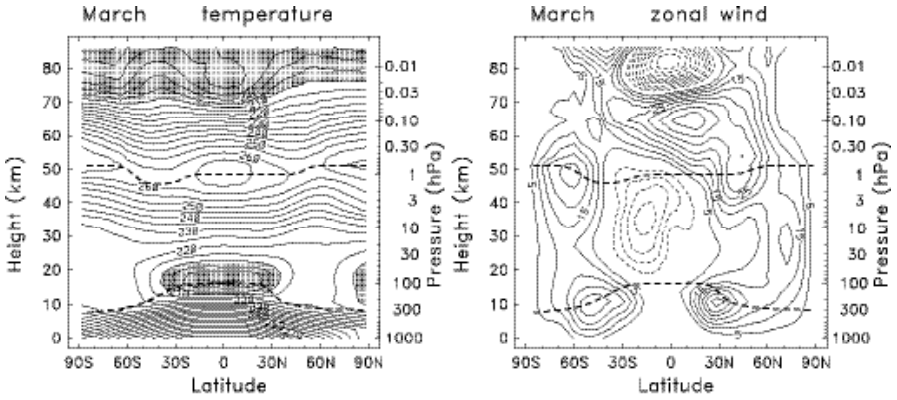
March temperature
March zonal wind
Height (km)
Pressure (hPa)
Latitude
90S 60S 30S 0 30N 60N 90N

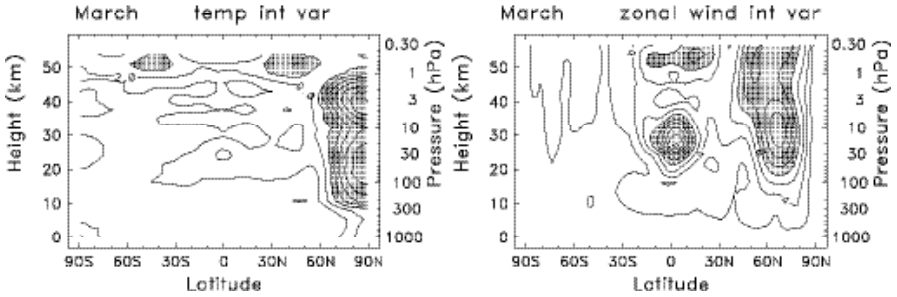
March temp int var
March zonal wind int var
Height (km)
Pressure (hPa)
Latitude
90S 60S 30S 0 30N 60N 90N

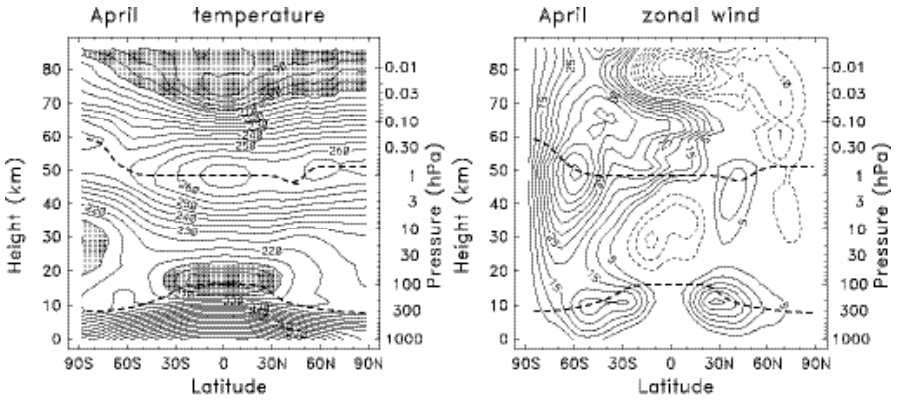
April temperature
April zonal wind
Height (km)
Pressure (hPa)
Latitude
90S 60S 30S 0 30N 60N 90N

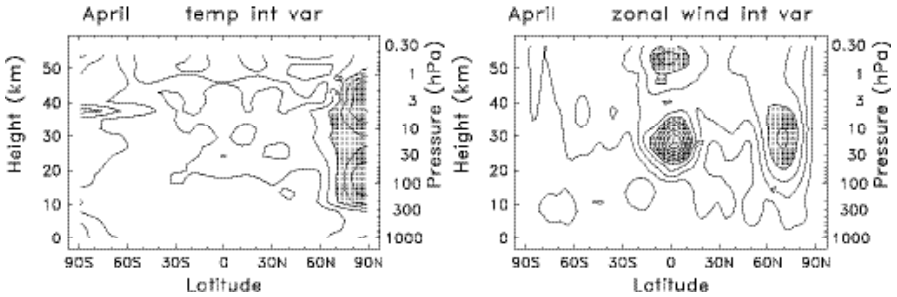
April temp int var
April zonal wind int var
Height (km)
Pressure (hPa)
Latitude
90S 60S 30S 0 30N 60N 90N

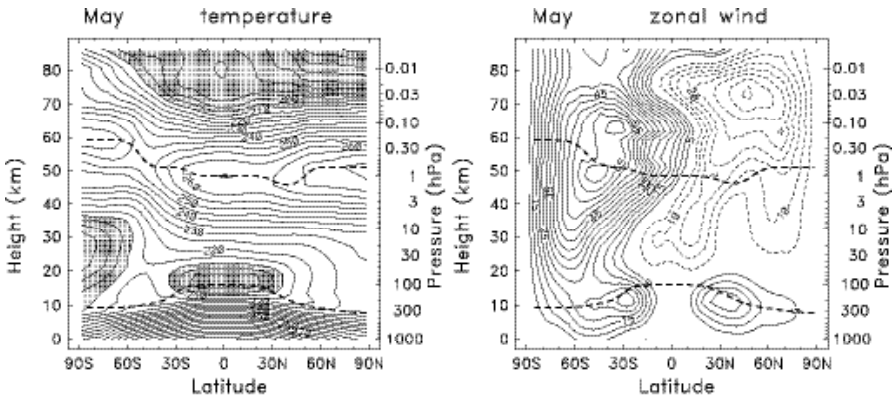
May temperature
May zonal wind
Height (km)
Pressure (hPa)
Latitude
90S 60S 30S 0 30N 60N 90N

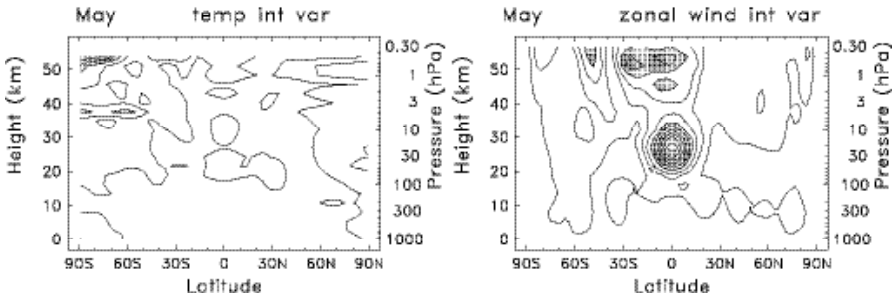
May temp int var
May zonal wind int var
Height (km)
Pressure (hPa)
Latitude
90S 60S 30S 0 30N 60N 90N

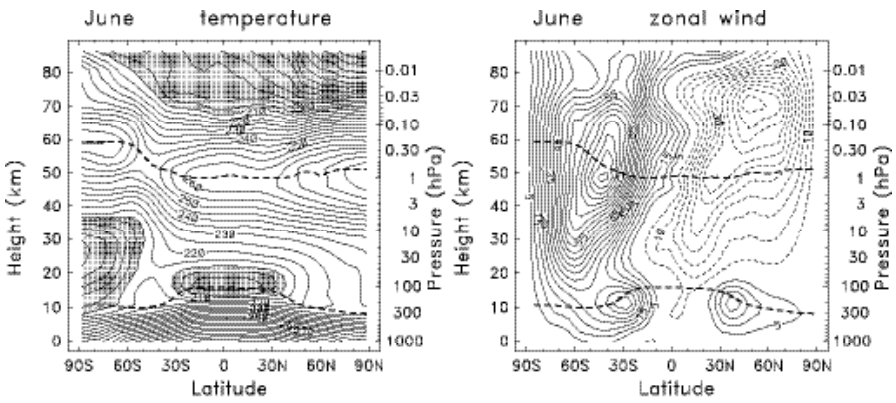
June temperature
June zonal wind
Height (km)
Pressure (hPa)
Latitude
90S 60S 30S 0 30N 60N 90N

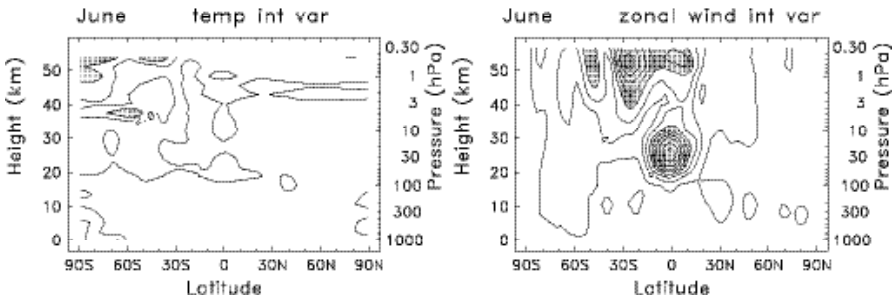
June temp int var
June zonal wind int var
Height (km)
Pressure (hPa)
Latitude
90S 60S 30S 0 30N 60N 90N

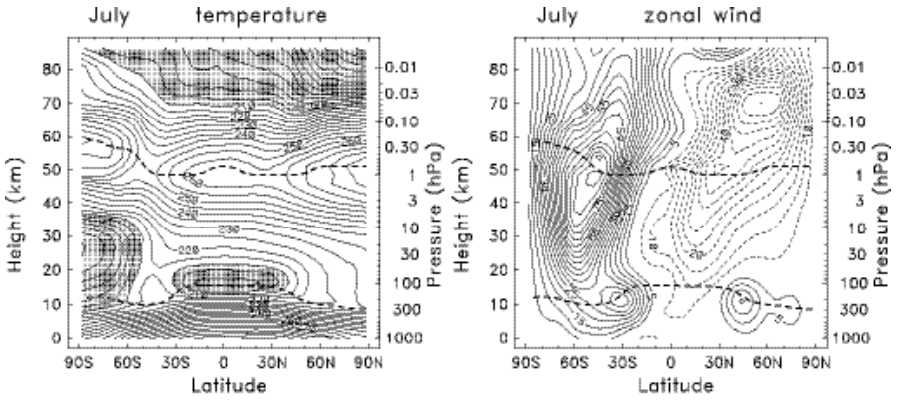
July temperature
July zonal wind
Height (km)
Pressure (hPa)
Latitude
90S 60S 30S 0 30N 60N 90N

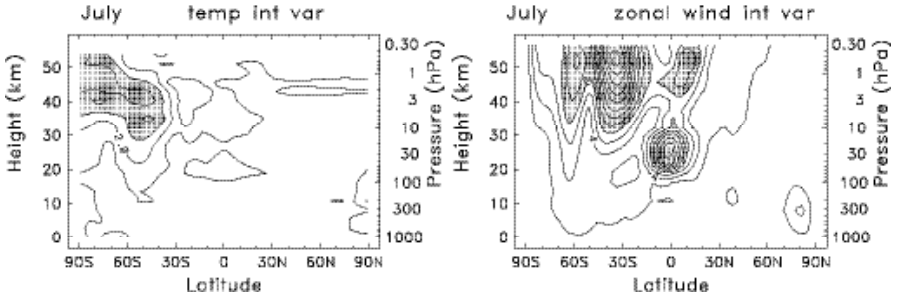
July temp int var
July zonal wind int var
Height (km)
Pressure (hPa)
Latitude
90S 60S 30S 0 30N 60N 90N

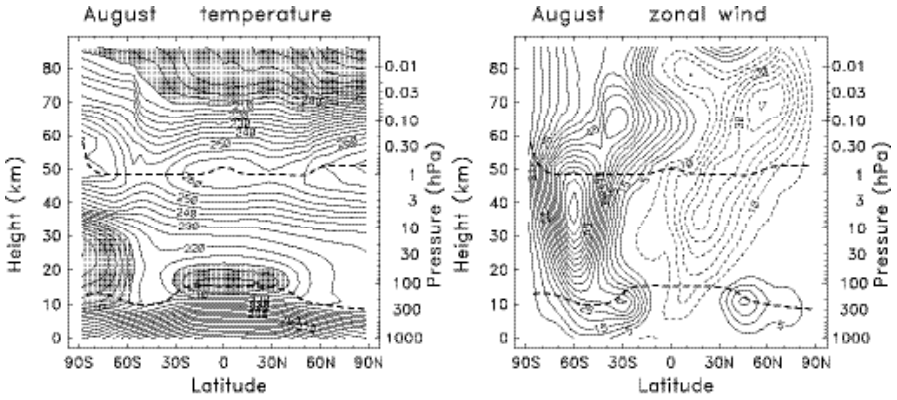
August temperature
August zonal wind
Height (km)
Pressure (hPa)
Latitude
90S 60S 30S 0 30N 60N 90N

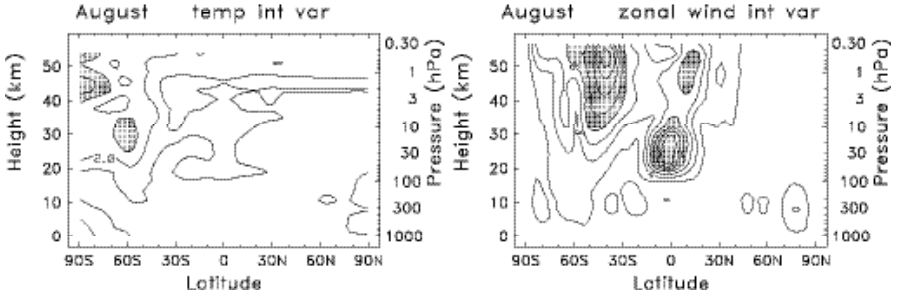
August temp int var
August zonal wind int var
Height (km)
Pressure (hPa)
Latitude
90S 60S 30S 0 30N 60N 90N

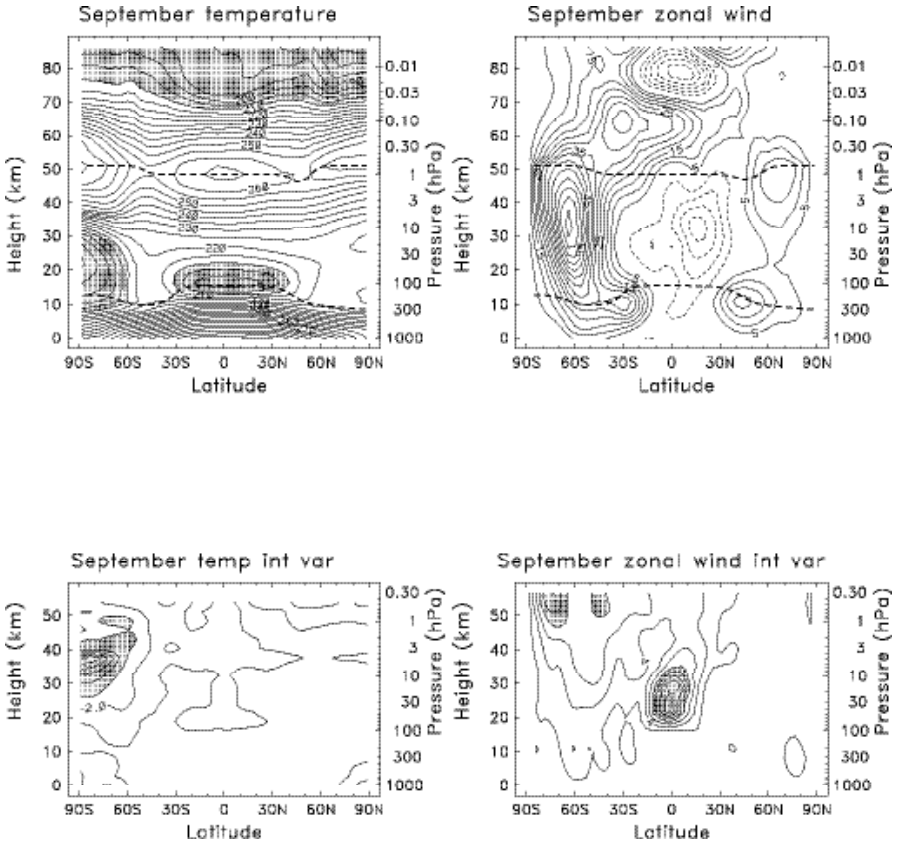
September temperature
September zonal wind
September temp int var
September zonal wind int var
Height (km)
Pressure (hPa)
Latitude
90S 60S 30S 0 30N 60N 90N

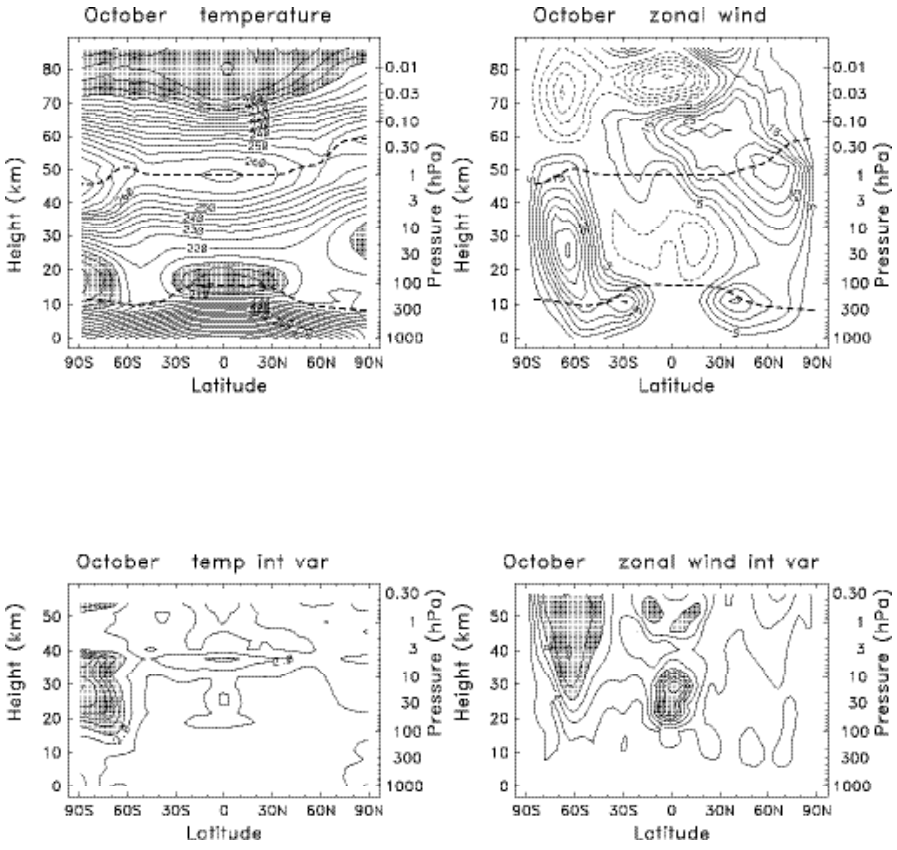
October temperature
October zonal wind
October temp int var
October zonal wind int var
Height (km)
Pressure (hPa)
Latitude
90S 60S 30S 0 30N 60N 90N

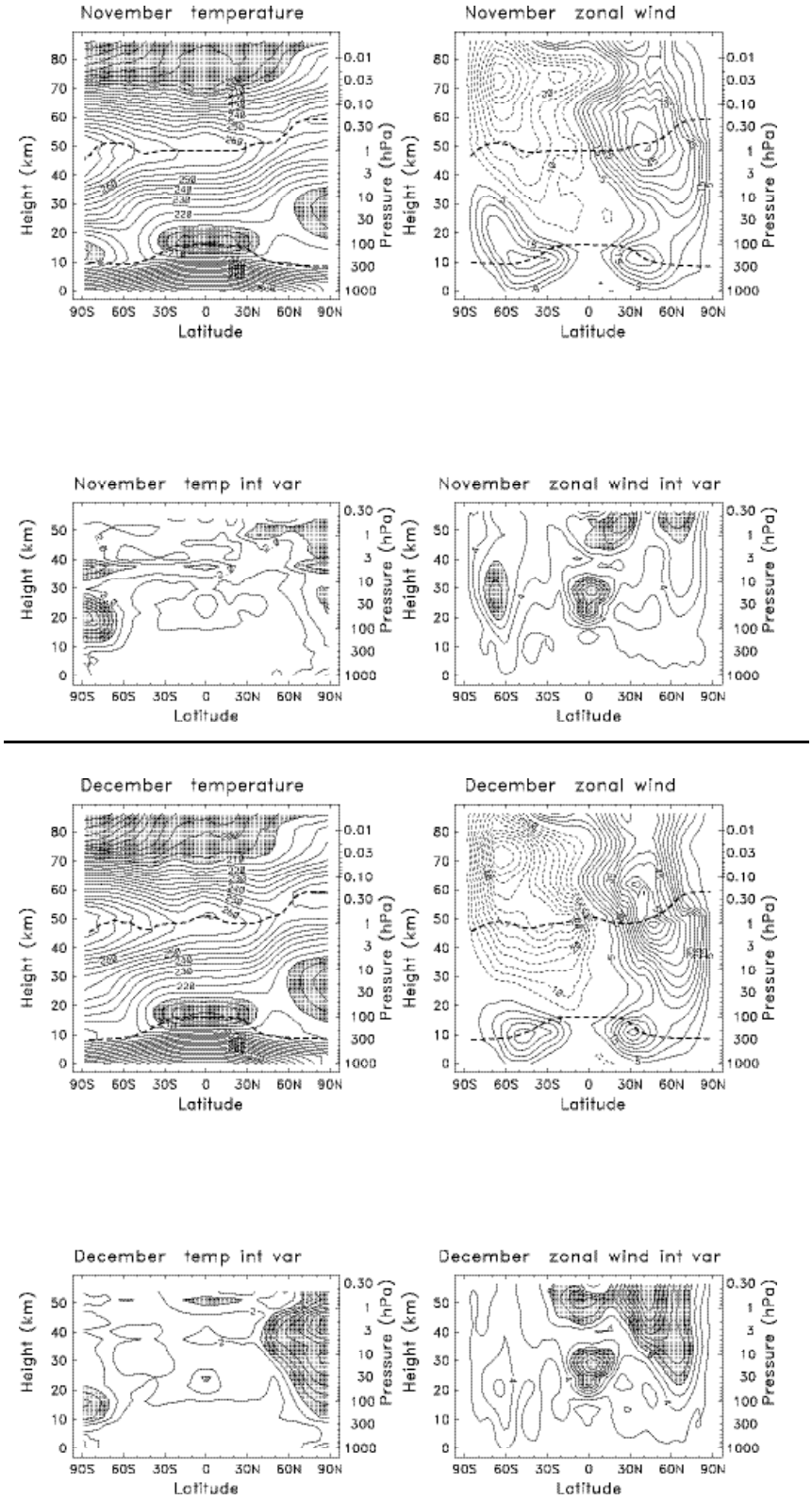

Figure 51. Meridional cross sections of climatological average zonal mean temperature (top left) and zonal wind (top right) for each month, derived from the data sets discussed in Section 5. Contour interval is 5 K for temperature (values below 210 K shaded), and 5 m/s for zonal wind (with zero contours omitted). The heavy dashed lines denote the tropopause and stratopause. Lower panels show the corresponding interannual variability of monthly means for temperature (left) and zonal wind (right) derived from UKMO analyses over 1992-2000. Contour interval is 1 K for temperature (values above 3 K shaded), and 2 m/s for zonal wind (values above 8 m/s shaded).

Figure 52. pp 80 to pp 82

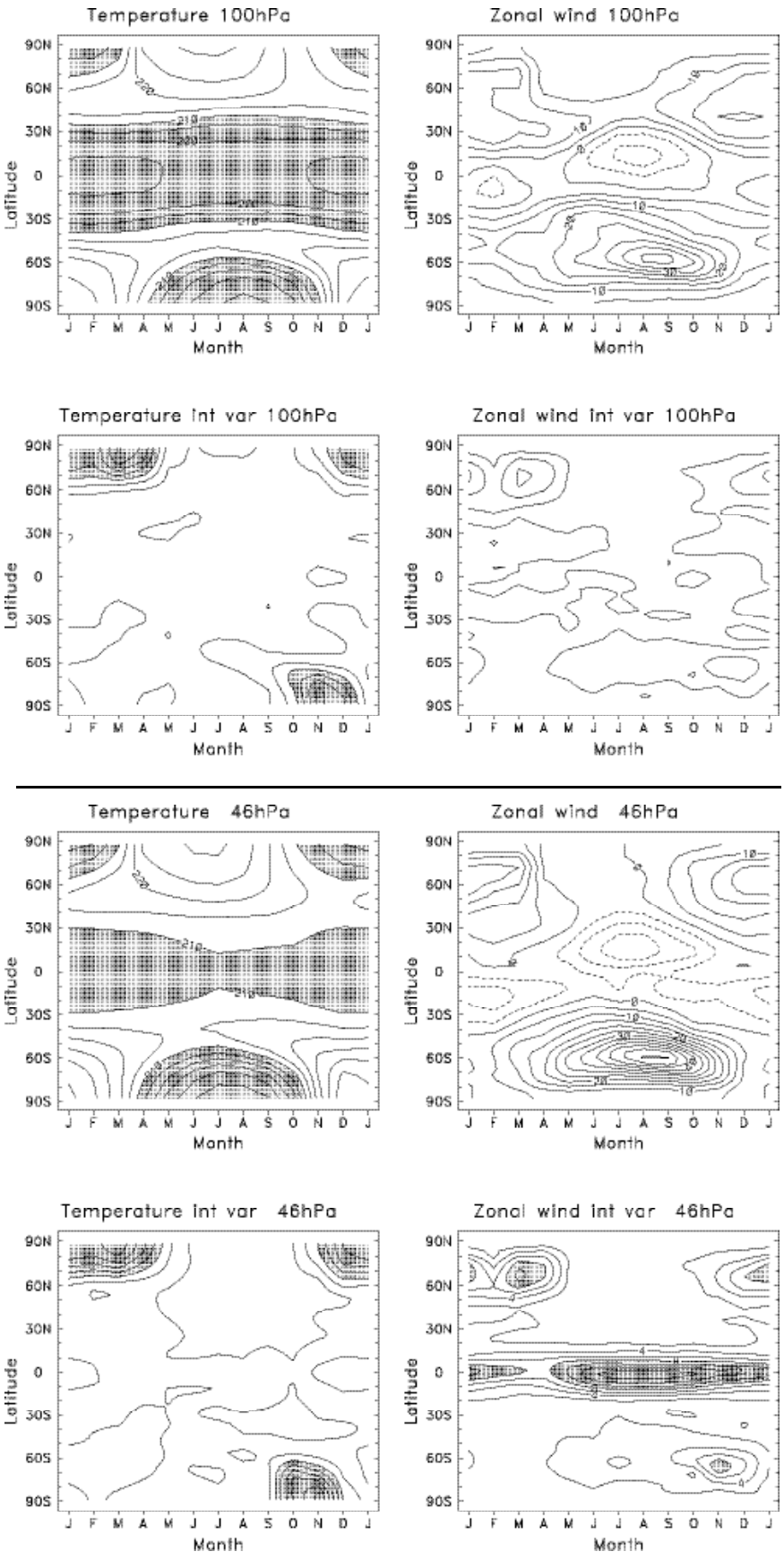

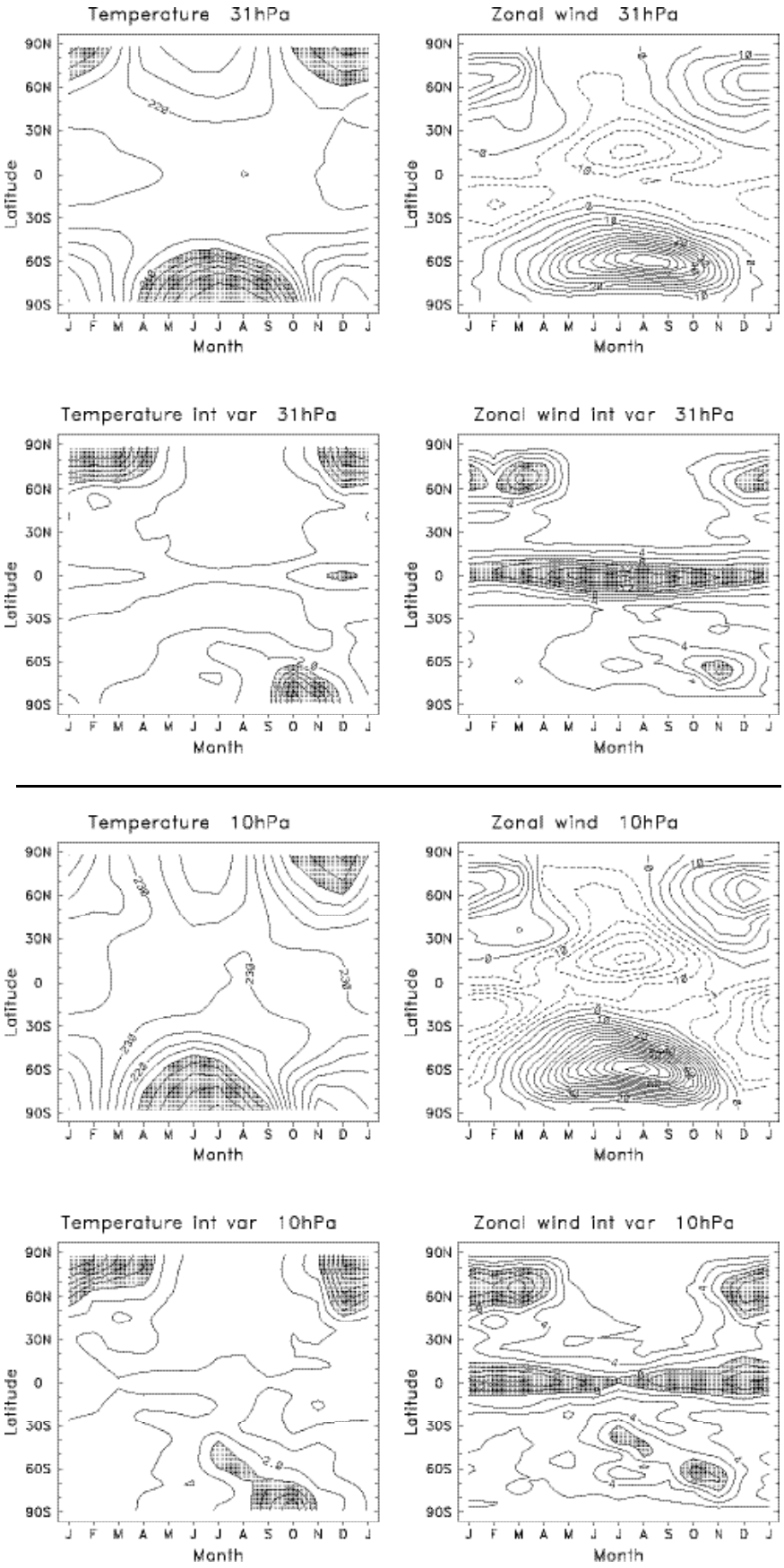
Temperature 31hPa
Zonal wind 31hPa
Temperature int var 31hPa
Zonal wind int var 31hPa
Temperature 10hPa
Zonal wind 10hPa
Temperature int var 10hPa
Zonal wind int var 10hPa
Latitude
Month
90N
60N
30N
0
30S
60S
90S
J F M A M J J A S O N D J

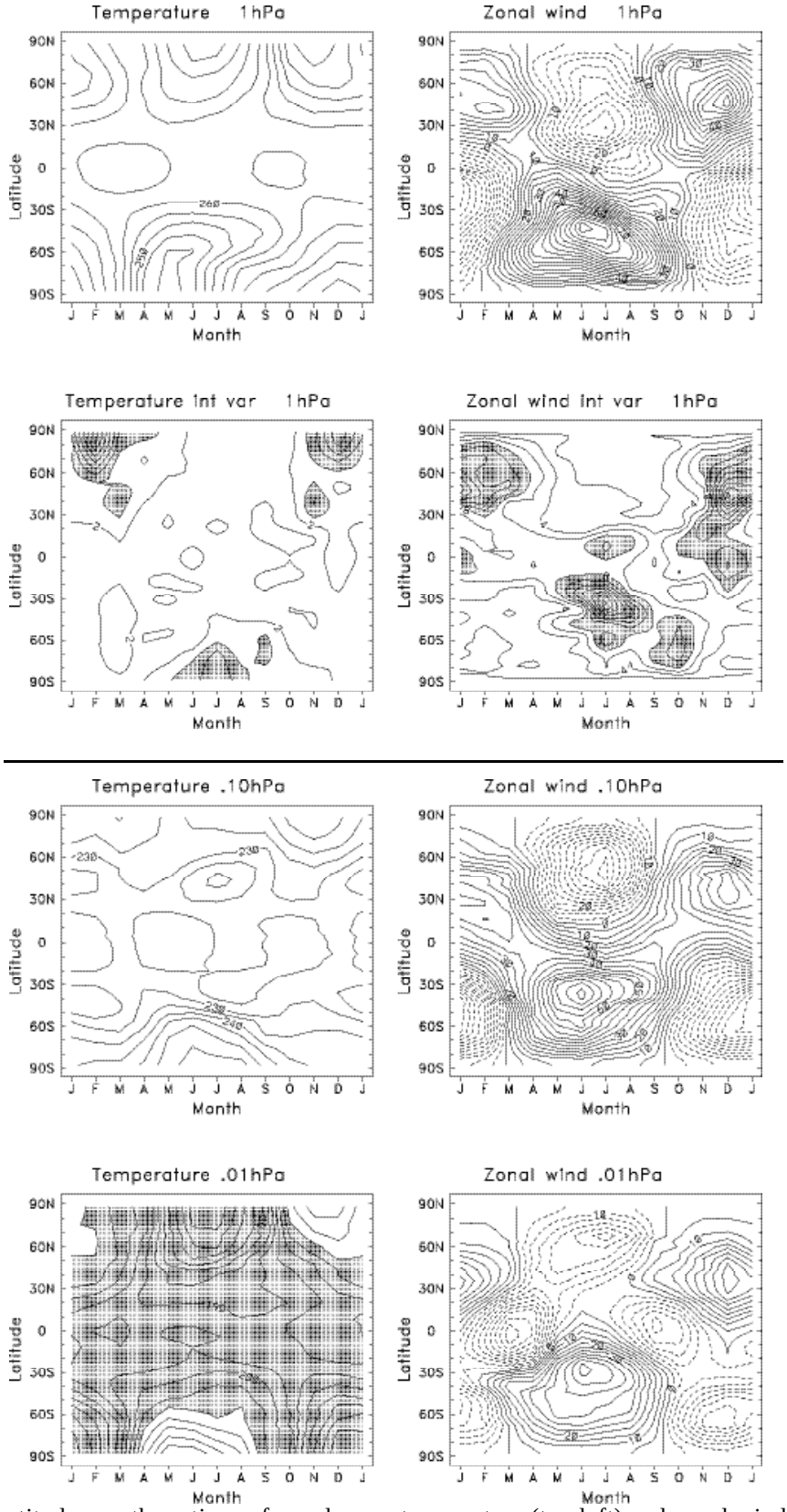

Figure 52. Latitude-month sections of zonal mean temperature (top left) and zonal wind (top right), together with estimates of interannual variability (lower panels), at a number of selected pressure levels. Contour intervals are 5 K and 5 m/s for the means (upper panels), and 1 K and 2 m/s for the lower panels. Interannual variability plots are only available for data at and below 1 hPa. Shading is included for mean temperatures below 210 K, and for wind (temperature) variability greater than 8 m/s (3 K), respectively.

Figure 53. pp 83 to pp 85

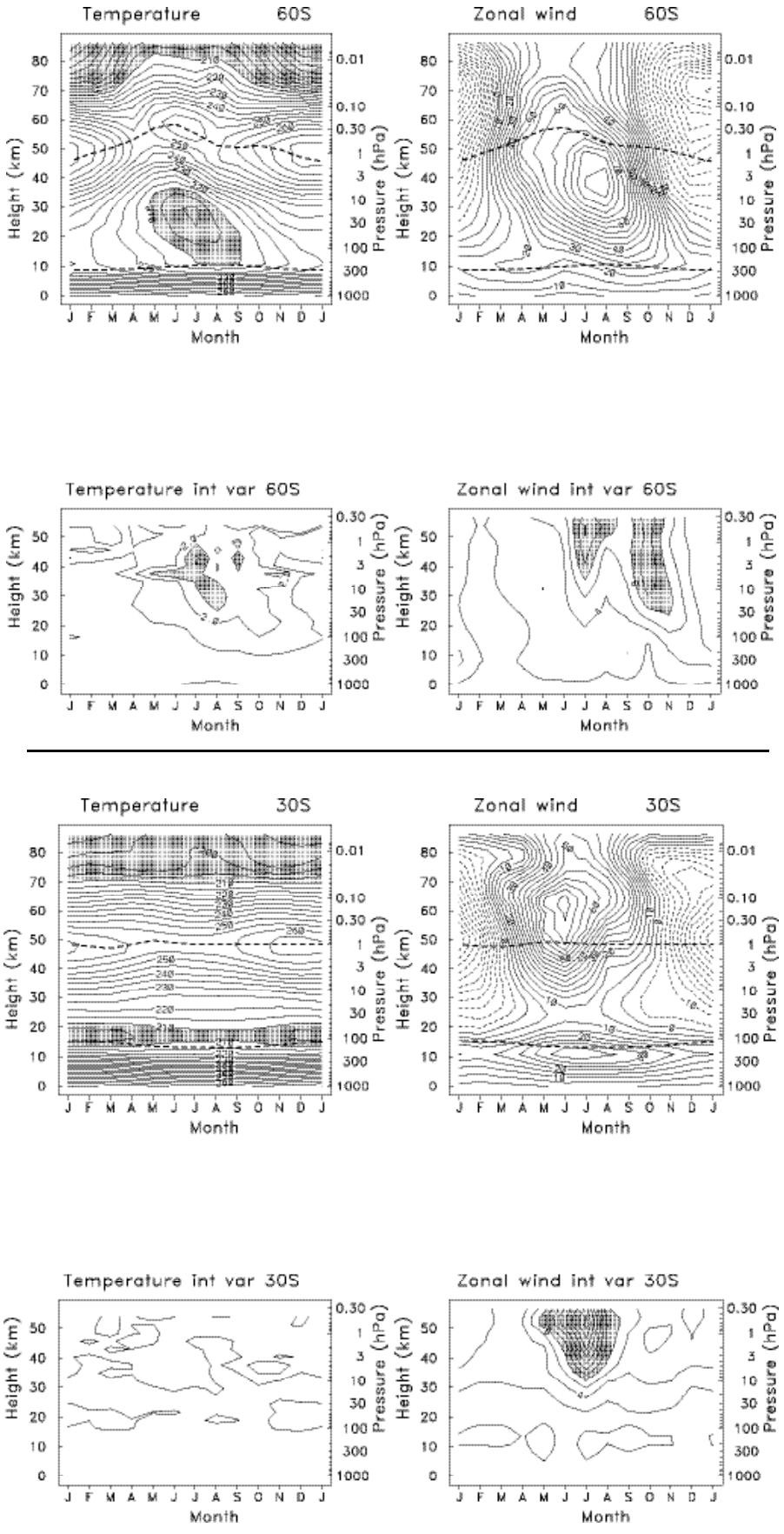

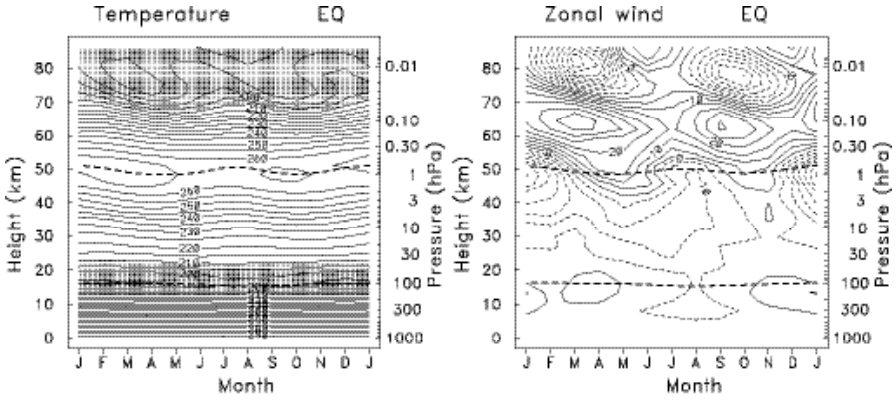
Temperature EQ
Zonal wind EQ
Height (km)
Pressure (hPa)
Month
J F M A M J J A S O N D J

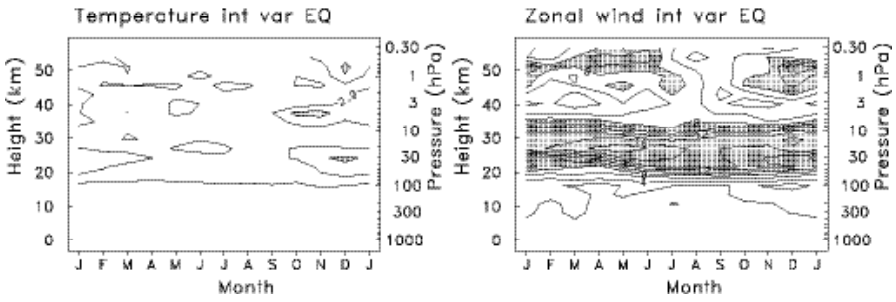
Temperature int var EQ
Zonal wind int var EQ
Height (km)
Pressure (hPa)
Month
J F M A M J J A S O N D J

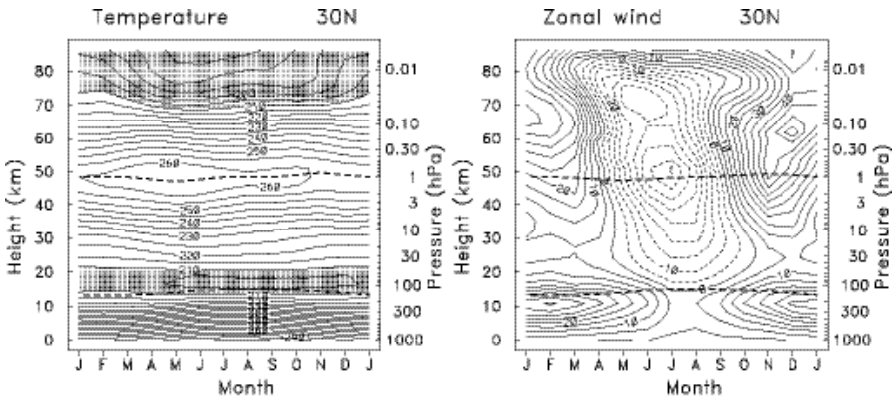
Temperature 30N
Zonal wind 30N
Height (km)
Pressure (hPa)
Month
J F M A M J J A S O N D J

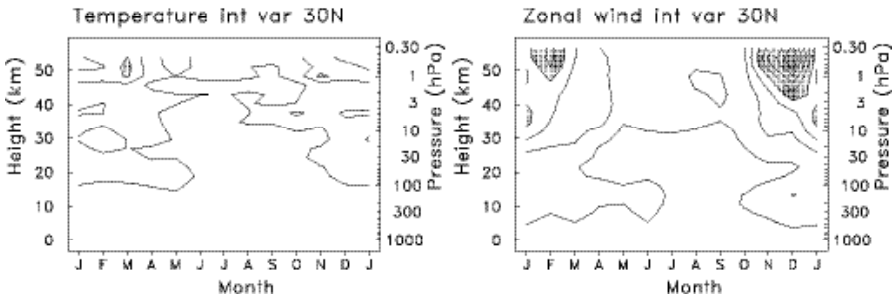
Temperature int var 30N
Zonal wind int var 30N
Height (km)
Pressure (hPa)
Month
J F M A M J J A S O N D J

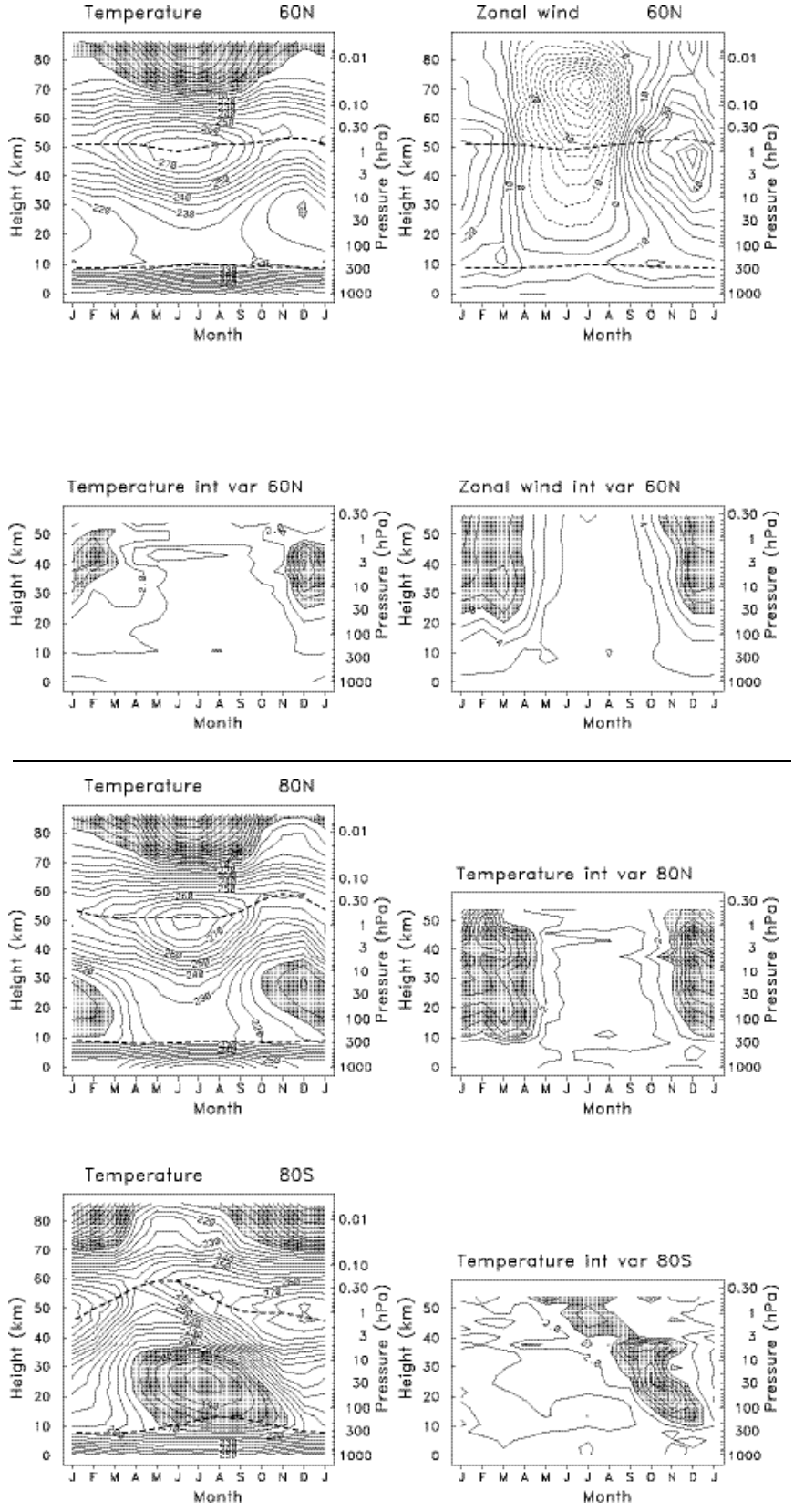

Figure 53. Height-time sections of zonal mean temperature and zonal mean zonal wind at a number of selected latitudes (zonal mean winds are not included for 80°N and 80°S). The heavy dashed lines indicate the tropopause and stratopause. Also included for each latitude are the respective interannual variability statistics derived from UKMO data for 1992-2000 (only available over 1000-0.3 hPa). Contours and shading are the same as in Figures 51-52.

Acronyms and Abbreviations

ACMAP	Atmospheric Chemistry Modelling and Analyses Program
ATOVS	Advanced-TOVS
CIRA	COSPAR International Reference Atmosphere
COSPAR	Committee On Space Research
CPC	Climate Prediction Center
DJF	December – January - February
ECMWF	European Center for Medium Range Weather Forecasts
ERA15	ECMWF 15-year ReAnalysis
ERA40	ECMWF 40-year ReAnalysis
FUB	Free University of Berlin, Germany
HALOE	Halogen Occultation Experiment
hPa	Hecto Pascal
HRDI	High Resolution Doppler Imager
ICSU	International Council of Sciences Union
JJA	June – July - August
MLS	Microwave Limb Sounder
MSIS	Mass Spectrometer and Incoherent Scatter
NASA	National Aeronautics and Space Administration, USA
NCAR	National Center for Atmospheric Research
NDSC	Network for the Detection of Stratospheric Change
NCEP	National Centers for Environmental Prediction
NH	North Hemisphere
NMC	National Meteorological Center
NOAA	National Oceanic and Atmospheric Administration, USA
OHP	Observatoire de Haute Provence, France
PMR	Pressure Modulator Radiometer
QBO	Quasi-Biennal Oscillation
SAO	Semi-Annual Oscillation
SCR	Selective Chopper Radiometer
SH	South Hemisphere
SME	Solar Mesosphere Explorer

SPARC	Stratospheric Processes and Their Role in Climate
SSU	Stratospheric Sounding Unit
TIROS	Television InfraRed Observation Satellites
TOVS	TIROS Operational Vertical Sounder
UARS	Upper Atmosphere Research Satellite
UKMO	United Kingdom Meteorological Office, UK
UKTOVS	United Kingdom TOVS
URAP	UARS Reference Atmosphere Project
UT	Universal Time
UTC	Coordinated Universal Time
WMO	World Meteorological Organisation
WCRP	World Climate Research Programme

LIST OF REPORTS

WCRP-1 VALIDATION OF SATELLITE PRECIPITATION MEASUREMENTS FOR THE GLOBAL PRECIPITATION CLIMATOLOGY PROJECT (Report of an International Workshop, Washington, D.C., 17-21 November 1986) (WMO/TD-No. 203) (out of print)

WCRP-2 WOCE CORE PROJECT 1 PLANNING MEETING ON THE GLOBAL DESCRIPTION (Washington, D.C., 10-14 November 1986) (WMO/TD-No. 205) (out of print)

WCRP-3 INTERNATIONAL SATELLITE CLOUD CLIMATOLOGY PROJECT (ISCCP) WORKING GROUP ON DATA MANAGEMENT (Report of the Sixth Session, Fort Collins, U.S.A., 16-18 June 1987) (WMO/TD-No. 210) (out of print)

WCRP-4 JSC/CCCO TOGA NUMERICAL EXPERIMENTATION GROUP (Report of the First Session, Unesco, Paris, France, 25-26 June 1987) (WMO/TD-No. 204) (out of print)

WCRP-5 CONCEPT OF THE GLOBAL ENERGY AND WATER CYCLE EXPERIMENT (Report of the JSC Study Group on GEWEX, Montreal, Canada, 8-12 June 1987 and Pasadena, U.S.A., 5-9 January 1988) (WMO/TD-No. 215) (out of print)

WCRP-6 INTERNATIONAL WORKING GROUP ON DATA MANAGEMENT FOR THE GLOBAL PRECIPITATION CLIMATOLOGY PROJECT (Report of the Second Session, Madison, U.S.A., 9-11 September 1988) (WMO/TD-No. 221) (out of print)

WCRP-7 CAS GROUP OF RAPPORTEURS ON CLIMATE (Leningrad, U.S.S.R., 28 October-1 November 1985) (WMO/TD-No. 226) (out of print)

WCRP-8 JSC WORKING GROUP ON LAND SURFACE PROCESSES AND CLIMATE (Report of the Third Session, Manhattan, U.S.A., 29 June-3 July 1987) (WMO/TD-No. 232) (out of print)

WCRP-9 AEROSOLS, CLOUDS AND OTHER CLIMATICALLY IMPORTANT PARAMETERS: LIDAR APPLICATIONS AND NETWORKS (Report of a Meeting of Experts, Geneva, Switzerland, 10-12 December 1985) (WMO/TD-No. 233) (out of print)

WCRP-10 RADIATION AND CLIMATE (Report of the First Session, JSC Working Group on Radiative Fluxes, Greenbelt, U.S.A., 14-17 December 1987) (WMO/TD-No. 235) (out of print)

WCRP-11 WORLD OCEAN CIRCULATION EXPERIMENT - IMPLEMENTATION PLAN - DETAILED REQUIREMENTS (Volume I) (WMO/TD-No. 242) (out of print)

WCRP-12 WORLD OCEAN CIRCULATION EXPERIMENT - IMPLEMENTATION PLAN - SCIENTIFIC BACKGROUND (Volume II) (WMO/TD-No. 243) (out of print)

WCRP-13 RADIATION AND CLIMATE (Report of the Seventh Session of the International Satellite Cloud Climatology Project (ISCCP) Working Group on Data Management, Banff, Canada, 6-8 July 1988) (WMO/TD-No. 252) (out of print)

WCRP-14 AN EXPERIMENTAL CLOUD LIDAR PILOT STUDY (ECLIPS) (Report of the WCRP/CSIRO Workshop on Cloud Base Measurement, CSIRO, Mordialloc, Victoria, Australia, 29 February-3 March 1988) (WMO/TD-No. 251) (out of print)

WCRP-15 MODELLING THE SENSITIVITY AND VARIATIONS OF THE OCEAN-ATMOSPHERE SYSTEM (Report of a Workshop at the European Centre for Medium Range Weather Forecasts, 11-13 May 1988) (WMO/TD-No. 254) (out of print)

WCRP-16 GLOBAL DATA ASSIMILATION PROGRAMME FOR AIR-SEA FLUXES (Report of the JSC/CCCO Working Group on Air-Sea Fluxes, October 1988) (WMO/TD-No. 257) (out of print)

WCRP-17 JSC/CCCO TOGA SCIENTIFIC STEERING GROUP (Report of the Seventh Session, Cairns, Queensland, Australia, 11-15 July 1988) (WMO/TD-No. 259) (out of print)

WCRP-18 SEA ICE AND CLIMATE (Report of the Third Session of the Working Group on Sea Ice and Climate, Oslo, 31 May-3 June 1988) (WMO/TD-No. 272) (out of print)

WCRP-19 THE GLOBAL PRECIPITATION CLIMATOLOGY PROJECT (Report of the third Session of the International Working Group on Data Management, Darmstadt, FRG, 13-15 July 1988) (WMO/TD-No. 274) (out of print)

WCRP-20 RADIATION AND CLIMATE (Report of the Second Session of the WCRP Working Group on Radiative Fluxes, Geneva, Switzerland, 19-21 October 1988) (WMO/TD-No. 291) (out of print)

WCRP-21 INTERNATIONAL WOCE SCIENTIFIC CONFERENCE (Report of the International WOCE Scientific Conference, Unesco, Paris, 28 November-2 December 1988) (WMO/TD-No. 295) (out of print)

WCRP-22 THE GLOBAL WATER RUNOFF DATA PROJECT (Workshop on the Global Runoff Data Set and Grid estimation, Koblenz, FRG, 10-15 November 1988) (WMO/TD-No. 302) (out of print)

WCRP-23 WOCE SURFACE FLUX DETERMINATIONS - A STRATEGY FOR IN SITU MEASUREMENTS (Report of the Working Group on In Situ Measurements for Fluxes, La Jolla, California, U.S.A., 27 February-3 March 1989) (WMO/TD-No. 304) (out of print)

WCRP-24 JSC/CCCO TOGA NUMERICAL EXPERIMENTATION GROUP (Report of the Second Session, Royal Society, London, U.K., 15-16 December 1988) (WMO/TD-No. 307) (out of print)

WCRP-25 GLOBAL ENERGY AND WATER CYCLE EXPERIMENT (GEWEX) (Report of the First Session of the JSC Scientific Steering Group for GEWEX, Pasadena, U.S.A., 7-10 February 1989) (WMO/TD-No. 321) (out of print)

WCRP-26 WOCE GLOBAL SURFACE VELOCITY PROGRAMME (SVP) (Workshop Report of WOCE/SVP Planning Committee and TOGA Pan-Pacific Surface Current Study, Miami, Florida, U.S.A., 25-26 April 1988) (WMO/TD-No. 323) (out of print)

WCRP-27 DIAGNOSTICS OF THE GLOBAL ATMOSPHERIC CIRCULATION (Based on ECMWF analyses 1979-1989, Department of Meteorology, University of Reading, Compiled as part of the U.K. Universities Global Atmospheric Modelling Project) (WMO/TD-No. 326) (out of print)

WCRP-28 INVERSION OF OCEAN GENERAL CIRCULATION MODELS (Report of the CCCO/WOCE Workshop, London, 10-12 July 1989) (WMO/TD-No. 331) (out of print)

WCRP-29 CAS WORKING GROUP ON CLIMATE RESEARCH (Report of Session, Geneva, 22-26 May 1989) (WMO/TD-No. 333) (out of print)

WCRP-30 WOCE - FLOW STATISTICS FROM LONG-TERM CURRENT METER MOORINGS: THE GLOBAL DATA SET IN JANUARY 1989 (Report prepared by Robert R. Dickinson, Eddy Statistics Scientific Panel) (WMO/TD-No. 337) (out of print)

WCRP-31 JSC/CCCO TOGA SCIENTIFIC STEERING GROUP (Report of the Eighth Session, Hamburg, FRG, 18-22 September 1989) (WMO/TD-No. 338) (out of print)

WCRP-32 JSC/CCCO TOGA NUMERICAL EXPERIMENTATION GROUP (Report of the Third Session, Hamburg, FRG, 18-20 September 1989) (WMO/TD-No. 339) (out of print)

WCRP-33 TOGA MONSOON CLIMATE RESEARCH (Report of the First Session of the Monsoon Numerical Experimentation Group, Hamburg, FRG, 21-22 September 1989) (WMO/TD-No. 349) (out of print)

WCRP-34 THE GLOBAL PRECIPITATION CLIMATOLOGY PROJECT (Report of the Fourth Session of the International Working Group on Data Management, Bristol, U.K., 26-28 July 1989) (WMO/TD-No. 356) (out of print)

WCRP-35 RADIATION AND CLIMATE (Report of the Third Session of the WCRP Working Group on Radiative Fluxes, Fort Lauderdale, U.S.A., 12-15 December 1989) (WMO/TD-No. 364) (out of print)

WCRP-36 LAND-SURFACE PHYSICAL AND BIOLOGICAL PROCESSES (Report of an ad-hoc Joint Meeting of the IGBP Co-ordinating Panel No. 3 and WCRP Experts, Paris, France, 24-26 October 1989) (WMO/TD-No. 368) (out of print)

WCRP-37 GLOBAL ENERGY AND WATER CYCLE EXPERIMENT (Report of the Workshop to Evaluate the Need for a Rain Radar in Polar Orbit for GEWEX, Greenbelt, U.S.A., 25-26 October 1989) (WMO/TD-No. 369) (out of print)

WCRP-38 GLOBAL ENERGY AND WATER CYCLE EXPERIMENT (Report of the First Session of the WCRP-GEWEX/IGBP-CP3 Joint Working Group on Land-Surface Experiments, Wallingford, U.K., 25-26 January 1990) (WMO/TD-No. 370) (out of print)

WCRP-39 RADIATION AND CLIMATE (Intercomparison of Radiation Codes in Climate Models, Report of Workshop, Paris, France, 15-17 August 1988) (WMO/TD-No. 371) (out of print)

WCRP-40 GLOBAL ENERGY AND WATER CYCLE EXPERIMENT (Scientific Plan), August 1990 (WMO/TD-No. 376) (out of print)

WCRP-41 SEA-ICE AND CLIMATE (Report of the Fourth Session of the Working Group, Rome, Italy, 20-23 November 1989) (WMO/TD-No. 377) (out of print)

WCRP-42 PLANETARY BOUNDARY LAYER (Model Evaluation Workshop, Reading, U.K., 14-15 August 1989) (WMO/TD-No. 378) (out of print)

WCRP-43 INTERNATIONAL TOGA SCIENTIFIC CONFERENCE PROCEEDINGS (Honolulu, U.S.A., 16-20 July 1990) (WMO/TD-No. 379) (out of print)

WCRP-44 GLOBAL ENERGY AND WATER CYCLE EXPERIMENT (Report of the 2nd Session of the JSC Scientific Steering Group, Paris, France, 15-19 January 1990) (WMO/TD-No. 383) (out of print)

WCRP-45 SEA ICE NUMERICAL EXPERIMENTATION GROUP (SINEG) (Report of the First Session, Washington, D.C., 23-25 May 1989) (WMO/TD-No. 384) (out of print)

WCRP-46 EARTH OBSERVING SYSTEM FOR CLIMATE RESEARCH (Report of a WCRP Planning Meeting, Reading, U.K., 2-3 July 1990) (WMO/TD-No. 388) (out of print)

WCRP-47 JSC/CCCO TOGA SCIENTIFIC STEERING GROUP (Report of the Ninth Session, Kona, Hawaii, U.S.A., 23-25 July 1990) (WMO/TD-No. 387) (out of print)

WCRP-48 SPACE OBSERVATIONS OF TROPOSPHERIC AEROSOLS AND COMPLEMENTARY MEASUREMENTS (Report of experts meeting at Science and Technology Corporation, Hampton, Virginia, U.S.A., 15-18 November 1989) (WMO/TD-No. 389) (out of print)

WCRP-49 TOGA MONSOON CLIMATE RESEARCH (Report of the Second Session of the Monsoon Numerical Experimentation Group, Kona, Hawaii, U.S.A., 26-27 July 1990) (WMO/TD-No. 392) (out of print)

WCRP-50 TOGA NUMERICAL EXPERIMENTATION GROUP (Report of the Fourth Session, Palisades, New York, U.S.A., 13-14 June 1990) (WMO/TD-No. 393) (out of print)

WCRP-51 RADIATION AND CLIMATE (Report of the First Session, International Working Group on Data Management for WCRP Radiation Projects, New York City, U.S.A., 21-23 May 1990) (WMO/TD-No. 398) (out of print)

WCRP-52 THE RADIATIVE EFFECTS OF CLOUDS AND THEIR IMPACT ON CLIMATE (Review prepared by Dr. A. Arking at request of IAMAP Radiation Commission) (WMO/TD-No. 399) (out of print)

WCRP-53 CAS/JSC WORKING GROUP ON NUMERICAL EXPERIMENTATION (Report of the Sixth Session, Melbourne, Australia, 24-28 September 1990) (WMO/TD-No. 405) (out of print)

WCRP-54 RADIATION AND CLIMATE (Workshop on Implementation of the Baseline Surface Radiation Network, Washington, D.C., 3-5 December 1990) (WMO/TD-No. 406) (out of print)

WCRP-55 GLOBAL CLIMATE MODELLING (Report of First Session of WCRP Steering Group on Global Climate Modelling, Geneva, Switzerland, 5-8 November 1990) (WMO/TD-No. 411) (out of print)

WCRP-56 THE GLOBAL CLIMATE OBSERVING SYSTEM (Report of a meeting convened by the Chairman of the Joint Scientific Committee for the WCRP, Winchester, U.K., 14-15 January 1991) (WMO/TD-No. 412) (out of print)

WCRP-57 GLOBAL ENERGY AND WATER CYCLE EXPERIMENT (Report of the 3rd Session of the JSC Scientific Steering Group, Hamilton, Bermuda, 21-25 January 1991) (WMO/TD-No. 424) (out of print)

WCRP-58 INTERCOMPARISON OF CLIMATES SIMULATED BY 14 ATMOSPHERIC GENERAL CIRCULATION MODELS (CAS/JSC Working Group on Numerical Experimentation, prepared by Dr. G.J. Boer et al) (WMO/TD-No. 425) (out of print)

WCRP-59 INTERACTION BETWEEN AEROSOLS AND CLOUDS (Report of Experts Meeting, Hampton, Virginia, U.S.A., 5-7 February 1991) (WMO/TD-No. 423) (out of print)

WCRP-60 THE GLOBAL PRECIPITATION CLIMATOLOGY PROJECT (Report of the Fifth Session of the International Working Group on Data Management, Laurel, Maryland, U.S.A., 20-21 May 1991) (WMO/TD-No. 436)

WCRP-61 GLOBAL ENERGY AND WATER CYCLE EXPERIMENT (Report of the Second Session of the WCRP-GEWEX/IGBP Core Project on BAHC Joint Working Group on Land-Surface Experiments, Greenbelt, Mayland, U.S.A., 3-4 June 1991) (WMO/TD-No. 437)

WCRP-62 SEA-ICE AND CLIMATE (Report of a Workshop on Polar Radiation Fluxes and Sea-Ice Modelling, Bremerhaven, Germany, 5-8 November 1990) (WMO/TD-No. 442)

WCRP-63 JSC/CCCO TOGA SCIENTIFIC STEERING GROUP (Report of the Tenth Session, Gmunden, Austria, 26-29 August 1991) (WMO/TD-No. 441)

WCRP-64 RADIATION AND CLIMATE (Second Workshop on Implementation of the Baseline Surface Radiation Network, Davos, Switzerland, 6-9 August 1991) (WMO/TD-No. 453)

WCRP-65 SEA-ICE AND CLIMATE (Report of the Fifth Session of the Working Group, Bremerhaven, Germany, 13-15 June 1991 (WMO/TD-No. 459)

WCRP-66 GLOBAL ENERGY AND WATER CYCLE EXPERIMENT (Report of the First GEWEX Temperature/Humidity Retrieval Workshop, Greenbelt, U.S.A., 23-26 October 1990) (WMO/TD-No. 460) (out of print)

WCRP-67 GEWEX CONTINENTAL SCALE INTERNATIONAL PROJECT (Scientific Plan, December 1991) (WMO/TD-No. 461) (out of print)

WCRP-68 SIMULATION OF INTERANNUAL AND INTRASEASONAL MONSOON VARIABILITY (Report of Workshop, Boulder, CO, U.S.A., 21-24 October 1991) (WMO/TD-No. 470)

WCRP-69 RADIATION AND CLIMATE (Report of Fourth Session of the WCRP Working Group on Radiative Fluxes, Palm Springs, U.S.A., 24-27 September 1991) (WMO/TD-No. 471)

WCRP-70 CAS/JSC WORKING GROUP ON NUMERICAL EXPERIMENTATION (Report of the Seventh Session, Boulder, CO, U.S.A., 24-29 October 1991) (WMO/TD-No. 477)

WCRP-71 GLOBAL CLIMATE MODELLING (Report of Second Session of WCRP Steering Group on Global Climate Modelling, Bristol, U.K., 18-20 November 1991) (WMO/TD-No. 482)

WCRP-72 SCIENTIFIC CONCEPT OF THE ARCTIC CLIMATE SYSTEM STUDY (ACSYS) (Report of the JSC Study Group on ACSYS, Bremerhaven, Germany, 10-12 June 1991 and London, U.K., 18-19 November 1991) (WMO/TD-No. 486) (out of print)

WCRP-73 TOGA NUMERICAL EXPERIMENTATION GROUP (Report of the Fifth Session, San Francisco, California, U.S.A., 9-11 December 1991) (WMO/TD-No. 487)

WCRP-74 GLOBAL ENERGY AND WATER CYCLE EXPERIMENT (Report of the Fourth Session of the JSC Scientific Steering Group for GEWEX, Tokyo, Japan, 27-31 January 1992) (WMO/TD-No. 490)

WCRP-75 HYDROLOGY AND SURFACE RADIATION IN ATMOSPHERIC MODELS (Report of a GEWEX Workshop, European Centre for Medium-range Weather

Forecasts, Reading, U.K., 28 October-1 November 1991) (WMO/TD-No. 492) (out of print)

WCRP-76 REVIEWS OF MODERN CLIMATE DIAGNOSTIC TECHNIQUES - Satellite data in climate diagnostics, (A. Gruber and P.A. Arkin, November 1992) (WMO/TD-No. 519) (out of print)

WCRP-77 INTERNATIONAL SATELLITE CLOUD CLIMATOLOGY PROJECT (Radiance Calibration Report, December 1992) (WMO/TD-No. 520) (out of print)

WCRP-78 GLOBAL OBSERVATIONS, ANALYSES AND SIMULATION OF PRECIPITATION (Report of Workshop, National Meteorological Center, Camp Springs, Maryland, U.S.A., 27-30 October 1992) (WMO/TD-No. 544) (out of print)

WCRP-79 INTERCOMPARISON OF TROPICAL OCEAN GCMS (TOGA Numerical Experimentation Group, prepared by T. Stockdale et al., April 1993) (WMO/TD-No. 545)

WCRP-80 SIMULATION AND PREDICTION OF MONSOONS - RECENT RESULTS (TOGA/WGNE Monsoon Numerical Experimentation Group, New Delhi, India, 12-14 January 1993) (WMO/TD-No. 546)

WCRP-81 ANALYSIS METHODS OF PRECIPITATION ON A GLOBAL SCALE (Report of a GEWEX Workshop, Koblenz, Germany, 14-17 September 1992) (WMO/TD-No. 558) (Out of print)

WCRP-82 INTERCOMPARISON OF SELECTED FEATURES OF THE CONTROL CLIMATES SIMULATED BY COUPLED OCEAN-ATMOSPHERE GENERAL CIRCULATION MODELS (Steering Group on Global Climate Modelling, September 1993) (WMO/TD-No. 574)

WCRP-83 STRATOSPHERIC PROCESSES AND THEIR ROLE IN CLIMATE (SPARC): INITIAL REVIEW OF OBJECTIVES AND SCIENTIFIC ISSUES (SPARC Scientific Steering Group, December 1993) (WMO/TD-No. 582) (out of print)

WCRP-84 PROCEEDINGS OF THE INTERNATIONAL CONFERENCE ON MONSOON VARIABILITY AND PREDICTION (Trieste, Italy, 9-13 May 1994) (WMO/TD-No. 619) (Out of print)

WCRP-85 INITIAL IMPLEMENTATION PLAN FOR THE ARCTIC CLIMATE SYSTEM STUDY (ACSYS) (September 1994) (WMO/TD-No. 627) (out of print)

WCRP-86 CLOUD-RADIATION INTERACTIONS AND THEIR PARAMETERIZATION IN CLIMATE MODELS (Report of international workshop, Camp Springs, Maryland, U.S.A., 18-20 October 1993) (WMO/TD-No. 648)

WCRP-87 PROCEEDINGS OF THE WORKSHOP ON GLOBAL COUPLED GENERAL CIRCULATION MODELS (La Jolla, California, USA, 10-12 October 1994) (WMO/TD-No. 655)

WCRP-88 INTRASEASONAL OSCILLATIONS IN 15 ATMOSPHERIC GENERAL CIRCULATION MODELS (Results from an AMIP diagnostic subproject) (WMO/TD-No. 661)

WCRP-89 CLIMATE VARIABILITY AND PREDICTABILITY (CLIVAR) Science Plan (August 1995) (WMO/TD-No. 690) (out of print)

WCRP-90 WORKSHOP ON CLOUD MICROPHYSICS PARAMETERIZATIONS IN GLOBAL ATMOSPHERIC CIRCULATION MODELS (Kananaskis, Alberta, Canada, 23-25 May 1995) (WMO/TD-No. 713)

WCRP-91 PROCEEDINGS OF THE INTERNATIONAL SCIENTIFIC CONFERENCE ON TOGA (Melbourne, Australia, 2-7 April 1995) (WMO/TD-No. 717)

WCRP-92 PROCEEDINGS OF THE FIRST INTERNATIONAL AMIP SCIENTIFIC CONFERENCE (Monterey, California, USA, 15-19 May 1995) (WMO/TD-No. 732)

WCRP-93 PROCEEDINGS OF THE WORKSHOP ON ACSYS SOLID PRECIPITATION CLIMATOLOGY PROJECT (Reston, VA, USA, 15-15 September 1995) (WMO/TD-No. 739) (out of print)

WCRP-94 PROCEEDINGS OF THE ACSYS CONFERENCE ON THE DYNAMICS OF THE ARCTIC CLIMATE SYSTEM (Göteborg, Sweden, 7-10 November 1994) (WMO/TD-No. 760) (out of print)

WCRP-95 WCRP WORKSHOP ON AIR-SEA FLUX FIELDS FOR FORCING OCEAN MODELS AND VALIDATING GCMS (Reading, UK, 24-27 October 1995) (WMO/TD-No. 762) (out of print)

WCRP-96 NORTHERN HEMISPHERE ATMOSPHERIC BLOCKING AS SIMULATED BY 15 ATMOSPHERIC GENERAL CIRCULATION MODELS IN THE PERIOD 1979-1988 (Results from an AMIP Diagnostic subproject) (WMO/TD-No. 784) (out of print)

WCRP-97 INTERNATIONAL WORKSHOP ON RESEARCH USES OF ISCCP DATASETS (NASA Goddard Institute for Space Studies, New York, NY, USA, 15-18 April 1996) (WMO/TD-No. 790) (out of print)

WCRP-98 PROCEEDINGS OF THE WORKSHOP ON THE IMPLEMENTATION OF THE ARCTIC PRECIPITATION DATA ARCHIVE (APDA) AT THE GLOBAL PRECIPITATION CLIMATOLOGY CENTRE (GPCC), (Offenbach, Germany, 10-12 July 1996) (WMO/TD-804)

WCRP-99 PROCEEDINGS OF THE FIRST SPARC GENERAL ASSEMBLY (Melbourne, Australia, 2-6 December 1996) (WMO/TD-No. 814) (2 volumes)

WCRP-100 MONSOON PRECIPITATION IN AMIP RUNS (Results from an AMIP diagnostic subproject) (WMO/TD-No. 837)

WCRP-101 CLIVAR - A RESEARCH PROGRAMME ON CLIMATE VARIABILITY AND PREDICTABILITY FOR THE 21ST CENTURY, 1997 (WMO/TD-No. 853)

WCRP-102 ORGANIZATION OF INTERNATIONALLY CO-ORDINATED RESEARCH INTO CRYOSPHERE AND CLIMATE (Proceedings of a meeting of experts on cryosphere and climate) (WMO/TD-No. 867)

WCRP-103 CLIVAR INITIAL IMPLEMENTATION PLAN (WMO/TD-No.869)

WCRP-104 PROCEEDINGS OF THE FIRST WCRP INTERNATIONAL CONFERENCE ON REANALYSES (Silver Spring, Maryland, USA, 27-31 October 1997) (WMO/TD-No. 876)

WCRP-105 SPARC IMPLEMENTATION PLAN (WMO/TD-No. 914)

WCRP-106 PROCEEDINGS OF THE ACSYS CONFERENCE ON POLAR PROCESSES AND GLOBAL CLIMATE (Rosario, Orcas Island, WA, USA, 3-6 November 1997) (WMO/TD-No. 908)

WCRP-107 COARE-98: PROCEEDINGS OF A CONFERENCE ON THE TOGA COUPLED OCEAN-ATMOSPHERE RESPONSE EXPERIMENT (COARE) (Boulder, CO, USA, 7-14 July 1998) (WMO/TD-No. 940)

WCRP-108 PROCEEDINGS OF THE INTERNATIONAL CLIVAR CONFERENCE(Paris, France, 2-4 December 1998) (WMO/TD No. 954)

WCRP-109 PROCEEDINGS OF THE SECOND WCRP INTERNATIONAL CONFERENCE ON REANALYSES (Wokefield Park, nr Reading, UK, 23-27 August 1999) (WMO/TD-No. 985)

WCRP-110 WORKSHOP ON CLOUD PROCESSES AND CLOUD FEEDBACKS IN LARGE-SCALE MODELS (ECMWF, Reading, Berkshire, UK, 9-13 November 1999) (WMO/TD-No. 993)

WCRP-111 PALEOCLIMATE MODELLING INTERCOMPARISON PROJECT (PMIP) (Proceedings of workshop, La Huardière, Canada, 4-8 October 1999) (WMO/TD-NO. 1007)

WCRP-112 INTERCOMPARISON AND VALIDATION OF OCEAN-ATMOSPHERE ENERGY FLUX FIELDS (Final report of the Joint WCRP/SCOR Working Group on Air-Sea Fluxes) (November 2000) (WMO/TD-No. 1036)

WCRP-113 SPARC ASSESSMENT OF UPPER TROPOSPHERIC AND STRATOSPHERIC WATER VAPOUR (WMO/TD-No. 1043) (limited distribution only)

WCRP-114 CLIMATE AND CRYOSPHERE (CLIC) PROJECT, SCIENCE AND CO-ORDINATION PLAN – VERSION 1 (WMO/TDNo. 1053)

WCRP-115 WCRP/SCOR WORKSHOP ON INTERCOMPARISON AND VALIDATION OF OCEAN ATMOSPHERE FLUX FIELDS (BOLGER CENTER, POTOMAC, MD, USA, 21-24 MAY 2001) (WMO/TD-No. 1083)

WCRP-116 SPARC INTERCOMPARISON OF MIDDLE ATMOSPHERE CLIMATOLOGIES (WMO/TD-No. 1142) (limited distribution only)